INHIBITION OF HSP90 IN TRYPANOSOMA BRUCEI AND PHARMACOKINETIC-PHARMACODYNAMIC RELATIONSHIPS OF ANTITRYPANOSOMALS

by

Kirsten J. Meyer

A dissertation submitted to Johns Hopkins University in conformity with the requirements for the degree of Doctor of Philosophy

Baltimore, Maryland

August 2016

ABSTRACT

Human African trypanosomiasis (sleeping sickness), caused by the protozoan parasite *Trypanosoma brucei,* is fatal if untreated. Current drugs are cumbersome to deliver and severely toxic. New antitrypanosomals are greatly needed. The molecular chaperone Hsp90 is conserved and highly expressed in eukaryotes, and essential for several regulatory cell pathways. Hsp90 inhibitors were investigated for anti-trypanosomal activity. Geldanamycin, radicicol, and NVP-AUY922 had nanomolar potency against bloodstream form *T. brucei* in vitro; CUDC-305 and novobiocin had micromolar activity. Structure–activity studies of geldanamycin analogs found 17-AAG and 17-DMAG were most selective against *T. brucei* compared to mammalian cells. Both oral and parenteral 17-DMAG cured mice of a normally lethal infection of *T. brucei.* 17-AAG treatment sensitized trypanosomes to heat shock and caused severe cell cycle disruption. Cytokinesis and kinetoplast replication were particularly affected. RNAi of trypanosome Hsp90s, *HSP83* and Tb427tmp.02.0250 (putative mitochondrial Hsp90), caused growth defects. Loss of HSP83 inhibited cytokinesis, and loss of Tb427tmp.02.0250 disrupted kinetoplast replication, similar effects to those seen with 17-AAG. These promising results support the use of inhibitors to study Hsp90 function in trypanosomes and to expand current clinical development of Hsp90 inhibitors to include *T. brucei.* Correct dosing can be the critical difference between efficacy and failure, not only in the total dose administered but also in the shape of the drug concentration-time curve produced. A hollow-fiber cartridge model was developed to study pharmacokinetic-pharmacodynamic relationships of antitrypanosomals. Contrasting pharmacokinetic profiles, with artificial kinetics favoring either high peak concentrations or sustained drug levels, were delivered to parasites. Simply changing the shape of exposure significantly shifted the dose-response curve of 17-AAG, affecting potency and efficacy. Hsp90 inhibitors from three chemical scaffolds were concentration-driven: significantly more efficacious applied as short-lived high peaks. For optimal efficacy, ideal pharmacokinetic properties and dosing regimens of Hsp90 inhibitors as antitrypanosomals will produce high peaks in vivo. The PK-PD system was also used to study four clinically used and two candidate antitrypanosomals. In vitro PK-PD methodology is expedient, versatile, and a valuable translational tool.

Advisor: Theresa Shapiro

Additional Reader: James Stivers

ACKNOWLEDGEMENTS

My sincere thanks and appreciation to Theresa Shapiro for her mentorship throughout this journey. Under her guidance I have learnt the value of detailed scientific investigation, thoughtful approach to subject matter, and critical analysis of results. I highly respect and admire Dr. Shapiro and am most grateful for training with her.

Thank you to my wonderful colleagues and friends from the Shapiro lab: Elizabeth Nenortas, Rahul Bakshi, Mary Barry, Sonya Tang Girdwood, Nathan Nenortas, Madhuri Manohar, Kathryn Champ, and a special mention to Emily Caton for all her technical support of my experiments.

This work would not have been possible without generous contributions from collaborators. Thanks to David Meyers for chemical synthesis; Nene Kalu for Hsp90 antibody; the Englund/Jensen lab, especially Calvin Tiengwe and Jianyang Wong, for reagents and protocol support; the BDIFL Flow Cytometry Core, Gibson, Cole, and Bumpus laboratories for equipment; Anne Moore from the Centers for Disease Control and Prevention for melarsoprol; and the National Cancer Institute's Developmental Therapeutics Program for chemicals.

My gratitude to my thesis committee for their support and intellectual critique: Charles Flexner, Sean Prigge, and a particular thank you to James Stivers as my dissertation reader.

I am grateful to have been a part of the Pharmacology Department and the Division of Clinical Pharmacology during my time at Johns Hopkins. Thank you to the staff, students, post-docs, and faculty for their collegiality and support.

The training I received in the BioMedical Science Honours program at Victoria University of Wellington and in the lab of John Miller gave me an excellent and thorough scientific foundation.

I am honoured to have been a Fulbright New Zealand Fellow (2010-2015) and a Harvey Fellow (2013-2015). Both provided valuable support, leadership training, and enriching experiences.

Finally, thank you to all my friends and family for their love, and to the One who created and sustains all life and grants the ability to learn, think, and creatively apply knowledge.

TABLE OF CONTENTS

LIST OF TABLES

LIST OF FIGURES

INTRODUCTION

Trypanosoma brucei is a protozoan parasite and causes human African trypanosomiasis (HAT, sleeping sickness). Passed by the bite of the tsetse fly, the parasite is extracellular and exhibits frequent antigenic variation of its surface glycoprotein coat, allowing evasion of the immune system (1). In mammals trypanosomes differentiate into the bloodstream form lifecycle stage, which divides rapidly by mitosis and survives by glycolysis. The parasites live in the blood, lymph, and tissues, and in late-stage disease move in to the CNS leading to devastating neurological symptoms and death (2). Subspecies *T. b. gambiense* is predominantly found in west and central Africa and typically causes an infection that takes several years to progress, whereas *T. b. rhodesiense* is located in east Africa and causes an acute and aggressive infection which leads to death within a few months if untreated (2).

There are currently five drugs used clinically to treat HAT (Fig. 1). Suramin was one of the very first antitrypanosomals, developed in the Bayer dye company in the early 1900s (3). It unfortunately has limited blood-brain barrier permeability, and is thus only effective against early-stage infection. Similarly pentamidine, introduced in the 1940s, is very effective against peripheral infection but inactive against late-stage disease (4). Originating from the work of Paul Ehrlich, organic arsenicals have been used for over a century to treat the CNS disease. The trivalent arsenical melarsoprol, introduced in the late 1940s, remains in use today as the only option for late-stage rhodesiense infection (5). Gambiense CNS disease is now predominantly treated with difluoromethylornithine (DFMO) in combination with nifurtimox. DFMO was repurposed from the oncology field as an antitrypanosomal in the 1980s (6). Although effective against trypanosomes, these drugs all have severe toxicities. Melarsoprol is particularly toxic, frequently causing a reactive encephalopathy that leads to death in 2-10% of treated patients (1). Along with the toxicities, the current antitrypanosomals have lengthy and cumbersome treatment regimens,

difficult to administer in the rural setting of this infection. There is unmet medical need for treatment of this deadly disease.

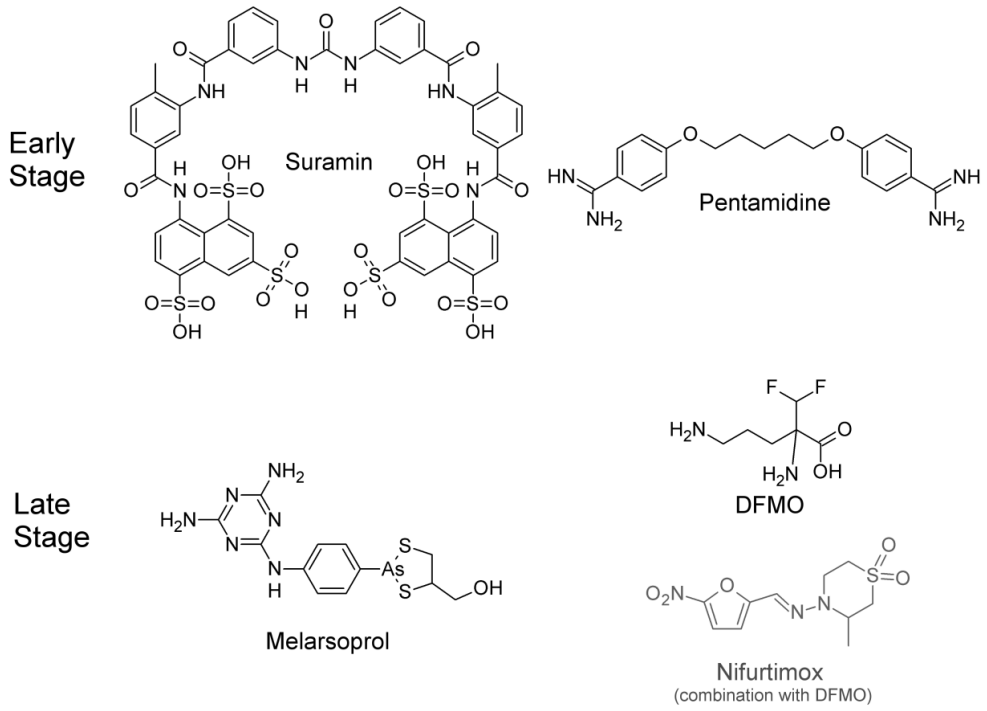

Figure 1. Chemical structures of clinically used antitrypanosomals

The repurposing of DFMO, which inhibits ornithine decarboxylase, illustrates that as a eukaryote *T. brucei* contains homologues of mammalian proteins and is thus susceptible to many compounds effective against mammalian cells. The converse is also true, and in fact suramin and melarsoprol are cytotoxic against cancer cells in vitro and have been tested in clinical oncology trials (7,8). Despite shared cytotoxicity, each of these compounds has a selectivity index for trypanosomes over mammalian cells. Preferential drug uptake in the parasite, divergent enzyme structure and regulation, and differential downstream consequences of compound action can all produce selective toxicity. Screening and repurposing oncology drugs is thus an effective drug development strategy for trypanosomes, as validated by the history of DFMO. This dissertation describes the investigation of heat shock protein 90 (Hsp90) inhibitors against trypanosomes, the molecular consequences of trypanosomal Hsp90 inhibition, and a pharmacokinetic-

pharmacodynamic technique to enhance the development of Hsp90 inhibitors and all antitrypanosomals.

Hsp90 is a molecular chaperone found in high abundance in all eukaryotes and bacteria (9). Chaperones are important for the correct folding and function of other proteins, and are thus essential for protein homeostasis. Hsp90 is a large 90 kDa protein that functions as a dimer and has ATPase capacity thought to drive conformational changes (Fig. 2) (10,11). Post-translational modifications and co-chaperones play an important role in regulating Hsp90 activity and in recruiting specific clients (12). In mammalian cells, Hsp90 clients are involved in multiple cell pathways; including receptor mediated signaling cascades, cell cycle regulation, stress responses, translation control, and even structural integrity and transport (13). Hsp90 is thus a node at the intersection of many essential pathways.

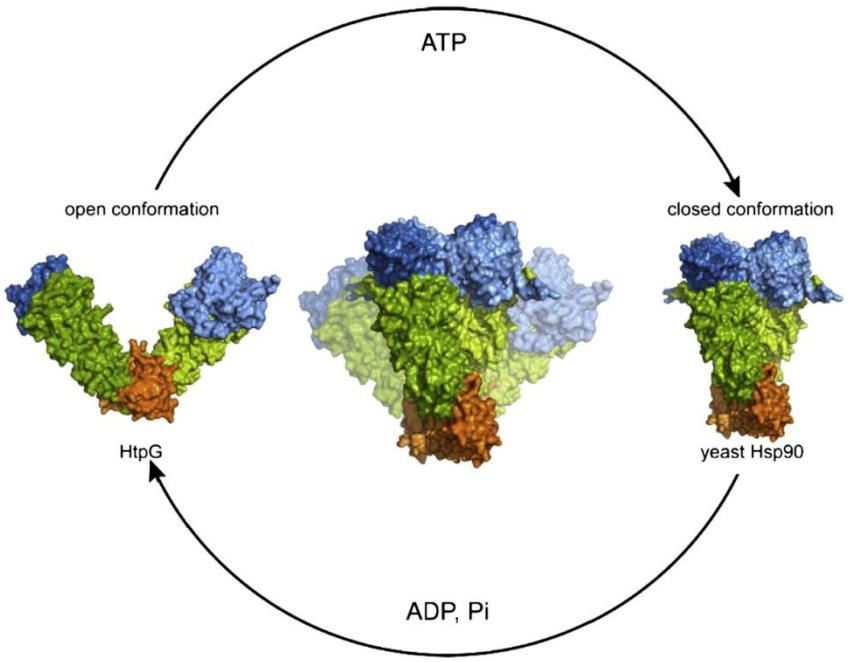

Figure 2. Hsp90 crystal structures

Crystal structure of full length Hsp90 from *E. coli* (HtpG) in the open conformation (left, PDB 2IOQ) and nucleotide-bound yeast Hsp90 in the closed conformation (right, PDB 2CG9). The N-domain is depicted in blue, the M-domain in green and the C-domain in orange. Reprinted from (11) with permission from Elsevier (License 3832560660752).

The trypanosome homologue of Hsp90 is HSP83. HSP83 is encoded by ten tandem genes in *T. brucei* (14), suggesting high abundance, and has been shown to associate with protein phosphatase 5, an important modulatory phosphatase (15). Little is known about the client repertoire of HSP83. Although trypanosomes lack homologues of mammalian clients such as receptor tyrosine kinases or steroid receptors, some translation and cell cycle regulators are conserved. Trypanosomes are ancient divergent eukaryotes and contain many unique cellular pathways that may intersect with HSP83 at some level. For example, in trypanosomes gene transcription is polycistronic and all mRNAs require a spliced 5'-leader sequence, the processing of which is heat-shock sensitive (16). Trypanosome redox stress response relies on the unique trypanothione reductase system rather than the glutathione reductase used in mammalian cells (17). The trypanosome also contains distinct structural features (Fig. 3)(18). Essential for viability is the single flagellum attached along the length of the cell. The flagellum originates from a basal body, anchored at one end of the trypanosome. Attached to the basal body is the kinetoplast, a unique feature to this family of parasites. The kinetoplast is the genome of the single mitochondrion, consisting of a complex network of interlocking DNA plasmids. During the cell cycle, the trypanosome has to faithfully replicate and segregate each structure and organelle in an ordered process, which requires complex regulation (19).

The first inhibitor of Hsp90 identified was the natural product geldanamycin, which binds in the ATP pocket of the *N*-terminal domain and inhibits Hsp90 ATPase activity (20). This pocket is formed by a Bergerat fold, which is also found in histidine kinase, topoisomerase II, and MutL proteins (21). Geldanamycin has potent cytotoxic activity against many cancer cell lines (22). Selectivity for cancer cells over non-transformed cells arises from an increased need for protein homeostasis buffering in the malignant cell due to aberrant mutations, cell stress, and rapid proliferation (23). The impressive in vitro results obtained with geldanamycin led to great interest in Hsp90 as an anti-cancer target, and development of many inhibitors, both semi-synthetically, structurally designed, and found by high-throughput screening (24). The three major classes to

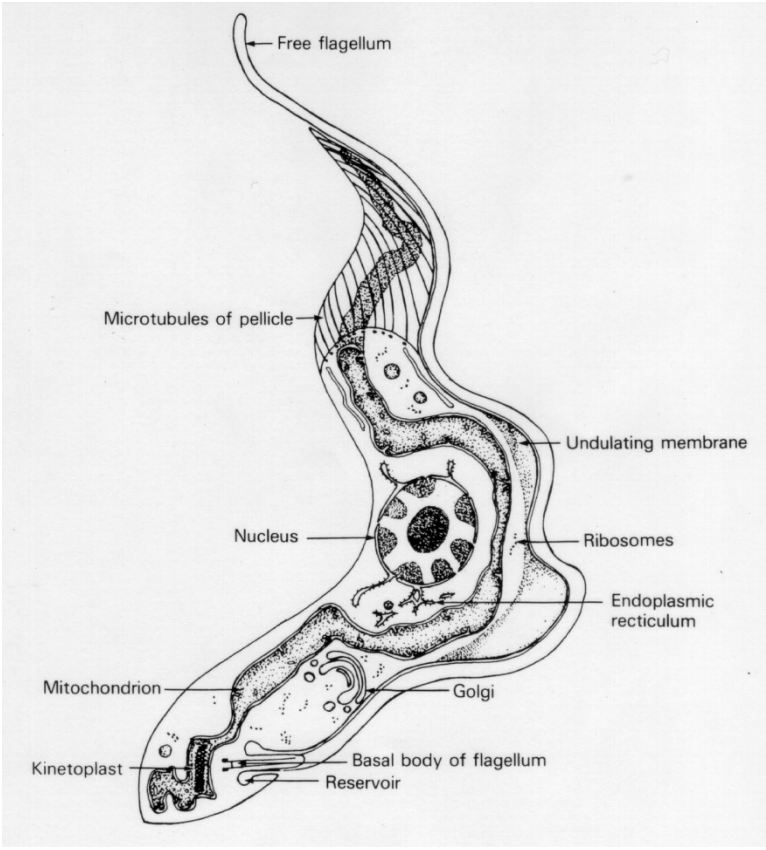

Figure 3. Sub-structure of *T. brucei*

The bloodstream form trypanosome is a slender polarized cell with a single flagellum attached along one undulating edge. Microtubules form a corset that maintains the trypanosome structure. The flagellum originates from the basal body at one end of the cell. The basal body is also attached to the kinetoplast, the densely packed mitochondrial genome. In the trypanosomes the Golgi is a single structure, and trypanosomes also have a single mitochondrion and nucleus. Vickerman and Cox, The Protozoa, 1967 (25).

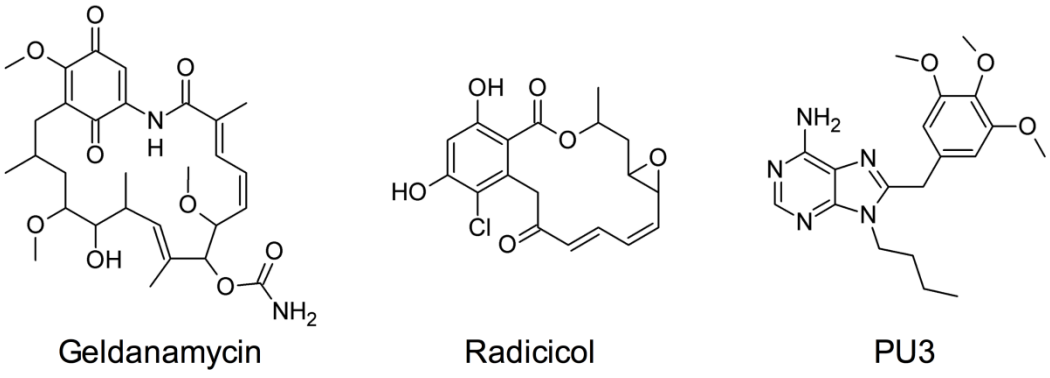

Figure 4. The original ansamycin, resorcinol, and purine scaffold Hsp90 inhibitors

enter the clinic are the benzoquinone ansamycins, derived from geldanamycin, resorcinols (using the pharmacophore of radicicol), and purines (based off a rationally designed inhibitor, PU3) (Fig. 4)(24). All of these bind in the Bergerat fold. Unfortunately no Hsp90 inhibitor has yet been licensed for oncology, as only modest success has been seen in clinical trials (24,26). Alternative indications for these inhibitors are of interest, including use as anti-infectives (27).

Development of any drug is enhanced by knowledge of its pharmacokinetic-pharmacodynamic (PK-PD) relationships, namely the connection between exposure and effect. In vivo, drugs are absorbed, distributed, metabolized, and eliminated by the body which produces a dynamically changing concentration-time profile (Fig. 5). The total exposure to drug is the area

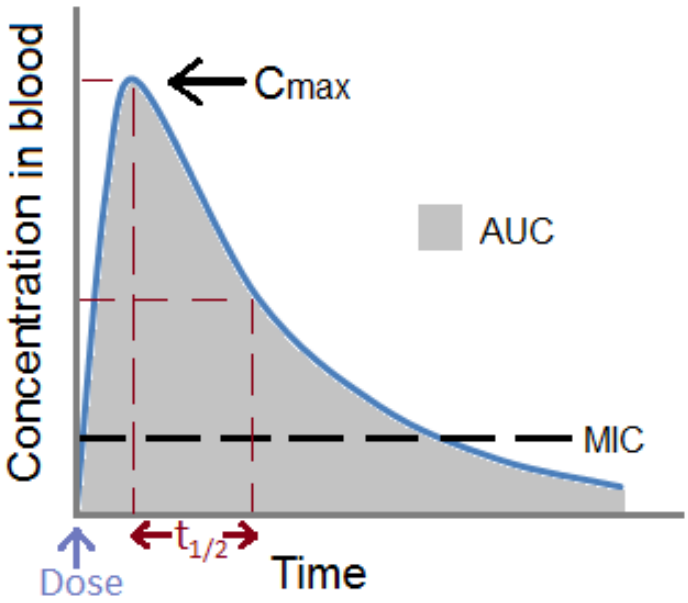

Figure 5. Typical concentration-time profile of drug in blood after an oral dose

After an oral dose of drug, the concentration in the blood rises as drug is absorbed from the gut. Concentration reaches a maximum, C_{max}, when distribution, metabolism, and elimination of the drug begin to dominate, and then falls with a certain half-life, $t_{1/2}$. The total exposure to the drug is described by the area under the curve (AUC). A minimum inhibitory concentration (MIC) can be defined below which the drug is not effective.

under the curve (AUC), and the same AUC can be produced by very differently shaped curves. Knowledge of the PK-PD relationships of a drug helps with optimization of physio-chemical properties and dosing schedules for pre-clinical and clinical evaluation (28,29).

To assess the potential of repurposing Hsp90 inhibitors against *T. brucei*, in vitro cytotoxicity was determined, in vivo activity in mice was examined, molecular consequences of Hsp90 inhibitor treatment were compared to genetic knockdown of trypanosome Hsp90s, and in vitro pharmacokinetic-pharmacodynamic relationships of Hsp90 inhibitors against trypanosomes were investigated.

CHAPTER I. Potent antitrypanosomal activities of Hsp90 inhibitors in vitro and in vivo

Published in part in:

Meyer, K. J., and Shapiro, T. A. (2013) Potent antitrypanosomal activities of heat shock protein 90 inhibitors in vitro and in vivo. *J Infect Dis* **208**, 489-499 (30)

INTRODUCTION

African sleeping sickness (human African trypanosomiasis, HAT) is caused by the protozoan parasite *Trypanosoma brucei* (1). *T. brucei* is transmitted by the tsetse fly and causes endemic disease in both livestock (nagana) and humans (HAT) in sub-Saharan Africa. The parasite propagates extracellularly and moves throughout the body, including in late disease into the central nervous system. In humans this infection is fatal unless treated. Current therapies require repeated parenteral dosing and have formidable toxicities, exemplified by the 2-10% lethality caused by the commonly used drug melarsoprol. New anti-trypanosomal drugs are long overdue.

Heat shock protein 90 (Hsp90) is a phylogenetically conserved, abundant, and essential molecular chaperone (reviewed in (11,31-35)). In mammalian cells it functions as a homodimer complexed with regulatory co-chaperones. Hsp90 stabilizes 'client' proteins, enabling their proper activities. Over two hundred clients have been identified, with many acting in signal transduction pathways, stress responses, and cell cycle regulation (11). Thus Hsp90 is a critical node coordinating many networks necessary for survival. This combinatorial function and a disproportionate dependence on Hsp90 activity in malignant cells have established it as a cancer chemotherapy target (33-36). Dozens of Hsp90 inhibitors have entered the drug development pathway, including derivatives of natural products geldanamycin (e.g., 17-*N*-allylamino-17-demothoxygeldanamycin (17-AAG), 17-dimethylaminoethylamino-17-demethoxygeldanamycin (17-DMAG)) and radicicol, and novel structural scaffolds identified in screens. 17-AAG has been in Phase III trials (34). Geldanamycin treatment leads to proteasomal degradation of Hsp90

client proteins, cell cycle arrest, and heat shock response in mammalian cells (37). Damage to multiple proteins and pathways may be the basis for reported synergism between Hsp90 inhibitors and several chemotherapeutic agents (38).

T. brucei contains a homologue of Hsp90, known as HSP83, for which there are ten tandem genes in the genome (14). Structurally diverse Hsp90 inhibitors, including some already studied in humans, were evaluated for their activity against bloodstream form trypanosomes in vitro; structure-activity relationships were explored for the geldanamycin scaffold; 17-AAG was tested in combination with other drugs; and efficacy of orally dosed 17-DMAG was demonstrated against *T. brucei* infection in mice.

MATERIALS AND METHODS

Cell Culture and Reagents. All studies utilized bloodstream *Trypanosoma brucei brucei* (MiTat 1.2 strain 427) maintained continuously in exponential growth (10^4-10^6 cells/mL) at 37°C, 5% CO_2, in phenol red-free HMI-9, 10% fetal bovine serum (Invitrogen) and 10% Serum Plus (SAFC Biosciences). Motile parasites were counted by hemocytometer. L1210 murine leukemia cells (ATCC CCL-219) were maintained in phenol red-free RPMI 1640 (Sigma-Aldrich), 15% fetal bovine serum. Compound stock solutions were aliquoted and stored at -20°C: radicicol (Sigma-Aldrich), CUDC-305 (ChemieTech), and ansamycins [including geldanamycin, 17-AAG, and 17-DMAG] (The NCI/DTP Open Chemical Repository, http://dtp.cancer.gov) were all in sterile DMSO (Hybri-Max, Sigma-Aldrich). Final DMSO ≤0.5% had no effect in cytotoxicity assay.

Cytotoxicity Assays and Combination Studies. Cytotoxicity was assayed by colorimetric 96-well plate acid-phosphatase method (39). Cells were exposed to various concentrations of compound in quadruplicate for 24 h (*T. brucei* seeded $1x10^5$ cells/mL) or 48 h (L1210 seeded $7x10^4$ cells/mL), reflecting respective doubling-times of 6 and 11 h. Cells were then lysed with addition of lysis buffer (1M sodium acetate, pH 5.5, 1% Triton X-100) and 20 mg/mL phosphatase substrate (Sigma). After incubation for 3-6 h, absorbance was read at 304 nm. Dose-response curves and EC_{50}s were obtained (Microsoft Excel, DeltaGraph Pro v3.5, and GraphPad Prism v6). Drug combinations were studied by cytotoxicity assays with one drug at fixed concentrations while the other was varied, and vice versa. EC_{50}s were then obtained for plotting isobolograms, and for calculating combination index values (CalcuSyn V1, Biosoft).

Animal Studies. Protocols were approved by the Johns Hopkins IACUC. Drug solutions were prepared immediately before use in 5% glucose vehicle. Six week-old female CD1 mice were infected with *T. brucei* (MiTat 1.2 427, $5x10^4$) intraperitoneally (ip) on day 0. On day 1, after confirmation of parasitemia, animals were divided into groups (3 to 5 mice each), then treated once daily with (i) vehicle (200 μL ip, 3 d), (ii) 3.5 mg/kg berenil (Sigma-Aldrich) (200 μL ip, 3 d),

(iii) single dose of 17-DMAG ip (150 mg/kg (400 μL) or 75 mg/kg (200 μL)), (iv) multiple doses of 17-DMAG ip (30mg/kg (200 μL ip, 5 d), 20 mg/kg (200 μL ip, 5 d), 50 mg/kg (200 μL ip, 3d)), or (v) multiple doses of 50 mg/kg 17-DMAG orally (200 μL by gavage, 5 d or 4 d). Mice were weighed prior to infection and daily during first week; parasitemia was monitored in tail snip blood samples for 30 d. Mice with $>5x10^8$ trypanosomes/mL or in evident distress were euthanized.

RESULTS

In vitro Anti-trypanosomal Activity of Parent Compounds. Initial studies were to determine whether structurally diverse Hsp90 inhibitors had cytotoxic activity against African trypanosomes in vitro. Geldanamycin, radicicol, and CUDC-305 are from three different chemical scaffolds but all bind to the *N*-terminal ATP-binding pocket of Hsp90 and inhibit ATPase activity (24,40-42). Novobiocin binds the *C*-terminal domain (43). Geldanamycin and radicicol had potent nanomolar EC_{50}s against *T. brucei* (Table 1), in agreement with reported 50% growth inhibition of *T. brucei* at 40 nM geldanamycin (15). CUDC-305 and novobiocin had micromolar activity.

Table 1. Activity of Hsp90 inhibitors against trypanosomes in vitro

Compound		EC_{50} (nM)[a]
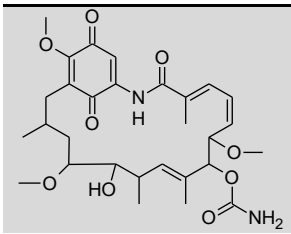	Geldanamycin	12 ± 4
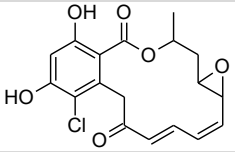	Radicicol	70 ± 14
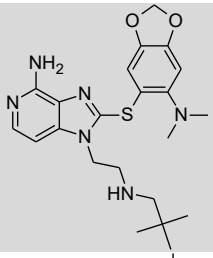	CUDC-305	1900 ± 400
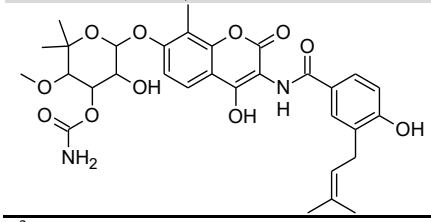	Novobiocin	180,000 ± 20,000

[a]Values are mean ± SD of at least 3 independent experiments. r^2 value for dose-response curves all exceeded 0.99

Published in part in (30).

Structure Activity Relationships on the Ansamycin Scaffold. Based on the impressive potency of geldanamycin, twelve related ansamycins were analyzed for structure-activity relationships (Tables 2 and 3). For some measure of therapeutic index, compounds were also evaluated against the mammalian cell line L1210 (mouse leukemia cells). Disruption of the geldanamycin quinone (compound 255108, Table 2) reduced activity severely against trypanosomes and moderately against L1210. Sterically demanding hydrazone moieties at R_4 (210753, 255112, 265482) substantially decreased activity against both cell types. Modifications at C17 were well tolerated. Replacement of the methoxy at R_1 with hydroxyl (255104) decreased potency some ten-fold against both cell types, but incorporation of chloroethylamino (320877) had little to no effect on potency. Importantly however, other amino moieties at R_1 enhanced selective toxicity against trypanosomes: a primary amine (255109) or allyl amino (330507) resulted in a 30- to 50-fold increase in selectivity, and dimethylaminoethylamino (707545) increased selectivity 300-fold. An even more substantial change, a large, rigid bromo-benzoxazine bridging R_1 and R_2 positions (255105), maintained good activity against both cell types, suggesting this position is not constrained in the drug and target interaction. Modifications in more remote ansamycin ring substituents and reduction of the quinone (330500, Table 3) impaired potency and selectivity, while opening the macrocycle (265481) resulted in complete loss of activity.

The general trends of these structure activity relationships correlate with crystal structure data of ansamycins complexed with mammalian Hsp90, where C17 modifications are solvent-exposed and outside the Bergerat-fold ATP-binding pocket (44). However, the series also reveals differences in susceptibility of mammalian and trypanosome cells. Many factors may account for this including phylogenetic differences in the target enzymes. This possibility is supported by the several log difference in ATPase activity of kinetoplastid HSP83 compared with mammalian Hsp90 (45). Compounds with most favorable selectivity were 17-AG (255109), 17-AAG (330507) and 17-DMAG (707545); the latter was also most potent against trypanosomes. As 17-AAG is the most widely studied, its anti-trypanosomal effect was characterized more fully.

Table 2. Structure activity relationships of ansamycins

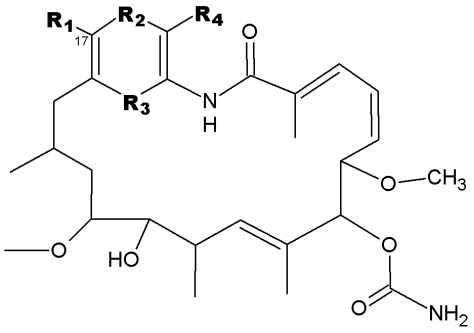

Ansamycin Scaffold

NSC Number	Modification				EC_{50} (nM)[a]		
	R1	R2	R3	R4	*T. brucei*	L1210	Selectivity[b]
122750 Geldanamycin	OCH_3	CO	CO	H	13	12	1
255108	OCH_3		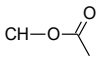	H	38000	7100	0.2[c]
210753	OCH_3	CO	CO	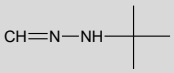	2800	940	0.3[c]
255112	OCH_3	CO	CO	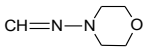	13000	9600	0.7
265482	OCH_3	CO	CO	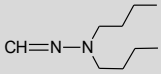	3400	5800	2
255104	OH	CO	CO	H	130	180	1
320877	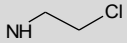	CO	CO	H	17	21	1
255109	NH_2	CO	CO	H	6.0	180	30[c]
330507 17-AAG	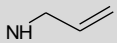	CO	CO	H	38	1800	50[c]
707545 17-DMAG	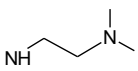	CO	CO	H	3.1	1000	300[c]
255105	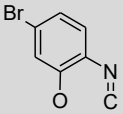		CO	H	27	23	0.9

[a]Values are mean of at least 3 independent determinations. Coefficients of variation for EC_{50} values were all ≤33%. r^2 value for dose-response curves all exceeded 0.98; within an assay the coefficients of variation for quadruplicate determinations were ≤10% and averaged 2.1%. [b]Ratio L1210 EC_{50} to *T. brucei* EC_{50}; large numbers are favorable. [c]P< 0.05 in two-tailed t-test comparison of *T. brucei* and L1210 values.

Published in (30).

Table 3. Structure activity relationships on the ansamycin scaffold

NSC Number	Structure	EC_{50} (nM)[a]		
		T. brucei	L1210	Selectivity[b]
330500 Macbecin II	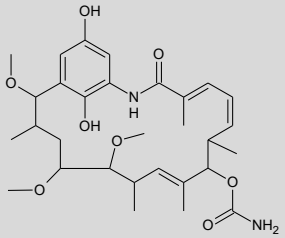	240	47	0.2[c]
265481	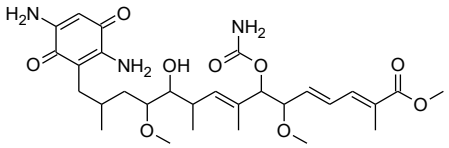	>80,000	>80,000	N/A

[a]Values are mean of at least 3 independent determinations. Coefficients of variation for EC_{50} values were all ≤35%. r^2 value for dose-response curves all exceeded 0.98; within an assay the coefficient of variation for quadruplicate determinations were ≤10% and averaged 2.6%. [b]Ratio L1210 EC_{50} to *T. brucei* EC_{50}; large numbers are favorable. [c]$P < 0.05$ in two-tailed t-test. *N/A*, Not Applicable.

Published in (30).

Additional Effects of 17-AAG. Heat shock chaperones were initially recognized as proteins whose levels increased after heat stress. Hsp90, among other chaperones, helps maintain protein quality control. We hypothesized that if 17-AAG inhibits HSP83, then 17-AAG might sensitize trypanosomes to heat shock. In control cells a 1 h heat pulse caused a 10 h arrest in trypanosome cell growth (Fig. 6). In a dose-dependent fashion, 17-AAG sensitized trypanosomes to heat shock. Cells shocked in 30 nM 17-AAG (ordinarily an EC_{30}) continuously declined in number and did not recover (Fig. 6).

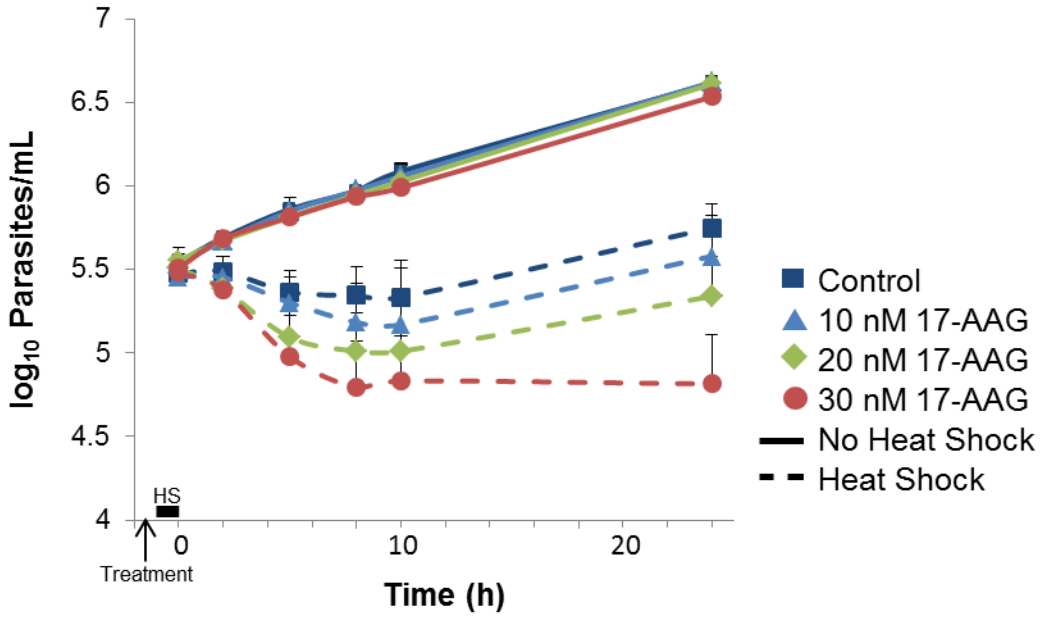

Figure 6. *T. brucei* treated with 17-AAG are more sensitive to heat shock.

Starting at -1.5 h, cells at 37 °C were treated with 17-AAG or solvent as indicated. Control cells continued at 37 °C for the remainder of the experiment. At -1 h, tubes containing cells to be heat shocked (*HS*) were transferred to a 41°C water bath, then returned to 37 °C at 0 h for the remainder of the experiment. Motile cells were counted by hemocytometer to determine parasite density. Values are mean ± SD of three determinations. Published in (30).

Somewhat surprisingly, trypanosomes differ from mammalian cells, and Hsp90 inhibitors did not synergize with etoposide, bortezomib, melarsoprol, pentamidine or novobiocin (Fig. 7). 17-AAG and etoposide, melarsoprol, or novobiocin was moderately antagonistic, whereas 17-AAG and bortezomib or pentamidine was severely antagonistic (Fig. 7).

Activity of 17-DMAG in *T. brucei*-infected Mice. The promising in vitro cytotoxicity of Hsp90 inhibitors supported evaluation in a mouse model of *T. brucei* infection. Three experiments were carried out with 17-DMAG. 17-DMAG was chosen for superior water solubility, potency and selectivity (Table 2). In this acute model, parasites rapidly proliferated in

A

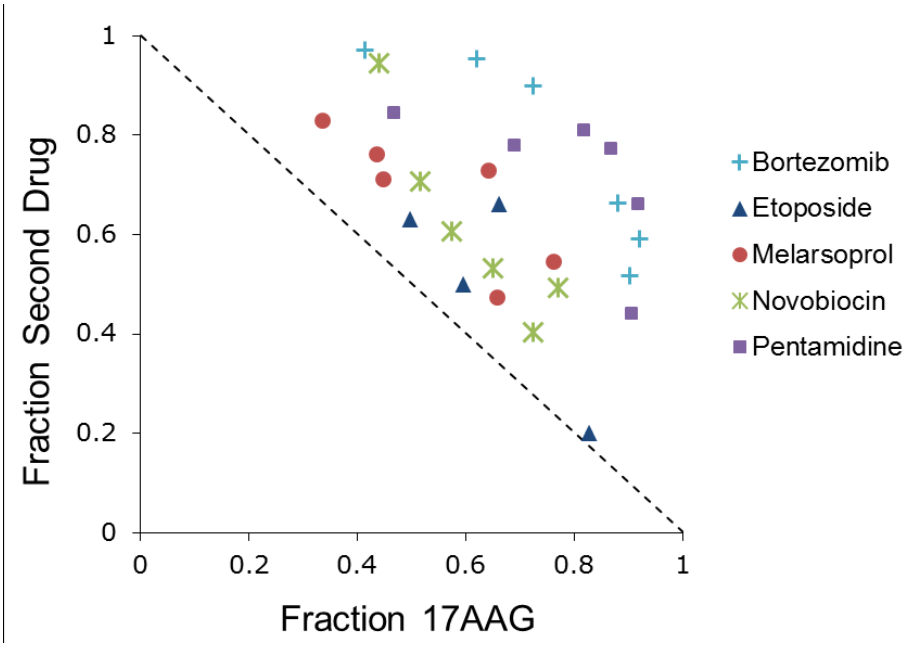

B

Drug	Combination Index Values		
	ED_{50}	ED_{75}	ED_{90}
Etoposide	1.42	1.49	1.61
Bortezomib	2.01	1.90	2.0
Melarsoprol	1.83	1.59	1.35
Pentamidine	1.94	1.66	1.57
Novobiocin	1.13	1.06	1.00

Figure 7. 17-AAG is not synergistic in combination with five other compounds

(A) EC_{50} isobolograms of 17-AAG in combination with each of five other drugs show no synergism. The concentrations of 17-AAG and partner drug required to produce a 50% growth inhibition in combination were plotted as a fraction of the concentrations of each as a single agent required to produce a 50% growth inhibition. All combinations show an antagonistic effect, falling to the right and above of the dotted additive EC_{50} line. *(B)* Combination Index (CI) values for 17-AAG combinations. Values are means of ≥ 2 experiments. 1 defines additivity, <1 is synergistic, >1 is antagonistic. CI values were calculated for a mutually nonexclusive mechanism of action; except for novobiocin which was calculated for a mutually exclusive mechanism of action (novobiocin also inhibits Hsp90). Published in part in (30).

vehicle controls and caused death within four days (Fig. 8). Veterinary anti-trypanosomal Berenil cured all mice. Three dosing strategies were used with 17-DMAG; a single high dose on day 1, multiple doses ip, or multiple doses orally. All provided initial clearance of parasitemia and prolonged survival relative to controls. A single high parenteral dose of 150 mg/kg led to dose-limiting toxicity, and day 10 recurrence of parasitemia in the surviving mouse (Fig. 8*A*). When this same total dose was divided over five days as 30 mg/kg a day, parasitemia dropped below detection by day 3 and all mice were cured, i.e., without detectable parasitemia for thirty days (Fig. 8*A*). Reducing the ip dose to 20 mg/kg for five days cured three out of five mice (Fig. 8*B*), reducing the number of doses to three days of 50 mg/kg cured two out of four mice (Fig. 8*C*), and a single ip dose of 75 mg/kg did not cure but prolonged survival an average of 7 days (Fig. 8*C*). Of considerable importance, oral 17-DMAG (50 mg/kg daily for 5 days) caused prompt reduction in parasitemia and cured three out of four mice in experiment A, and three out of five mice in experiment B (Fig. 8*A,B*). The mice which died had been clear of parasitemia for four or more days, so likely died from gavage-induced trauma and/or drug toxicity. Oral 17-DMAG dosed at 50 mg/kg for 4 days also cured four out of five mice, with one dying from toxicity (Fig. 8*B*). The remaining mice in these groups appeared healthy and remained parasite-free for 30 d. Weight change as an index of health was consistent with these outcomes. In experiment A, on day 0 the average weight was 21.6 g. Between days 0 and 7 average weight changes were: +2.2 g (Berenil), -0.75 g (17-DMAG, 150 mg/kg ipx1), +3.5 g (17-DMAG, 30 mg/kg ipx5), and +3.2 g (17-DMAG, 50 mg/kg oralx5).

Figure 8. 17-DMAG has anti-trypanosomal activity in vivo.

Mice were infected with *T. brucei* on day 0. Starting on day 1 they were treated once daily with vehicle or drug as indicated then monitored for up to 30 d for survival and parasitemia (average value for group) by visual analysis and hemocytometer counts of trypanosomes in tail snip blood samples. Negative control in blue, positive control in yellow, single ip doses in green, multiple ip doses in red, oral doses in black. Experiments A, B, and C as described in text. Published in (30).

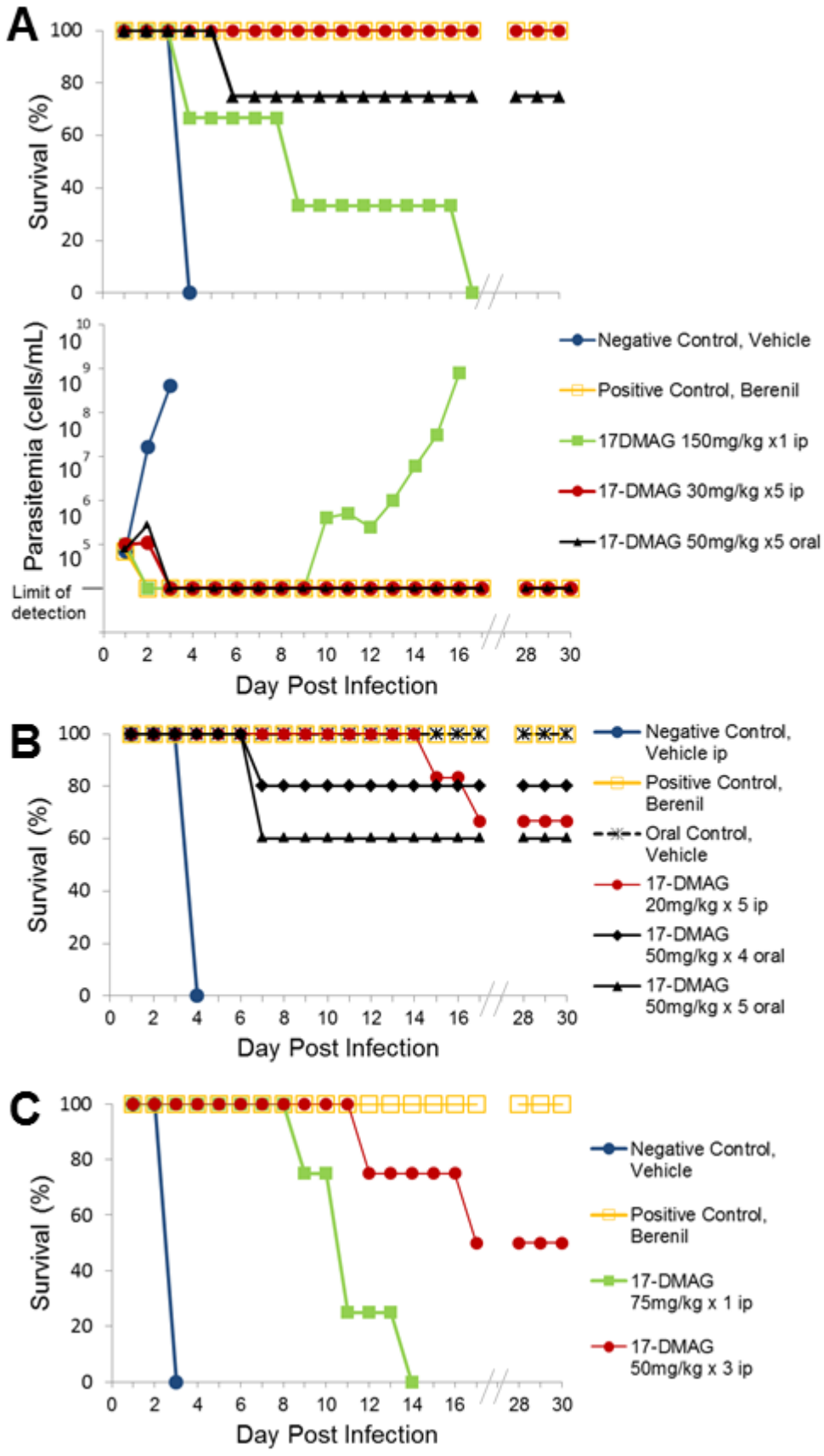
A
Survival (%)
100
80
60
40
20
0
Parasitemia (cells/mL)
10^{10}
10^{9}
10^{8}
10^{7}
10^{6}
10^{5}
Limit of detection
0 2 4 6 8 10 12 14 16 28 30
Day Post Infection
Negative Control, Vehicle
Positive Control, Berenil
17DMAG 150mg/kg x1 ip
17-DMAG 30mg/kg x5 ip
17-DMAG 50mg/kg x5 oral
B
Survival (%)
100
80
60
40
20
0
0 2 4 6 8 10 12 14 16 28 30
Day Post Infection
Negative Control, Vehicle ip
Positive Control, Berenil
Oral Control, Vehicle
17-DMAG 20mg/kg x 5 ip
17-DMAG 50mg/kg x 4 oral
17-DMAG 50mg/kg x 5 oral
C
Survival (%)
100
80
60
40
20
0
0 2 4 6 8 10 12 14 16 28 30
Day Post Infection
Negative Control, Vehicle
Positive Control, Berenil
17-DMAG 75mg/kg x 1 ip
17-DMAG 50mg/kg x 3 ip

Figure 8

DISCUSSION

African sleeping sickness, caused by the protozoan parasite *Trypanosoma brucei,* is universally fatal if untreated and current drugs are limited by severe toxicities and difficult administration. New antitrypanosomals are greatly needed. Hsp90 is a conserved and ubiquitously expressed molecular chaperone essential for stress responses and cellular signaling. Hsp90 inhibitors were investigated for their anti-trypanosomal activity. Several inhibitors with different chemical scaffolds (namely certain ansamycins and resorcinols) had potent activity in vitro against bloodstream form *T. brucei*; purine CUDC-305 and C-terminal inhibitor novobiocin had micromolar activity. In structure–activity studies of geldanamycin analogs, 17-AAG and 17-DMAG were most selective against *T. brucei* compared to mammalian cells. Despite important differences, major structural requirements on the ansamycin scaffold are similar for anti-trypanosomal and anti-tumor activities, likely due to the high degree of conservation between the HSP83 and mammalian Hsp90 ATP binding pockets (46).

17-AAG treatment sensitized trypanosomes to heat shock. These two stressors potentiate each other, likely due to a lower capacity of the trypanosome Hsp90 system to help buffer heat damage. Interestingly in antitrypanosomal cytotoxicity assays 17-AAG did not synergize with five other compounds. Etoposide and bortezomib were each tested in combination with 17-AAG due to reported synergy against cancer cells (47,48). The lack of synergy in trypanosomes may result from many factors, including alternative regulation of damage responses and death pathways, or divergence in drug targets. Bortezomib and 17-AAG were decidedly antagonistic; perhaps the downstream damage from proteasome inhibition relies on HSP83 function or vice versa. Novobiocin was used to assess the combination of an *N*-terminal and *C*-terminal Hsp90 inhibitor; however the combination was not beneficial for efficacy. Melarsoprol and pentamidine were tested as partner drugs to assess the interaction of 17-AAG with these commonly used clinical antitrypanosomals. The substantial antagonism observed between 17-AAG and pentamidine suggests these agents should not be used in combination.

Both oral and parenteral 17-DMAG cured mice of a normally lethal infection of *T. brucei*. Single doses provided substantial survival benefits over controls, with parasitemia reappearing on day 7 with 75 mg/kg ip treatment and on day 10 with 150 mg/kg ip; however, were unable to cure mice. Single dose 150 mg/kg was toxic to the mice, with two out of three mice dying on days 4 and 9 after having cleared the initial parasitemia. Multiple doses of 17-DMAG were curative, with 50 mg/kg ip for three days curing two out of four mice, and 20 mg/kg ip for five days curing three out of five mice. 30 mg/kg ip for five days achieved 100% cures. In oral experiments, 50 mg/kg was given for four or five days and led to cure of parasitemia. Unfortunately, dosing 50 mg/kg a day by gavage for four or five days led to death of one out of five, and three out of nine mice respectively, a week after parasitemia had cleared and several days after dosing had finished. As 17-DMAG is only 50% bioavailable in mice (49), it seems unlikely that this toxicity was caused by systemic 17-DMAG, as 30 mg/kg ip for five days was well tolerated. Dosing by oral gavage is traumatic for the mice and 17-DMAG is known to cause gastrointestinal toxicity (50), so the gavage dosing may have potentiated the 17-DMAG gastrointestinal toxicity in some way leading to death in susceptible animals. The rest of the mice appeared healthy. 17-DMAG can cure aggressive mouse trypanosomiasis, both ip and orally, crucial proof of therapeutic index for 17-DMAG against trypanosomes.

Hsp90 inhibitors can be potent and selective anti-trypanosomal agents, as clearly demonstrated by in vitro cytotoxicity assay activity and more importantly by cure of acute mouse trypanosomiasis. Given the 61% protein sequence identity between Hsp90 and HSP83, it is interesting to speculate on the basis for this therapeutic index. Precedent for selective toxicity to Hsp90 inhibitors exists in the up to 200-fold greater susceptibility of tumor cells compared to non-transformed cells (36,51). Cancer cells are thought to be unusually dependent on Hsp90 to chaperone up-regulated oncogene clients and mutant proteins and to counter the toxic metabolic environment commonly present in tumors (33-36). The unique cellular pathways in

trypanosomes suggest downstream processes, not present in host cells, which may be unusually dependent on HSP83. These include the heat shock-sensitive requisite *trans*-splicing of a 5'-leader sequence onto all mRNAs (16) (disruption of which would globally cripple protein synthesis), or the production of essential variable surface glycoprotein for the cell surface coat (which requires chaperone activity) (52,53). Trypanosomes also have less stringent checkpoints lowering the threshold for cell cycle disruption (19).

The promising in vitro and in vivo activity of Hsp90 inhibitors against trypanosomes supports further investigation of their potential for clinical development for human African trypanosomiasis.

CHAPTER II. Chemical or genetic interference with trypanosome Hsp90s causes cell cycle dysregulation

Published in part in:

Meyer, K. J., and Shapiro, T. A. (2013) Potent antitrypanosomal activities of heat shock protein 90 inhibitors in vitro and in vivo. *J Infect Dis* **208**, 489-499 (30)

INTRODUCTION

The protozoan kinetoplastid parasite *Trypanosoma brucei* causes human African trypanosomiasis (sleeping sickness) (1). Kinetoplastids, including human pathogens *T. cruzi* and *Leishmania sp.*, are early diverging eukaryotes named for the kinetoplast, the characteristic dense granule of DNA at the base of the flagellum that comprises the mitochondrial genome. The kinetoplast is visible by light microscopy and is a unique structure composed of a network of thousands of interlocking plasmids of DNA (Fig. 9*A*). Several dozen 20-30 kb 'maxicircles' contain protein coding genes, but the majority of kinetoplast DNA (kDNA) is 1 kb 'minicircles' which encode guide RNAs to help edit maxicircle transcripts (54). The complex kinetoplast network has to be replicated faithfully once per cell cycle and is thus a carefully timed and regulated process (Fig. 9*B*), which differs dramatically from the mitochondrial DNA replication of mammalian host cells. Replication and separation of the kinetoplast precedes that of the trypanosome nucleus (Fig. 9*B*), and is linked to the separation of the basal bodies that nucleate the flagella. Once the kinetoplast, nucleus, and each substructure in the trypanosome has been replicated and precisely positioned, cytokinesis occurs via cleavage furrow ingression (55). The complex temporal requirements of these processes, coupled with a lack of tight checkpoints characteristic in higher eukaryotes, make trypanosomes particularly vulnerable to cell cycle disaster (19,56,57).

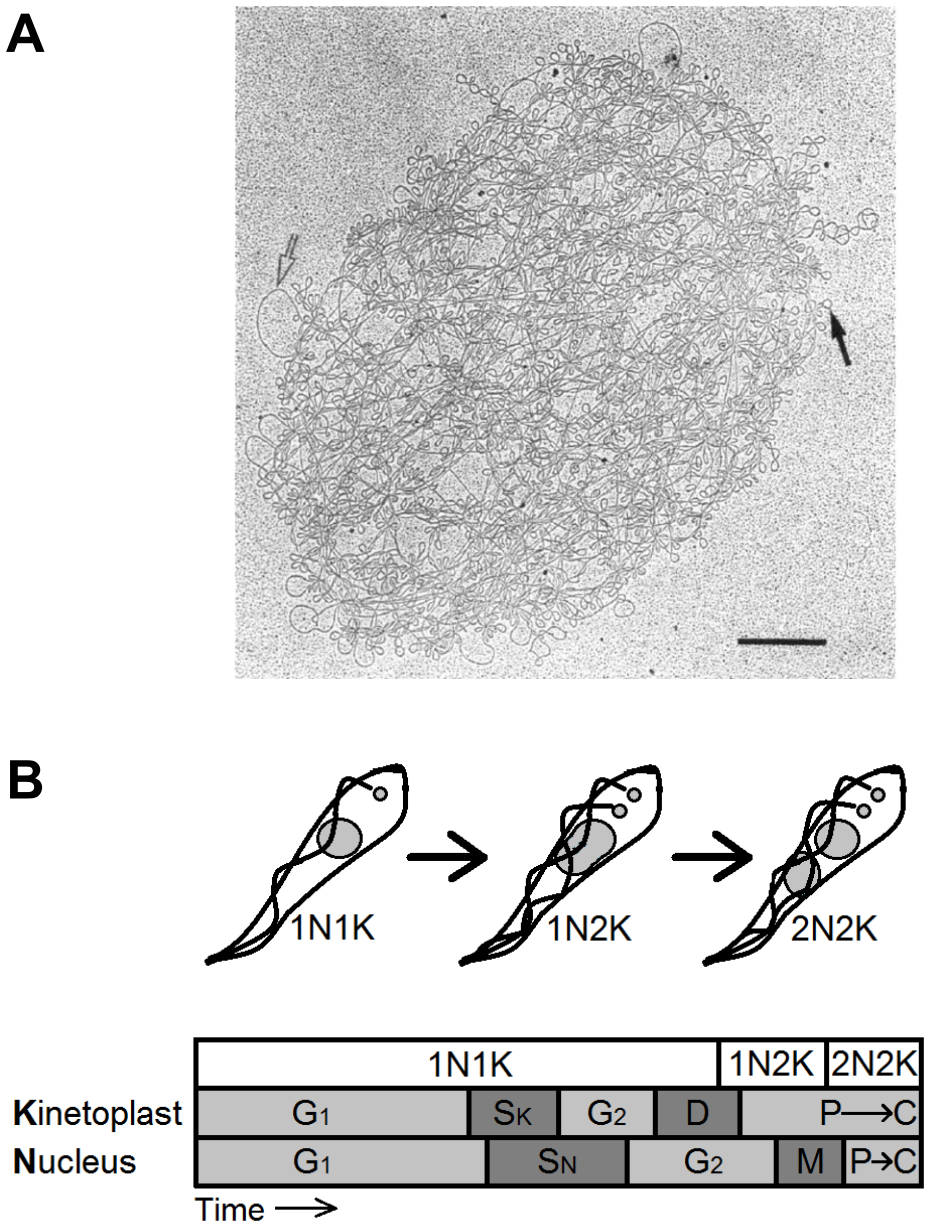

Figure 9. Kinetoplast replication in *T. brucei*

(A) Electron micrograph of an isolated kDNA network from *T. equiperdum*. Black arrow highlights a minicircle, clear arrow highlights a maxicircle. Bar is 1 μM. Reprinted from (58) with permission from Elsevier (License number 3833661438027). *(B)* In trypanosomes both the nuclear and the mitochondrial genomes can be visualized by light microscopy, and their replication is temporally linked but not strictly synchronous. Cells progress from having one nucleus and kinetoplast (1N1K), to one nucleus and two kinetoplasts (1N2K), and finally to two nuclei and kinetoplasts (2N2K) before the cells divide by cleavage furrow ingression to yield two daughter cells (adapted from (56)). G_1, Gap 1; $S_{K/N}$, Synthesis kinetoplast/nuclear DNA; G_2, Gap 2; *D*, Kinetoplast division; *M*, Nuclear mitosis; *P*, Pause; *C*, Cytokinesis.

In mammalian cells several important cyclins, cyclin dependent kinases, and other cell cycle regulators, such as Polo-like and Aurora kinase, are clients of the molecular chaperone, Hsp90. Hsp90 inhibition leads to various cell cycle malfunctions in different cell types. The kinetoplastid homologue of Hsp90 is HSP83, with *T. brucei* carrying ten tandem copies of *HSP83* in its genome (14). Initial studies have suggested that the Hsp90 inhibitor geldanamycin does cause cell cycle arrest in kinetoplastids *L. donovani* and *T. cruzi*, however, this has not been characterized in detail (59-61). Little is known about the role of HSP83 in *T. brucei* cellular metabolism and its clients and co-chaperones remain to be identified. As in mammalian cells, HSP83 does interact with deacetylase Sir2 in *Leishmania* and with protein phosphatase 5 in *T. brucei* (15,62). There are several forms of Hsp90 in mammalian cells. Hsp90α and Hsp90β differ in transcriptional regulation and are found throughout the cell, and there are two organelle Hsp90s, TRAP-1 in the mitochondria and GRP94 in the endoplasmic reticulum. TRAP-1 and GRP94 have only 34% and 49% identity to Hsp90α/β and may have different evolutionary origins (11). They both contain a conserved Bergerat fold in the *N*-terminus for ATP binding and hydrolysis, but their *C*-termini differ substantially, likely reflecting different interactions with other proteins and specific functions (63). TRAP-1 in mammalian cells has been implicated in apoptosis pathways, protection from oxidative stress, mitochondrial dynamics, and mitochondrial metabolism (64).

Cell cycle defects due to the Hsp90 inhibitor 17-AAG and arising from selective genetic interference through RNAi of *HSP83* or *TbTRAP* were characterized.

MATERIALS AND METHODS

Cell Culture and Reagents. All studies used bloodstream form *T. b. brucei* maintained in HMI9 (phenol red-free, 10% FBS, 10% Serum Plus) at 5% CO_2, 37°C. For work with 17-AAG, MiTat 1.2 strain 4.7 was used. RNAi was carried out in the Single-Marker Bloodstream (SMB) line (obtained from ATCC) in HMI9 (made with tetracycline (Tet) tested FBS) containing G418 (2.5 μg/mL) to maintain dual expression of the Tet repressor and T7 RNA polymerase (65). 17-AAG was obtained from the Open Chemical Repository of the Developmental Therapeutics Program (National Cancer Institute) and stored aliquoted in DMSO at -20°C.

Flow Cytometry. For each time-point, $3x10^6$ cells from treated cultures (seeded at $2x10^5$ cells/mL) were pelleted (1000xg, 10 min), washed twice (glucose and sucrose supplemented PBS: vPBS (66)), fixed by dropwise addition of ice-cold 70% EtOH (PBS), and stored (4°C). Cells were pelleted (3000xg, 10 min), washed (PBS), resuspended in 500 μL 10 μg/mL RNaseA (PBS), and incubated (37°C, 45 min). After addition of propidium iodide (Sigma-Aldrich) (final, 20 μg/mL), 10,000 cells were analyzed on a FACSCalibur (BD Biosciences), gated on FL2-A vs FL2-W to exclude doublets, and the G_1 peak of controls centered at 200 units FL2-A (CellQuest Pro v5.2, BD Biosciences).

DAPI Staining and Fluorescence Microscopy. For whole cell DAPI staining of 50 nM 17-AAG treated cells, at each time-point $2x10^6$ cells from treated cultures (seeded at $2x10^5$ cells/mL) were pelleted (1000xg, 10 min), washed (vPBS), fixed with 3% paraformaldehyde (PBS) (10 min on ice), diluted 5-fold (vPBS), pelleted (3000xg, 10 min), washed (vPBS), applied to polylysine-coated slides (1 h), permeabilised with 0.1% Triton X-100 (Sigma-Aldrich) (PBS) (10 min), washed thrice (PBS), and mounted using Fluoroshield with DAPI (Sigma-Aldrich) (66). For 100 nM 17-AAG treated cells and RNAi experiments, a simpler method was used. $1x10^6$ cells were centrifuged at 1000xg for 10 min and supernatant aspirated to 50 μL. Pellet was resuspended and

25 μL spread on a glass slide and left to dry. Slide was immersed in ice cold methanol for at least 1 h, then air dried. DAPI-containing mounting medium (Fluoroshield) was used to mount a coverslip. Cells were imaged on a Zeiss Axioskop with Retiga Exi charge-coupled-device camera (QImaging Corp) using iVision v4.0.13 (Biovision Technologies).

TdT Labelling. $5x10^6$ -$1x10^7$ trypanosomes (seeded at $2x10^5$ cells/mL) were spun (1000xg for 10 min) and washed in 1 mL vPBS. Supernatant was removed to 100 μL, pellet resuspended, and 100 μL lysis buffer (10 mM Tris.HCl, 75 mM EDTA, pH 8.0, 1% SDS) containing 2 mg/mL proteinase K added and incubated (55°C for 2 h). After storage at 4°C, RNaseA (final concentration 0.1 mg/mL) was added and incubated at 37°C for 30min-1h. 300 μL of 20% sucrose in TE was layered underneath the lysate, and spun (13000 rpm for 30 min). Supernatant was aspirated to 100 μL and washed with 700 μL of TE. Supernatant was removed to 50 μL, and networks resuspended. Networks (20 μL) were then settled on to 8-well Teflon coated slides (pre-treated with 0.01% polylysine) for 1 h. Networks were equilibrated with terminal deoxynucleotidyl transferase (TdT) reaction buffer (plus 2.25 mM $CoCl_2$) for 20 min (Roche), then incubated with reaction buffer including 2.25 mM $CoCl_2$, 10 μM dATP, 5 mM Fluorescein-12-dUTP (Thermo Scientific), and 10 U TdT (Roche) for 1 h. Reaction was quenched (2xSSC, three times for 5 min each), networks were washed twice with PBS, stained with 5 μg/mL DAPI (in H_2O) for 15 min, washed thrice with PBS, and then sealed using Vectashield mounting medium (Vector). Networks were imaged on a Zeiss Axioskop with Retiga Exi charge-coupled-device camera (QImaging Corp) using iVision v4.0.13 (Biovision Technologies).

Southern Blots. To isolate DNA for Southern analysis, $2x10^6$ cells (seeded at $2x10^5$ cells/mL) were pelleted (1000xg, 10 min) and washed with vPBS. Pellet was resuspended in lysis buffer (10 mM Tris.HCl, 75 mM EDTA, pH 8.0, 1% SDS) containing 2 mg/mL proteinase K (Invitrogen) and incubated at 55°C for 2 h. After storage at 4°C, RNase A was added (final concentration 0.1

mg/mL) and incubated at 37°C for 1 h. Samples were mixed with DNA loading dye, loaded on 20 cm agarose gels (1.5% or 0.6%) and run at 70 V for 17 h in TBE (90 mM Tris/Borate, 2.5 mM EDTA), 1 μg/mL EtBr. Gels were processed in 0.25 N HCl (15 min); rinsed in H_2O (10 min); neutralized in 0.6 M NaCl, 0.2 M NaOH (45 min); and finally incubated with 25 mM sodium phosphate (pH 6.5, 30 min x2) and transferred overnight in 10xSSC onto nylon Amersham Hybond™-N^+ membrane (GE Healthcare). Membranes were cross-linked twice with 1200 μJ UV. To probe the membranes, *T. equiperdum* full length minicircle DNA (1 kb excised from pJN6 with SmaI and XbaI) (67), or a 770 bp maxicircle sequence (amplified from whole cell DNA using 5'-CTAACATACCCACATAAGACAG-3' and 5'-ACACGACTCAATCAAAGCC-3') was radiolabeled with [^{32}P]-ATP using random primers (Invitrogen) and Klenow polymerase (37°C, 1 h), purified through Sephadex-G50, and hybridized with membranes in Church-Gilbert solution (0.5 M $NaHPO_4$, pH 7.2, 1 mM EDTA, 7% SDS, 1% BSA (68)) overnight at 45°C. Membranes were washed thrice (1xSSC, 0.1% SDS) at 45°C and exposed to PhosphorImager (Fuji) plates that were then scanned (Fuji Bas 2500 PhosphorImager, ImageGauge v3.45 Fuji).

RNAi of Trypanosome Hsp90s. The sequences of human TRAP1 mRNA variants (NM_016292.2 and NM_001272049.1) were compared to the *T. brucei* Lister Strain 427 genome sequence on TriTrypDb using the blastn program with an expectation value of 10, resulting in the identification of (Tb427tmp.02.0250/Tb11.02.0250), a putative heat shock protein, with an E value of 6e-12 (69). RNAiT software (TrypanoFan)(70) was used to choose a 487 bp sequence for *HSP83* (Tb10.26.1080/Tb927.10.10980) and a 592 bp sequence for putative *TbTRAP* (Tb427tmp.02.0250) that had no greater overlap than 20/21 bp with any other sequence in the trypanosome genome (Appendix I). These RNAi sequences were amplified from *T. brucei* whole cell DNA (*HSP83* and *TbTRAP* genes lack introns) incorporating 5' XbaI/XhoI and 3' NdeI/AscI sites, then sequentially inserted in to the plew100v5X:pex11 vector (71) as inverted repeats using XhoI/AscI digestion and then XbaI/NdeI digestion. Primers used were: *HSP83* forward XbaI 5'-CCC CTC TAG ATA TTG TGA AGA AGG CCC TGG-3', XhoI 5'-CTC

TCT CGA GTA TTG TGA AGA AGG CCC TGG-3'; *HSP83* reverse NdeI 5'-CCC CCA TAT GCT CTT TCA TTG CCT TGC ACA-3', AscI 5'-CTT TGG CGC GCC CTC TTT CAT TGC CTT GCA CA-3'; *TbTRAP* forward XbaI 5'-CCC CTC TAG AGA GCT CTC CTT TTG CAC ACC-3' , XhoI 5'-CTT CCT CGA GAG CTC TCC TTT TGC ACA CC-3'; *TbTRAP* reverse NdeI 5'-CCC CCA TAT GTG TGA ACC TGG TCG GTA CAA-3', AscI 5'-GTA TGG CGC GCC TGT GAA CCT GGT CGG TAC AA-3'. Correct insertion was confirmed by sequencing across insertions sites in both directions. The vectors were amplified in *E. coli* DH5α, purified, linearized with NotI, and transfected in to SMB *T. brucei* constitutively expressing the Tet repressor and T7 RNA polymerase (65). Transfection was performed using Human T-cell Nucleofector™ (Lonza) and an AMAXA electroporator on program X-001. $1x10^7$ cells were transfected with 10 μg DNA and immediately diluted into 30 mL of HMI9. A further 1:10 dilution was made. Both dilutions were then plated into 24 well plates. After 6 h, 2.5 μg/mL phleomycin was added to each well to select for transfectants. Three independent rounds of transfection were performed generating 11 clones for *HSP83* RNAi and 12 clones for *TbTRAP* RNAi. Tet (100 ng/mL) was added to induce RNAi.

Tagging *TbTRAP* with cmyc. Endogenous *TbTRAP* was tagged with a terminal 3xcmyc-tag using homologous recombination. The terminal 400 bp sequence of *TbTRAP* minus the STOP codon was ligated in frame into a modified pMOTag33M vector (72) (modified to contain a blasticidin resistance gene) using Kpn1 and XhoI. The first 400 bp of the 3'UTR sequence from *TbTRAP* was ligated into the vector using BamHI and SacI. The sequences were amplified from genomic DNA using the high fidelity PfU Turbo DNA Polymerase (Agilent), isolated on a 1% agarose gel (TBE) and purified using a Qiagen Gel extraction kit. The vector was amplified in DH5α *E.coli*. Kpn1 and SacI were used to digest out the fragment containing the *TbTRAP* terminal sequence, cmyc tag, blasticidin resistance gene, and *TbTRAP* 3'UTR, and this fragment was electroporated into $2x10^7$ cells of a *TbTRAP* RNAi clone (in SMB cells) using LONZA

Nucleofector™ as described above. Transfectants were selected using blasticidin pressure (5 μg/mL) and 6 out of 43 were chosen for clonal dilution and analysis.

Northern Blots. $1x10^7$ cells (seeded at $2x10^5$ cells/mL) were centrifuged (1000xg, 10 min) and supernatant removed to 10 μL. RNA was purified using a Qiagen RNeasy Mini kit (350 μL Buffer RLT, vortex, 350 μL 70% EtOH, RNeasy column, wash RWI and RPE x2, eluted with 30 μL water). RNA concentration was measured using a NanoDrop™ (Thermo Scientific) and 700 ng mixed with formaldehyde loading dye (Invitrogen), heated at 65°C for 15 min, cooled on ice, mixed with EtBr (final 12.5 μg/mL) and loaded on to a formaldehyde (6.6%) agarose (1%) gel cast and run in MOPS (20 mM MOPS, 8 mM NaOAc, 1 mM EDTA, pH 7.0). The gel was run at 5V/cm for 3 h. Gel was then processed in 1M NH_4OAc for 45 min, and the RNA transferred with 1M NH_4OAc overnight onto nylon Amersham Hybond™-N^+ membrane, then crosslinked with 2x 1200 μJ UV. Membranes were wet in 2xSSC, pre-hybridized in Church-Gilbert solution for ≥1 h, and probed with random primer radiolabeled [^{32}P]-dATP template (labeled as described for Southern blots) overnight at 56°C. Templates were gene sequences outside of the RNAi region that had no more than 40 bp overlap with other *T. brucei* genes. *HSP83* template 413 bp, primers 5'CCAGAGTCTGACGAACCAGTC3', 5' CCAGGTATTCCTGCTGGTCT3'; *TbTRAP* template 525 bp, primers 5'CTAAAGGGCAATGCAGGGGA3', 5'CCGGCTGTACACCTTGACAT3'. Membranes were washed thrice (1xSSC, 0.1% SDS) at 56°C and exposed to PhosphorImager (Fuji) plates that were then scanned (Fuji Bas 2500 PhosphorImager, ImageGauge v3.45 Fuji).

Western Blots. $5x10^6$ cells (seeded at $2x10^5$ cells/mL) were centrifuged (1000xg, 10 min), washed twice in vPBS, and supernatant aspirated to 20 μL. SDS loading dye was added (6 μL, 6 X) and sample boiled for 5-10 min in a boiling water bath then stored at 4°C. Samples were warmed to room temperature, loaded on an acrylamide gel (5% stacking, 8% running) and run at

200 V for 45 min in SDS-PAGE buffer. Proteins were transferred to Amersham Hybond™-ECL (GE Healthcare) membrane at 100 V for 1 h at room temperature. Blots were blocked in 5% milk, washed twice with TTBS (20 mM Tris.HCl, 1.5 M NaCl, pH 7.6, 0.1% Tween-20), incubated with primary antibody overnight at 4°C (1:5000 Hsp90 (sc-7947, H-114, lot e2611, Santa Cruz Biotechnology), 1:500 cmyc (C3956, Sigma), in 5% BSA in TTBS), washed three time with TTBS, incubated with secondary antibody at room temperature for 1 h (1:30000 goat-antirabbit-HRP in 5% BSA in TTBS, sc-2054, Santa Cruz Biotechnology), and washed thrice with TTBS. Blots were developed with "ECL Plus" western blotting detection system (RPN2132, Amersham Biosciences) and imaged on an Image Station 4000R Pro (Kodak) with Carestream software.

17-AAG Affects Growth Rate, Mitosis and Cytokinesis. Previous reports indicate that for insect form *T. cruzi* or *L. donovani*, 24 h geldanamycin treatment arrests the cell cycle at either G_1 or G_2 (59-61). Within 5 h, 50 or 100 nM 17-AAG (EC_{80} or EC_{99}, respectively) arrested growth of bloodstream *T. brucei* and cell numbers declined thereafter (Fig. 10). Cell cycle progression was inhibited, and this was examined by flow cytometry and microscopy of DAPI-stained cells, across time and concentration.

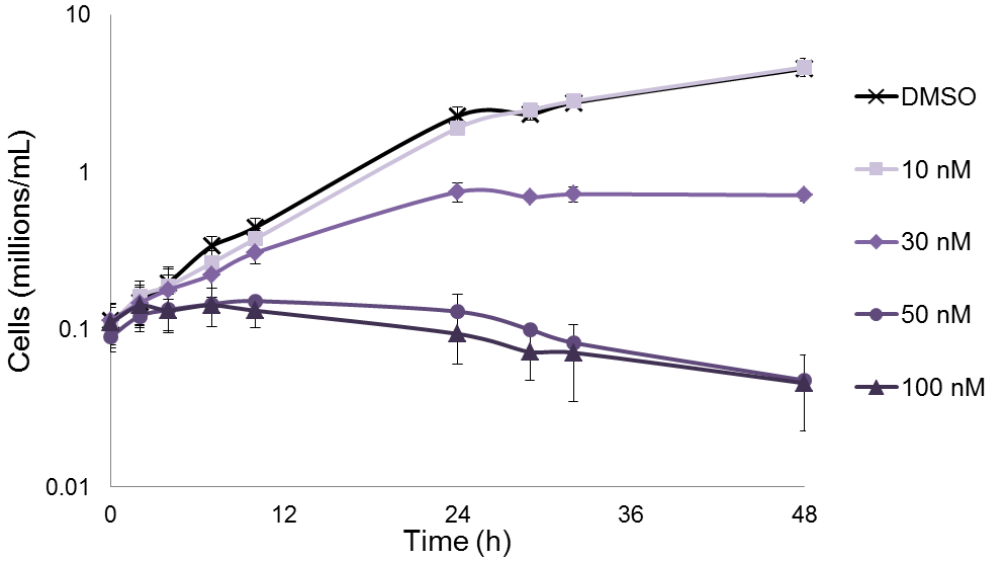

Figure 10. 17-AAG arrests trypanosome growth and kills trypanosomes

Trypanosomes were treated with indicated concentrations of 17-AAG or vehicle control (DMSO) and cell concentration counted over 48 h. n ≥ 2. Error bars SD for n ≥ 3.

Figure 11. The cell cycle of *T. brucei* is disrupted by 17-AAG

Trypanosomes were treated with solvent, 50 nM 17-AAG, or 100 nM 17-AAG for the indicated times then examined by flow cytometry for propidium iodide staining. This method focuses on the nuclear genome as kDNA comprises only 5% of total cell DNA (73). *(A)* Histograms of 10000 cells. *(B)(C)(D)* Quantification (n ≥ 5, means±SD) for DMSO, 50 nM 17-AAG and 100 nM 17-AAG respectively. G_1, Gap 1; *S*, Synthesis; G_2/M, Gap 2/Mitosis; *2C*, non-replicating diploid cells with two copies of nuclear genomic DNA; *4C*, cells late in replication with four copies of genomic DNA; *6C* or *8C*, abnormal cells with six or eight copies of the nuclear genome. Published in (30).

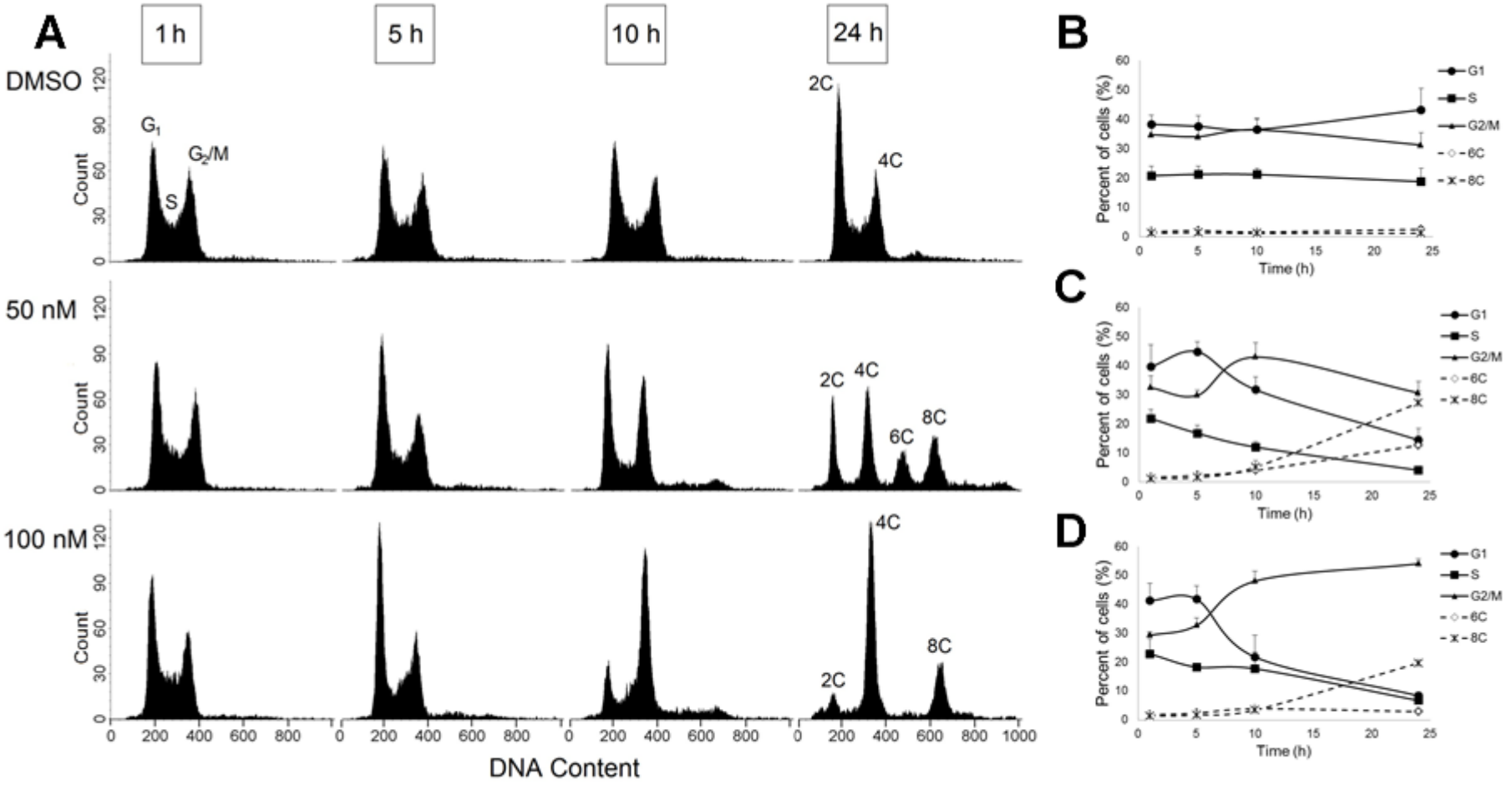
A
1 h
5 h
10 h
24 h
DMSO
50 nM
100 nM
Count
G1
S
G2/M
2C
4C
6C
8C
DNA Content
B
C
D
Percent of cells (%)
Time (h)
G1
S
G2/M
6C
8C

Figure 11

Based on nuclear DNA content as measured by flow cytometry, control cultures in mid-log growth were 38% G_1 (2C DNA content for the diploid trypanosome), 21% S, and 35% G_2/M (4C DNA content). This distribution was maintained until the culture reached stationary phase at 24 h (Fig. 11). 50 nM 17-AAG caused a transient increase in the G_1 peak at 5 h, which decreased progressively thereafter. At 10 h the G_2/M (or 4C) peak was increased, indicating a problem with mitosis and/or cytokinesis. At 24 h the 4C peak remained significant, but substantial 6C and 8C peaks were also present. These abnormal forms are possible in bloodstream trypanosomes due to inadequate or missing checkpoints to stop re-replication of DNA when cytokinesis is delayed or inhibited (19). With 100 nM 17-AAG the 5 h increase in G_1 and 10 h increase in G_2/M (or 4C) were also seen, but at 24 h the dominant population was 4C, along with an 8C but no 6C peak. With both concentrations the percentage of cells in S phase declined (Fig. 11).

To obtain further insight into this cell cycle disruption, trypanosomes were examined by fluorescence microscopy. Unlike flow cytometry, which reflects nuclear DNA content, visual analysis of DAPI-stained cells assays both nuclear and kinetoplast DNA, and phase contrast provides concomitant analysis of cytokinesis. Control cells can be divided into three populations. *First*, 1N1K cells, with a single nucleus and kinetoplast, are 68% of the total; *second*, in 1N2K cells mitochondrial DNA has divided but nuclear mitosis has not occurred (21%); and *finally*, in 2N2K cells the kinetoplast and nucleus have both divided (8%) (Fig. 12*Ai-iii, B*). These proportions are in good agreement with flow cytometry: G_1 plus S (38+21%) are a subset of 1N1K (68%); and 1N2K plus 2N2K (21+8%) are a subset of G_2/M (35%) (Fig. 11*B*). Likewise consistent with flow cytometry, treatment with 50 nM 17-AAG reduced 1N cells, and increased 2N cells and forms containing greater than 2N (Fig. 12*B*). Simultaneous accounting for both nuclei and kinetoplasts revealed the vivid loss of coordinate replication of these genomes. Flawed nuclear mitosis was evidenced by cells with abnormally high numbers of kinetoplasts but only one or two giant nuclei (Fig. 12*Ci, ii*). Conversely, defective kinetoplast segregation, with unchecked nuclear

mitosis, produced cells with multiple nuclei and a single large kinetoplast, demonstrated numerically by the increase in 2N1K cells (Fig. 12*B*; *Ciii, iv*). Grouping cells by ratio of nuclei to kinetoplasts established kinetoplast segregation as more defective than nuclear mitosis: 29% had more nuclei than kinetoplasts (Fig. 12*D*). Of cells that retained a 'normal' census of nuclei and kinetoplasts, many still had evident dysregulation, including 2N2K cells whose kinetoplasts had begun to re-replicate prior to cytokinesis (Fig. 12*Cv)*. Phase contrast confirmed the cytokinesis inhibition suggested by 6C and 8C flow cytometry peaks. At 24 h cells with multiple partially ingressed cleavage furrows indicated repeated failed attempts at cell division (Fig. 12*Ci,iii*) and some cells were arrested at abscission (Fig. 12*Cvi*).

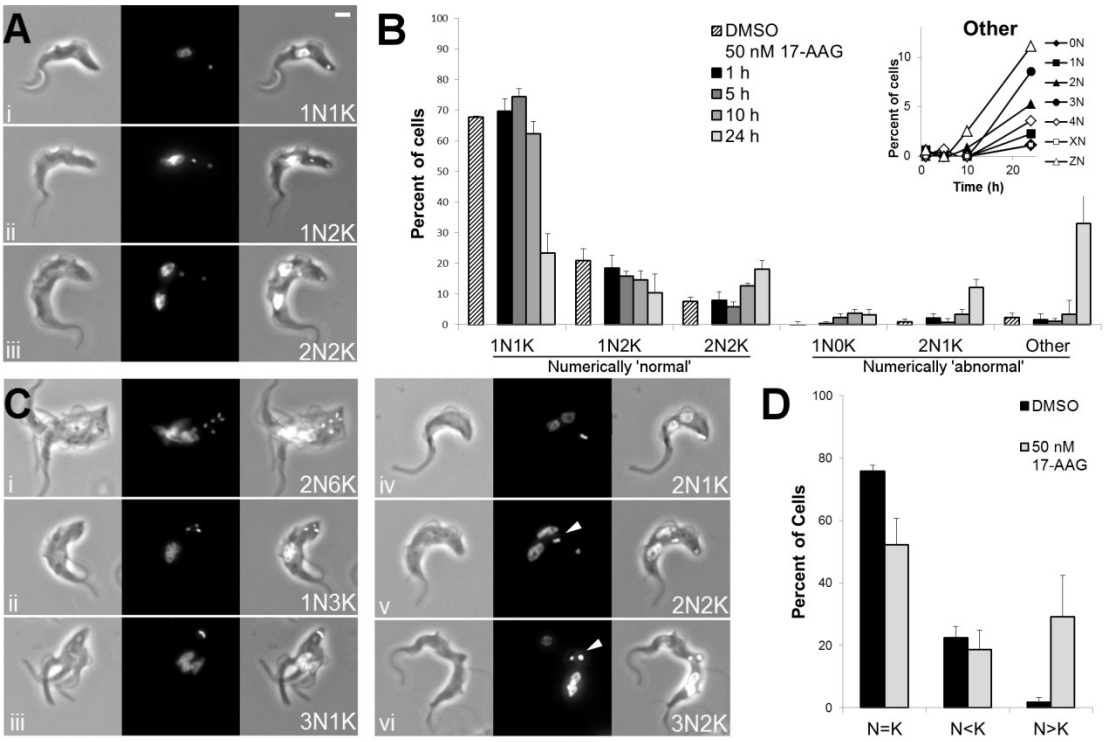

Figure 12. 50 nM 17-AAG causes multiple cell cycle abnormalities

Analyses of trypanosome nuclear and kinetoplast content by DAPI staining and fluorescence microscopy. *(A)* Examples, as indicated, of normal 1N1K, 1N2K and 2N2K cells in control cultures; *bar*, 1µm. *(B)* Trypanosomes were treated with 50 nM 17-AAG or solvent for the indicated times, then scored for nuclear and kinetoplast content based on DAPI staining. Values are the means ± SD of counts made in a blinded fashion by three observers. Insert shows nuclear content of 'Other' cells across time. *X*, ≥5, *Z*, not-identifiable *(C)* Examples of aberrant cells after 24 h 50 nM 17-AAG. *White arrowhead*, re-replicating kinetoplast *(D)* Panel B data analyzed to determine percentage of cells with number of nuclei equal to, less than, or greater than kinetoplasts. Published in (30).

Interestingly, abnormalities from 100 nM 17-AAG were substantially less varied. There was a large increase in 2N populations (including aberrant 2N1K) (Fig. 13*A*), but few trypanosomes had more than two nuclei or kinetoplasts. Once again the increased 2N population correlated with the flow cytometry result of increased 4C DNA content, although the substantial 8C peak in flow cytometry suggests that some of these 2N cells have undergone a second round of nuclear DNA synthesis without mitosis. There was also a large increase in trypanosomes displaying a partially ingressed cleavage furrow, primarily seen with 2N cells (Fig. 13*B,C*), and in keeping with the number of nuclei this was primarily one cleavage furrow and not multiple in contrast to

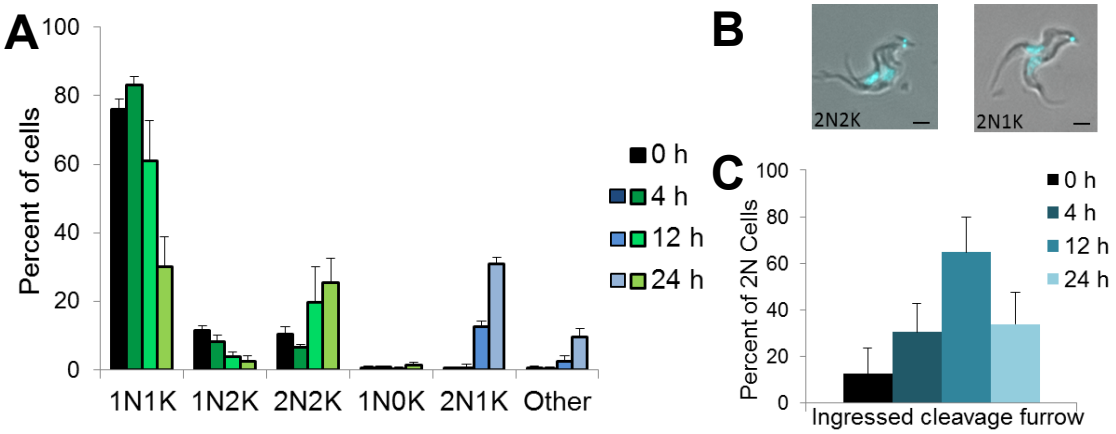

Figure 13. 100 nM 17-AAG causes cytokinesis defect

Analyses of trypanosome nuclear and kinetoplast content by DAPI staining and fluorescence microscopy. *(A)* Trypanosomes were treated with 100 nM 17-AAG for the indicated times, then scored for nuclear and kinetoplast content based on DAPI staining. *(B)* Examples of aberrant cells after 12 h treatment with 100 nM 17-AAG. *Bar*, 1μM. *(C)* Percentage of 2N cells with a visible partially ingressed cleavage furrow after treatment with 100 nM 17-AAG. *Mean±SD,* n ≥ 3. n > 100 cells were counted for each condition.

Figure 14. Kinetoplast separation is impaired with 17-AAG treatment.

(A) Trypanosomes were treated with 100 nM 17-AAG for the indicated times, then scored for nuclear and kinetoplast content based on DAPI staining, and kinetoplasts were further scored as either single (*Ks*), elongated (*Ke*), proximal (*Koo*), or clearly separated (*Ko o*). *(B), (C), (D)* Percentage of total, 1 N, or 2 N cells, respectively, with different kinetoplast morphologies. Values are the means ± SD of three experiments. n > 100 cells were counted for each condition.

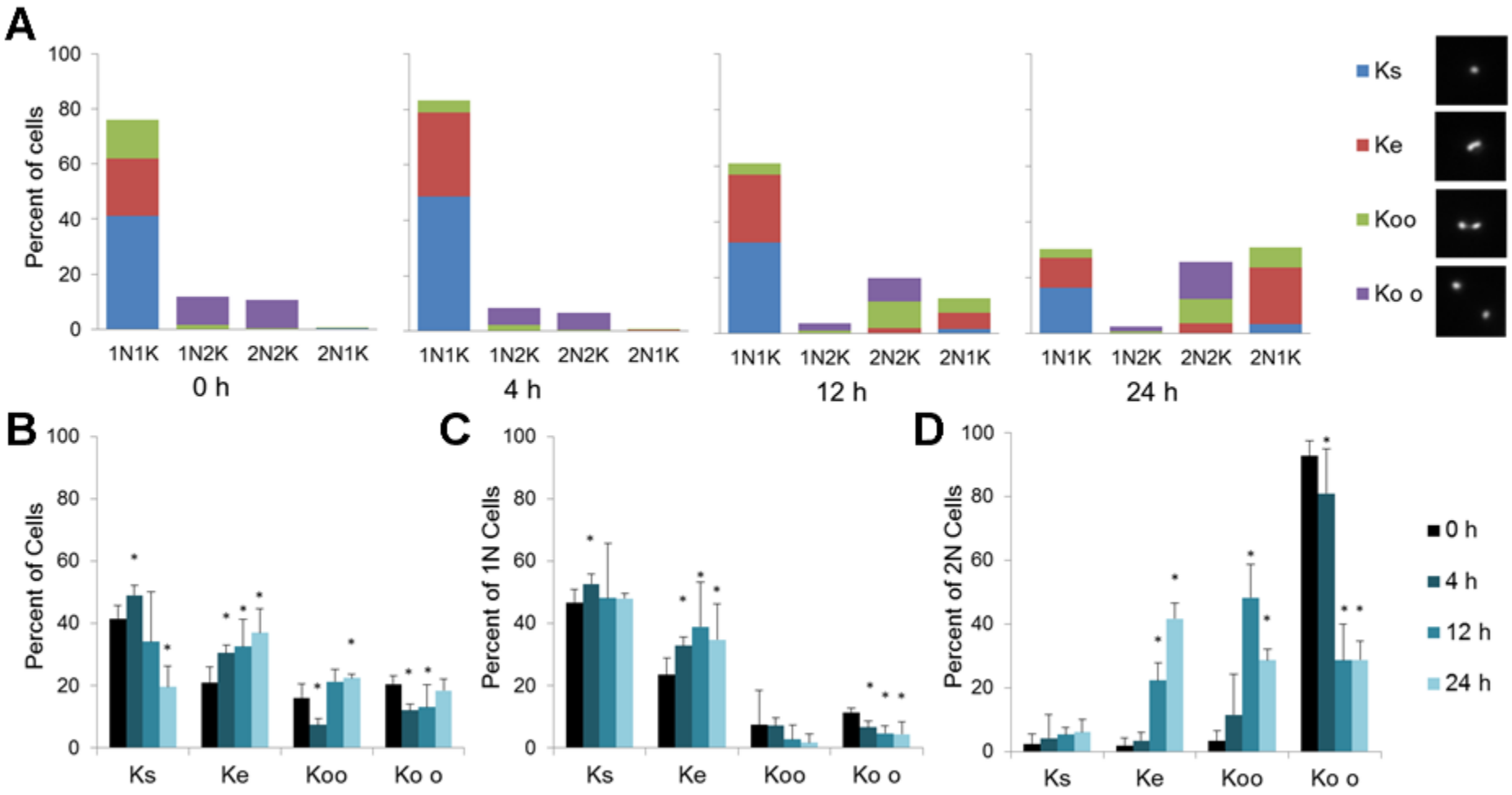
A
Percent of cells
100
80
60
40
20
0
1N1K
1N2K
2N2K
2N1K
0 h
4 h
12 h
24 h
Ks
Ke
Koo
Ko o
B
Percent of Cells
C
Percent of 1N Cells
D
Percent of 2N Cells
0 h
4 h
12 h
24 h

Figure 14

50 nM (Fig. 12*Ciii*). The strong 2N1K population prompted a closer look at kinetoplast morphology. Cells were scored according to presence of single, elongated, proximal, or fully separated kinetoplasts (Fig. 14). The percentage of cells containing a single kinetoplast or clearly separated kinetoplasts decreased, and elongated kinetoplasts increased, suggesting 17-AAG treatment slows kinetoplast separation (Fig. 14*B*). This is clearly seen when looking at just 2N cells (Fig. 14*D*), with the percentage containing fully separated kinetoplasts decreasing from 90% at 0 h to just 25% by 12 h. The separation defect worsens over time with increasing percentages of 2N cells containing proximal and elongated kinetoplasts. The presence of a cleavage furrow and an abnormal kinetoplast were not clearly correlated suggesting these processes are likely due to separate pathway malfunctions.

To test whether structurally different Hsp90 inhibitors caused cell cycle disruption, cells were treated with 350 nM radicicol (EC_{99}) (Fig. 15). The same broad patterns were seen by microscopy and flow cytometry (Fig. 15*A,B*), indicating the effects are likely attributable to HSP83 inhibition.

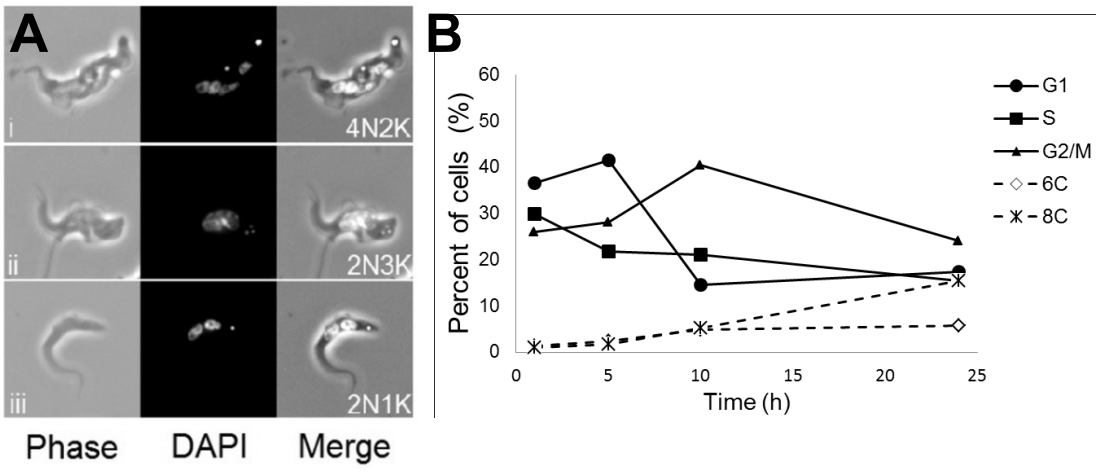

Figure 15. Radicicol causes cell cycle dysfunction

Trypanosomes were treated with 350 nM radicicol for 24 h. *(A)* Examples of aberrant cells using DAPI staining, fluorescent and light microscopy. (*B*) Quantifications of flow cytometry histograms of radicicol treated cells stained with propidium iodide to measure nuclear DNA content. G_1, Gap 1; *S*, Synthesis; G_2/M, Gap 2/Mitosis; *6C* or *8C*, abnormal cells with six or eight copies of the nuclear genome. Published in (30).

The multiple abnormalities caused by Hsp90 inhibitors suggest that HSP83 deficiency affects several cell cycle proteins. At sub-maximal inhibition the lack of effective checkpoints results in abnormal nuclear and kinetoplast content and abortive cytokinesis. With more stringent inhibition of HSP83 the regulated ability of cells to initiate and complete kDNA segregation and cytokinesis is more severely impaired which limits the variety of abnormalities. Overall, and different from previous reports with the insect forms of other kinetoplastids (59-61), these results indicate time- and concentration-dependent disruption of both G_1 and G_2/M phases.

17-AAG Slows Kinetoplast Division. Mitochondrial kDNA replication is a fascinating process unique to trypanosomatids, the regulation of which is very complex (54). As a solution to the topological problem of duplicating a catenated network, minicircles are decatenated from the network for replication (Fig. 16). The daughter minicircles are reattached at opposite poles of the network without closing all replication gaps, perhaps a book-keeping tool to ensure complete replication of all minicircles (54). This leads to a growing oval shaped network. At the final stages of replication the network appears dumbbell shaped, the gaps in the minicircles are filled, and the network divides into two new round networks (Fig. 16). The free minicircles have different topological forms depending on their progress through replication. Released as covalently closed plasmids, a theta structure is formed while the polymerase is synthesizing new strands. The daughter minicircles are either 'gapped', or 'nicked', depending on whether the new strand of DNA was the continuously synthesized leading strand or the lagging strand of Okazaki fragments (Fig. 16). Each of these forms runs at a different speed on an EtBr containing agarose gel. 17-AAG treatment (100 nM) led to a transient decrease in actively replicating theta structures and nicked daughters at 4 h, then a small increase in protein-bound linears over the next 20 h (Fig. 17*A*). 17-AAG also caused an increase in free maxicircles over 24 h (Fig. 17*B*). The abnormal protein-bound linears are evidence of topoisomerase dysfunction.

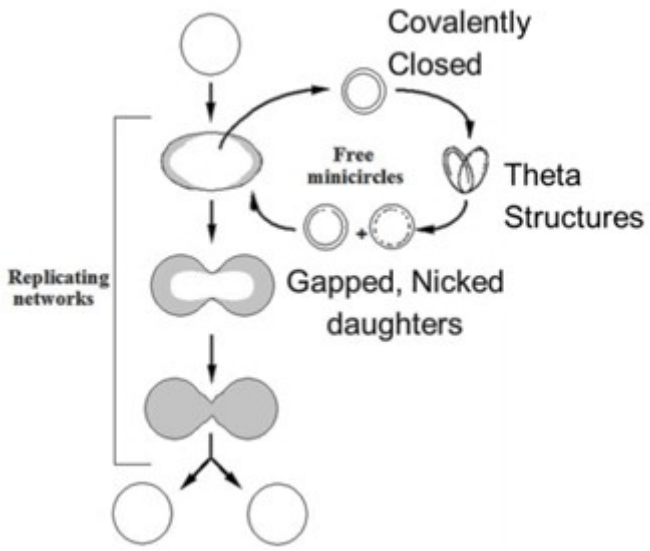

Figure 16. Kinetoplast DNA network replication schematic

A single network (circle) replicates minicircles gradually via decatenation of covalently closed plasmids then polymerase replication via a theta structure to produce a 'gapped' daughter (leading strand) or 'nicked' daughter (lagging strand). These daughters are reattached at opposite poles of the network without ligation of all gaps (grey). This process leads to a growing network that is at first oval and finally dumbbell shaped. When all minicircles have been replicated, the gaps are filled and ligated and the network divides to two new single round networks. Adapted from Theresa Shapiro.

Kinetoplast networks were isolated from 17-AAG treated cells, spread on slides, and the gaps in DNA filled in with fluorescent nucleotides to reveal the progress of kDNA replication (Fig. 18). With just 2 h of 100 nM 17-AAG treatment (2 h) there was a significant decrease in partially replicated networks (labeled poles), and an increase in fully labeled dumbbell-shaped networks. This suggests lagging initiation of replication, but also problems with closing minicircle gaps and separating daughter networks. After 4 h, labeled dumbbells declined whilst abnormal populations of first fully labeled ovals, followed by unlabeled ovals, became significant (together over 40% of networks by 24 h). This positioning and segregation defect suggests decatenation problems, perhaps due to the topoisomerase defects evidenced by the protein-bound linear minicircles (Fig. 17). These results explain the increased elongated kinetoplasts and the 2N1K population in whole-cell DAPI staining (Fig. 14).

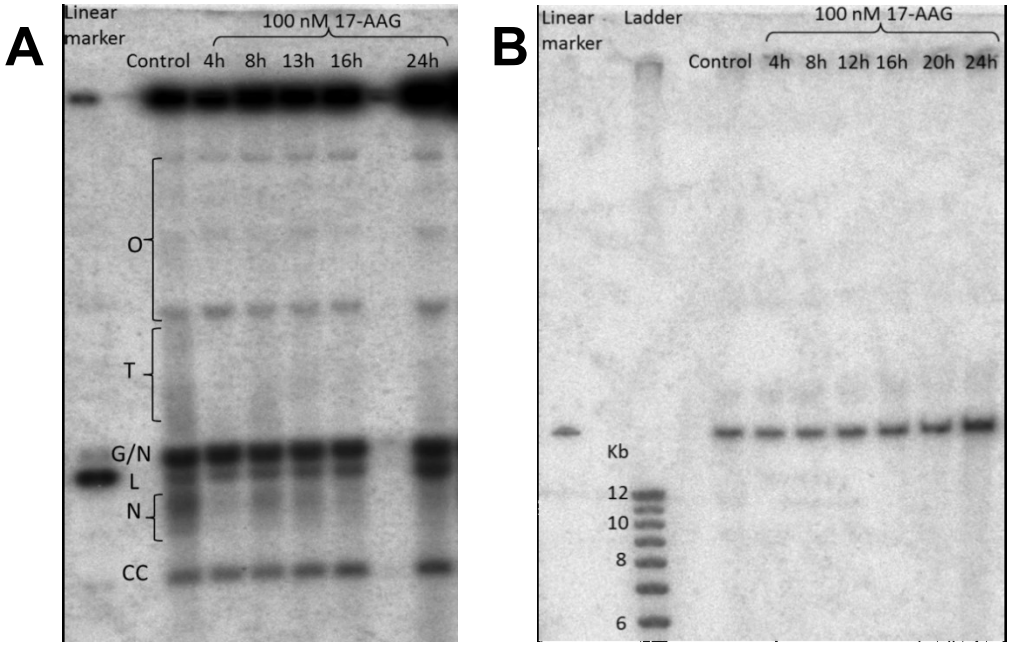

Figure 17. Free minicircles and maxicircles in cells treated with 17-AAG

DNA from cells treated with 100 nM 17-AAG was separated on agarose gels, transferred to nylon membranes, and probed with a kDNA minicircle *(A)* or maxicircle *(B)* sequence. Lanes were loaded by cell equivalents. *O* – Oligos, *T* – Theta structures, *G* – Gapped minicircles, *N* – Nicked minicircles, *L* – Linears, *CC* – Covalently closed minicircles.

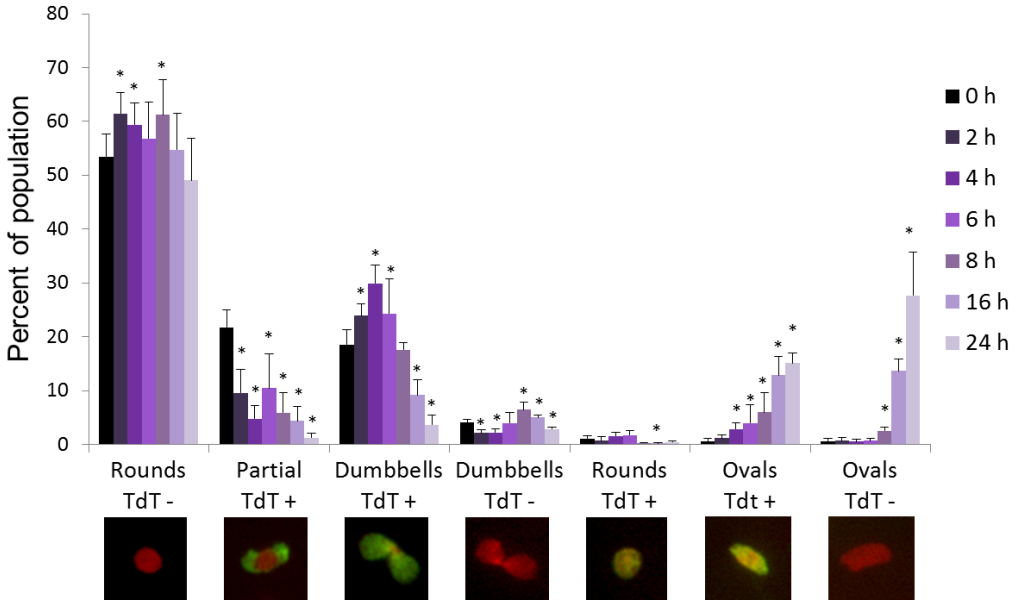

Figure 18. TdT labelling of kinetoplast networks from 17-AAG treated trypanosomes

Networks were isolated from 100 nM 17-AAG treated cells, spread on slides, stained with DAPI (*red*) and labelled with fluorescent dUTP (*green*) using TdT. *Means±SD* of $n \geq 3$, $^*p < 0.05$ compared to 0 h.

RNAi of *HSP83*. To further explore the role of trypanosome HSP83 in cell cycle regulation, RNAi constructs were generated to knock-down *HSP83*. The ten tandem copies of *HSP83* are 99.7% identical and thus a single RNAi sequence was sufficient to knock-down all gene products (Appendix I). The sequence selected for RNAi was inserted into the plew100v5X:pex11 vector (71), which integrates into an rRNA spacer region of the trypanosome genome and expresses the RNAi sequence as a stem-loop construct under a Tet controlled rRNA promoter. SMB trypanosomes were the recipient cells, containing both T7 RNA polymerase and the Tet repressor under a single neomycin resistance gene (G418 selection) (65). Three independent rounds of transfection were carried out, giving rise to 11 clones resistant to phleomycin (plew100v5X:pex11 carries a *Sh ble* gene). These clones were tested for growth phenotypes on addition of Tet to initiate RNAi. 9 out of 11 displayed a similar rapid and severe growth defect. Interestingly, although the growth defect was rapid cell kill was slow and took several days (representative clone Fig. 19*A*). Northern blotting was used to confirm that *HSP83* mRNA decreased on addition of Tet, although across 48 h mRNA was never completely ablated

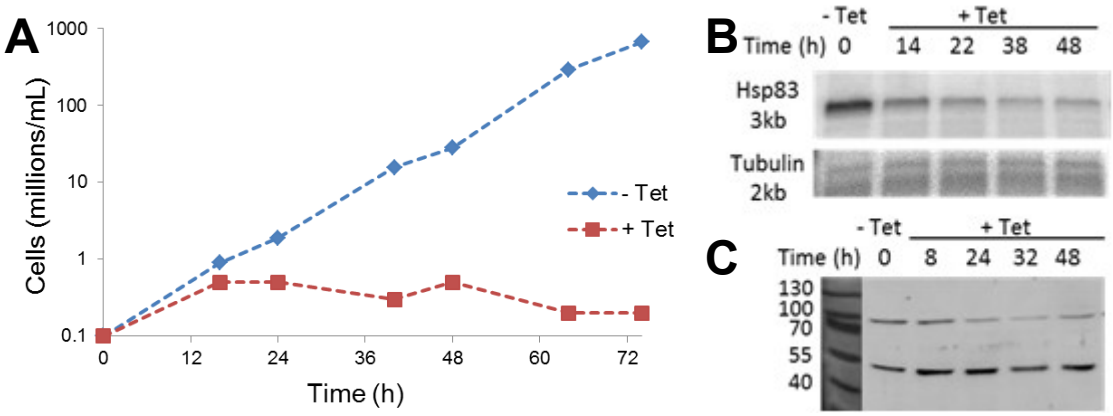

Figure 19. *HSP83* RNAi causes rapid and severe growth defect.

(A) Cumulative cell growth of a representative clone carrying plew100v5X:pex11 configured for *HSP83* RNAi, plus or minus Tet addition. Numbers adjusted for dilutions, which occurred each time concentrations exceeded $1x10^6$/mL in order to maintain log growth. *(B)* Northern probing *HSP83* mRNA on the same representative clone treated with Tet. Tubulin probed as a loading control. *(C)* Western blot using a human Hsp90 antibody on the same representative clone treated with Tet. *Ladder, kDa*.

(Fig. 19*B*). Protein lysates were probed with several human Hsp90 antibodies, and SC-7947 (Santa Cruz) detected a band between 80-90 kDa that decreased significantly with Tet treatment, but like the mRNA was not completely ablated (Fig. 19*C*).

Cell cycle progression after RNAi induction was investigated through DAPI staining and fluorescent microscopy. *HSP83* RNAi caused a large increase in 2N2K cells, a substantial cytokinesis defect (Fig. 20). This defect was at or prior to cleavage furrow initiation, as the number of 2N cells containing a visible cleavage furrow did not increase significantly (Fig. 20*C*). At 48 h a small 2N1K population accumulated. KDNA replication was investigated with a free minicircle profile, which showed an increase in abnormal linears at 48 h (Fig. 21). A census of network shapes and labeling patterns with TdT found decreased partially replicated forms and substantial populations of labeled and unlabeled ovals (Fig. 22), confirming kinetoplast segregation lesions and explaining the 2N1K population.

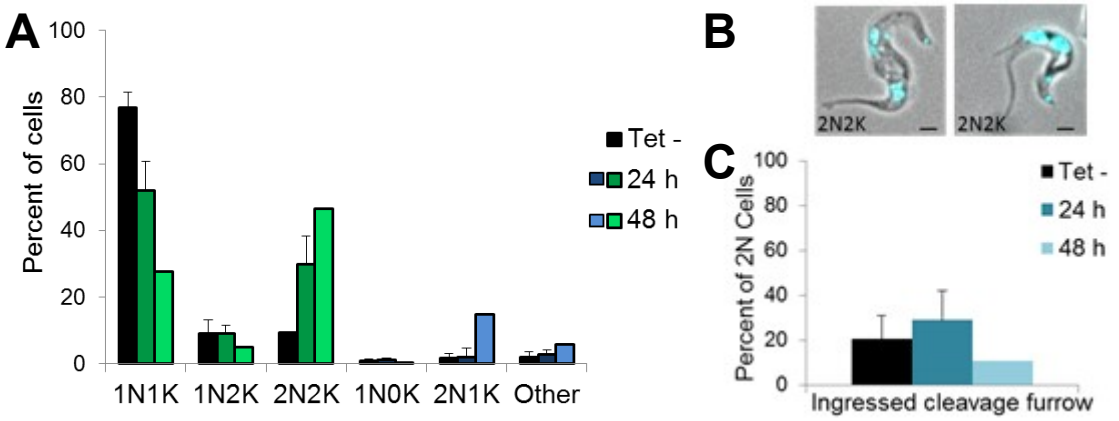

Figure 20. *HSP83* RNAi inhibits cytokinesis

HSP83 RNAi cells were treated with Tet and examined by DAPI staining and fluorescent microscopy for cell cycle progression. *(A)* Nuclear and kinetoplast contents of cell population. Cells counted for each time point ≥ 100. *(B)* Representative image of 2N2K cells. *Bar*, 1 μM. *(C)* Percent of 2N cells with a visible cleavage furrow. At 0 and 24 h mean±SD n = 5, 48 h mean of n = 2.

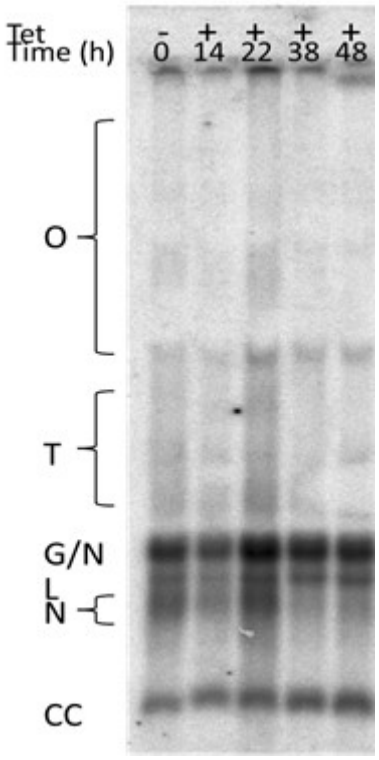

Figure 21. *HSP83* RNAi leads to an increase in linear minicircles at late timepoints

DNA from *HSP83* RNAi cells was separated on a 1.5% agarose gel and probed with a minicircle sequence. Lanes were loaded by cell equivalents. *O* – Oligos, *T* – Theta structures, *G* – Gapped minicircles, *N* – Nicked minicircles, *L* – Linears, *CC* – Covalently closed minicircles.

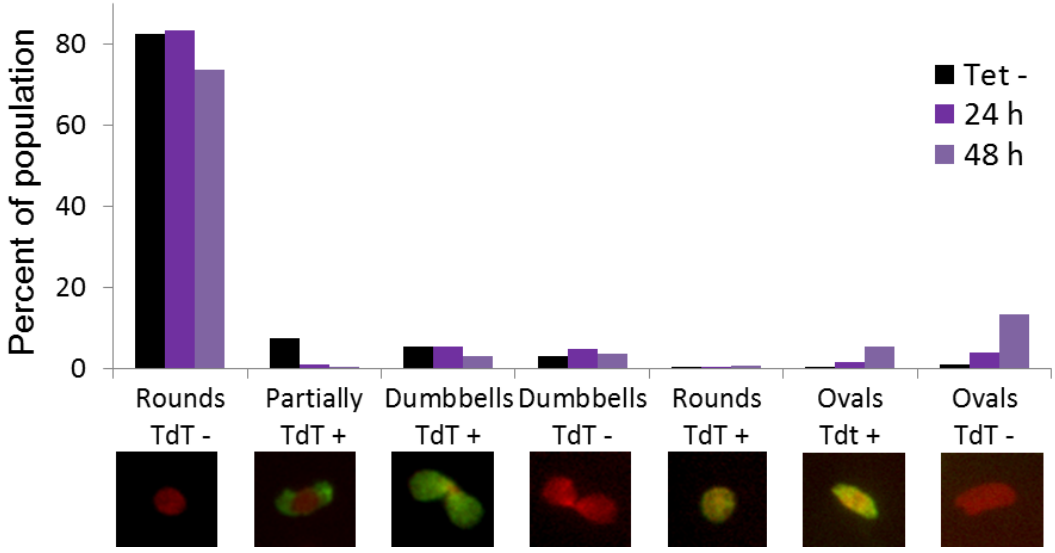

Figure 22. Abnormal TdT labeled and unlabeled ovals increase in *HSP83* RNAi cells

Networks were isolated from *HSP83* RNAi Tet induced cells, spread on slides, stained with DAPI (*red*) and labelled with fluorescent dUTP (*green*) using TdT. Networks ≥1500 counted for each treatment.

RNAi of *TbTRAP*. A BLAST search was performed against the trypanosome genome with the human mitochondrial Hsp90, TRAP-1, sequence (69). Tb427tmp.02.0250 was identified as a homologue with an Expect value of $2e^{-151}$ in predicted amino acid sequence with 62% positive and 43% identical matches. The Expect value for the mRNA sequence was $6e^{-12}$ with 68% and 75% identity in a 177 bp and 91 bp segment of the genetic sequence. Tb427tmp.02.0250 is annotated as a putative heat shock protein, and contains a mitochondrial targeting sequence. In the literature, Tb427tmp.02.0250 was identified as part of the trypanosome mitochondrial proteome (74). Hereafter Tb427tmp.02.0250 is termed *TbTRAP*. As with *HSP83* RNAi, a portion of *TbTRAP* was cloned into the plew100v5pex11 vector, and then transfected into SMB trypanosomes. Three independent rounds of transfection were carried out, giving rise to 12 clones. All 12 displayed a similar post 48 h growth defect on addition of Tet (Fig. 23*A*). Northern blotting was used to confirm that *TbTRAP* mRNA decreased (Fig. 23*B*). A human TRAP antibody was tested but did not detect any correctly sized bands in western blots. In one clone an endogenous copy of *TbTRAP* was tagged at the C-terminus using homologous

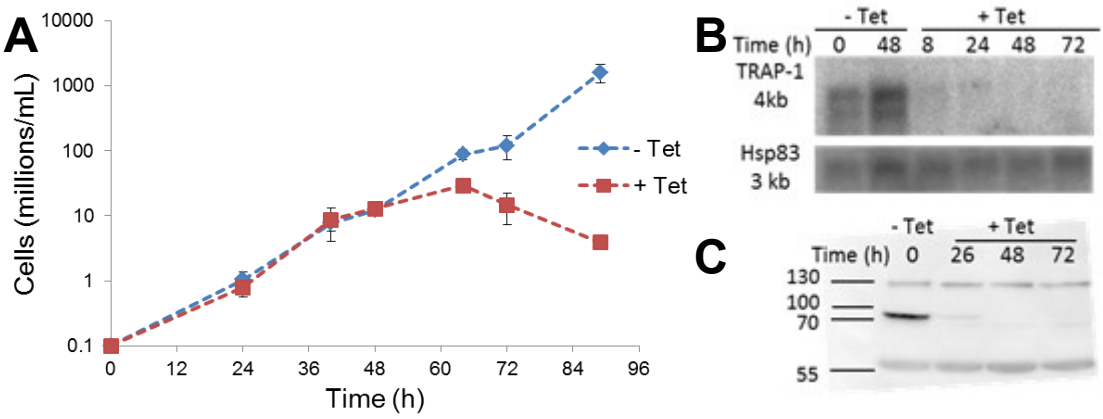

Figure 23. *TbTRAP* RNAi causes growth defect after 48 h

(A) Cumulative cell growth of eleven clones carrying plew100v5X:pex11 configured for *TbTRAP* RNAi, plus or minus Tet. Numbers adjusted for dilutions when cells concentrations exceeded $1x10^6$/mL in order to maintain log growth. *Mean±SD, n*=11 *(B)* Northern probing *TbTRAP* mRNA on a representative clone treated with Tet. *HSP83* probed as a loading control. *(C)* Western blot against cmyc of a *TbTRAP* RNAi cell line with an endogenous copy of *TbTRAP* modified to carry a C-terminal cmyc tag (one out of four which retained the same growth defect with Tet). *Ladder, kDa*.

recombination to insert a 3xcmyc tag and a blasticidin resistance gene in between the 3' end of the *TbTRAP* coding sequence and the 3'UTR. Six blasticidin resistant clones were subjected to Tet treatment and to western probing with a cmyc antibody. Four clones expressed a band between 80-90 kDa that decreased after 72 h of Tet treatment (Fig. 23*C*). These clones retained the same growth defect on Tet addition, but two clones lost their sensitivity to Tet and in these clones the 80-90 kDa band did not decrease.

In both the parent clones and in a cmyc tagged clone (that retained the same Tet induced growth defect) cell cycle progression was examined by microscopy. Interestingly, concurrent with the growth defect an abnormal 1N0K population, lacking a visible kinetoplast, appeared and increased with prolonged RNAi, and a small 2N1K population built up (Fig. 24). 1N0K cells are possible either when there is a kinetoplast replication defect without a cytokinesis defect, so that one daughter cell receives a kinetoplast and one does not, or when the cleavage furrow is positioned so that one daughter receives two kinetoplasts and the other none. As there was no increase in 1N2K cells, and there was evidence of 2N1K cells at abscission (Fig. 24*B*), the former scenario of a strong kinetoplast replication defect with no concomitant cytokinesis defect is

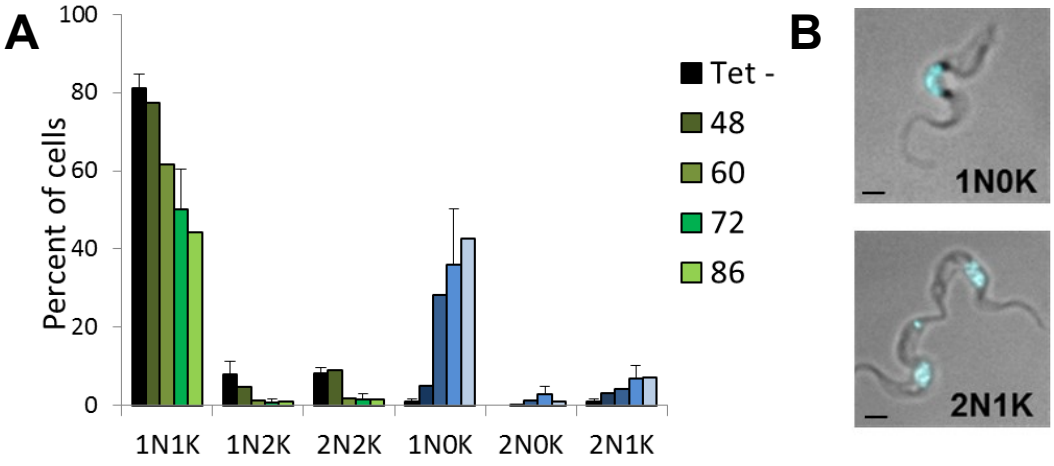

Figure 24. *TbTRAP* RNAi causes abnormal 1N0K cells and 2N1K cells

TbTRAP RNAi cells were treated with Tet and examined by DAPI staining and fluorescent microscopy. *(A)* Nuclear and kinetoplast contents of cell population. At 0 and 72 h error bars are SD for n ≥ 3. Cells counted for each time point ≥ 100. *(B)* Representative image of a 1N0K and a 2N1K cell. *Bar*, 1μM

likely. This is in contrast to the cell cycle defects observed with 17-AAG treatment and *HSP83* RNAi, but unsurprising if *TbTRAP* is indeed a mitochondrial Hsp90 as there would be no need to suppose it chaperoned cytokinesis regulators.

The free minicircle population was investigated and simultaneous with the growth defect a vivid alteration occurred. Replicating minicircle intermediates (theta and nicked smears) vanished, and multiple forms of abnormal oligomers appeared (Fig. 25). These changes point to an inhibition of kDNA synthesis and topoisomerase difficulties with catenation and decatenation of minicircles. Interestingly imaging of TdT labeled networks did not reveal vivid changes, although there was a small but significant increase in abnormal labeled and unlabeled oval networks, as had been seen with 17-AAG treatment and *HSP83* RNAi (Fig. 26). This, together with the DAPI whole cell staining (Fig. 24), suggests a strong halt on kinetoplast replication. TbTRAP is essential for kDNA integrity.

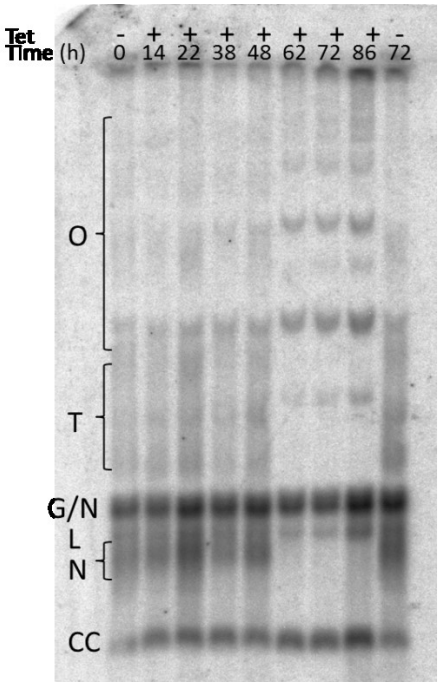

Figure 25. *TbTRAP* RNAi causes abnormal free minicircle populations

DNA from *TbTRAP* RNAi cells was separated on a 1.5% agarose gel and probed with a minicircle sequence. Lanes were loaded by cell equivalents. *O* – Oligos, *T* – Theta structures, *G* – Gapped minicircles, *N* – Nicked minicircles, *L* – Linears, *CC* – Covalently closed minicircles.

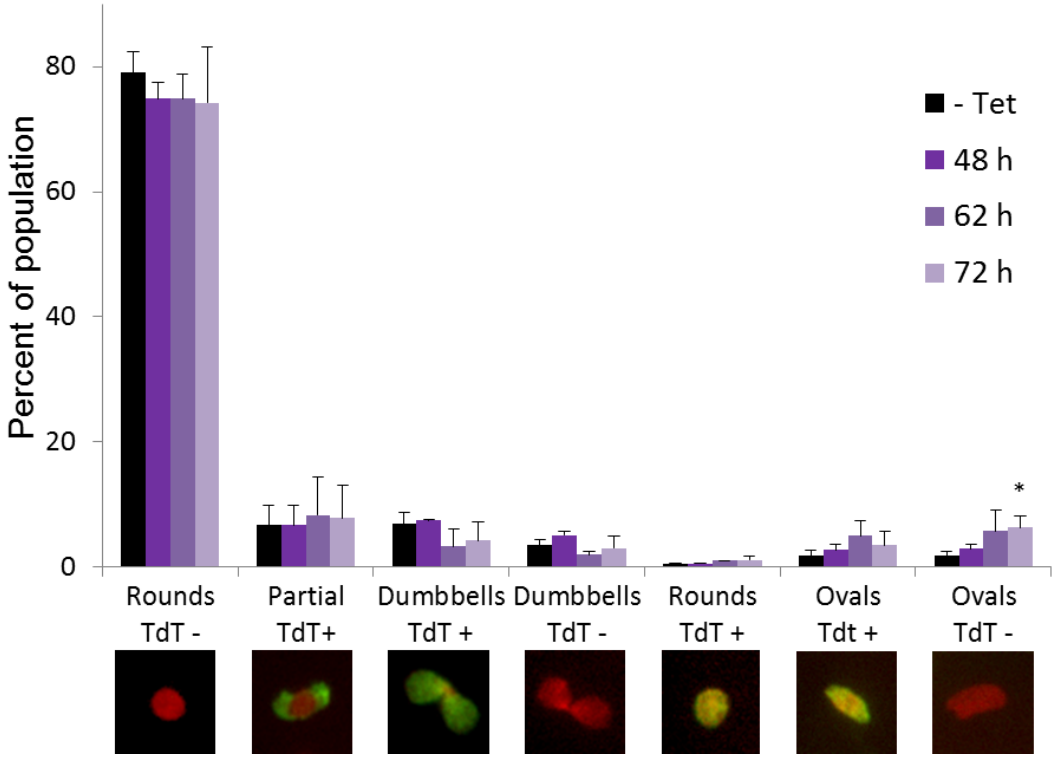

Figure 26. Abnormal TdT unlabeled ovals increase in *TbTRAP* RNAi cells

Networks were isolated from *TbTRAP* RNAi Tet induced cells, spread on slides, stained with DAPI (*red*) and labelled with fluorescent dUTP (*green*) using TdT. Networks ≥500 counted for each treatment.

DISCUSSION

17-AAG causes rapid growth-defects in trypanosomes. In higher eukaryotes, the toxicity of Hsp90 inhibitors is attributed to subsequent functional loss of client proteins, which include key cell cycle regulators. There was vivid evidence of cell cycle dysregulation in trypanosomes treated with Hsp90 inhibitors. Many gene products essential for orderly progression through the trypanosome cell cycle have been identified via RNAi silencing, including kinases (e.g., cyclin-related, Aurora, Polo-like (PLK), nuclear DBF-2 related (NDR) (75-77)) and kinase regulators (e.g., cyclins, kinase activator MOB1, kinase receptor TRACK (78-80)), several of whose mammalian homologs are recognized Hsp90 clients (81-84). Individual knockdown of these proteins in kinetoplastids generates a cell cycle defect, such as abnormal numbers of kinetoplasts or nuclei, arrested or misplaced cleavage furrows. Unlike these discrete phenotypes, however, with Hsp90 inhibitors multiple abnormalities were seen in the same cell and pleomorphic abnormalities in the population (Fig. 12*C*). These complex and profound disruptions of nuclear and kinetoplast segregation and cytokinesis support the notion that HSP83, like Hsp90 in higher eukaryotes, is an important node in the midst of numerous regulatory pathways. Cytokinesis and kinetoplast segregation defects dominate at high concentrations of 17-AAG suggesting key regulators of these processes are clients particularly sensitive to loss of Hsp90 function.

Initiation and completion of cleavage furrow ingression was impaired after 17-AAG treatment with many cells containing a visible partially ingressed furrow. Cell cycle proteins found particularly associated with this process are PLK, NDR kinases and their activator MOB1, and TRACK, along with cytoskeletal associated proteins such as katanins and kinesins (85-88). RNAi silencing of these genes leads to incomplete cleavage of the cell or failure to initiate cleavage furrow ingression (77,79,80,87,88). PLK is a client of mammalian Hsp90, and thus an attractive candidate for being the sensitive HSP83 client in *T. brucei* responsible for the cleavage furrow defects observed. Kinetoplast replication was also disrupted with 17-AAG treatment, particularly the architectural positioning of newly replicated minicircles and the dividing of the

network. Topoisomerases play an important role in this process, as do many other proteins, some of which have not yet been identified (54).

RNAi of *HSP83* and of Tb427tmp.02.0250, putative *TbTRAP*, led to inhibition of growth, proving both of these genes are essential for *T. brucei*. This confirms the severe growth defect observed in bloodstream forms after *HSP83* knockdown in a genome wide RNAi screen of *T. brucei* (89). Tb427tmp.02.0250 was not identified as essential in bloodstream forms in that genome wide screen, but our observation of a delayed growth defect explains its absence. In the same screen, it was found to be essential in procyclics, the insect form of *T. brucei*. Procyclics, unlike glycolytic bloodstream forms, rely on electron transport for energy production. Human TRAP-1 plays a role in the mitochondrial electron transport chain (64), and TbTRAP may also chaperone trypanosome components of this essential process in procyclics. In bloodstream forms, simultaneous with growth defects, we observed a halting of kinetoplast replication with RNAi of *TbTRAP*. Cells lacked kinetoplasts, or had two nuclei but only one kinetoplast (Fig. 24). There was a marked decrease in replicating theta and nicked minicircles and also an increase in catenated oligomers (Fig. 25). This suggests problems with the topoisomerases that ensure the correct catenation and decatenation of minicircles. The delay in appearance of this phenotype suggests a need to reach a threshold of dysfunction in certain kinetoplast replication regulators, the timing of which is likely determined by the size and rates of turnover of the protein pools of TbTRAP and of its clients. The growth defect due to RNAi of *HSP83* was immediate, even without complete loss of HSP83 protein by western blot. This likely reflects the importance of having abundant HSP83, so that even with a small amount of protein loss sensitive clients are unable to function correctly. Although the growth defect was rapid, cells took 48 h to begin to die, consistent with the delayed death seen with 17-AAG treatment (Fig. 10 and 19). The major cell cycle defect seen was cytokinesis inhibition, along with a more delayed kinetoplast replication defect. Perhaps HSP83 in the cytosol chaperones a nuclear encoded but mitochondrion targeted protein essential for kDNA network architecture. The phenotype observed with *HSP83* RNAi

was very similar to that observed with 17-AAG treatment, suggesting HSP83 is indeed the target of 17-AAG in trypanosomes. The RNAi phenotypes and 17-AAG treatment outcomes were not identical, which is unsurprising considering the difference between the gradual loss of protein that occurs with RNAi versus rapid chemical inhibition of ATPase activity with drug treatment. Cytokinesis and kinetoplast replication are particularly sensitive to chemical and genetic inhibition of Hsp90s in *T. brucei*.

The tightly coordinated duplication in trypanosomes of the mitochondrial genome within the cell cycle differs dramatically from mitochondrial DNA replication in mammalian cells. KDNA sensitivity to loss of TbTRAP suggests that this mitochondrial Hsp90 chaperones certain key regulators of kDNA replication. HSP83 chaperones multiple cell cycle regulators, with cytokinesis and kinetoplast replication particularly sensitive to HSP83 loss. These results validate HSP83 as a target for anti-trypanosomal agents.

CHAPTER III. Hsp90 inhibitors display class-wide concentration-driven efficacy against *Trypanosoma brucei*

INTRODUCTION

Drug action, and ultimately clinical response, is determined by pharmacokinetic-pharmacodynamic (PK-PD) relationships, the connection between drug exposure and effect. Understanding these relationships allows rational and optimal use of medicines. This is imperative in an era where incisive drug development, and control of drug toxicity and resistance, are critical needs. Drugs have dynamic concentration-time curves in vivo, with the typical pattern in blood after an oral dose being a rapid rise to the maximum concentration, C_{max}, followed by decay at a rate corresponding to the half-life ($t_{1/2}$). The resulting area under the concentration-time curve (AUC) comprises total exposure to drug (Fig. 5). Crucially, shape of the curve (and correspondingly, shape of its AUC) can be manipulated by dosing strategy, resulting in striking differences in the outcome of drug action (PK-PD reviewed in (28,29,90)).

Total drug exposure (AUC) is an integral of concentration and time, thus for the same total exposure peak concentration is inversely related to the time drug levels are sustained above a threshold (Fig. 27). One useful PK-PD relationship is the simplistic discrimination between concentration- or time-driven activity, reflecting better efficacy from a steep or flat concentration-time curve, respectively. For some agents there is apparently no shape preference, in which case total AUC is said to determine efficacy. Famously the antibacterial penicillins are time-driven and require sustained levels to exert maximal clinical effect (91). The tendency in drug development is to lengthen the half-life of candidates, assuming this will improve activity and require less frequent dosing; however, for a peak concentration-driven drug the resulting constant and extended exposure can be inappropriate for efficacy, toxicity, and the risk of resistance (90). For example, the antibacterial activity of aminoglycosides depends on peak concentration and is not enhanced by sustained drug levels, which worsen their nephrotoxicity

(92,93). Likewise the antileukemia bcr-abl kinase inhibitor dasatinib ($t_{1/2}$ 3 h) has maximal efficacy and minimal toxicity dosed once rather than twice daily, consistent with the in vitro finding that a 20 min exposure is sufficient to trigger apoptosis (94,95). Highly short-lived artemisinins, the last line of drug defense against malaria, are efficacious with once daily dosing (96). For these drugs, with varying targets and therapeutic indications, brief intermittent exposures are adequate, indeed optimal, for activity. Requiring long half-lives for drug candidates, while ideal for time-driven compounds, may needlessly cause useful leads to be abandoned. Likewise, frequent dosing to maintain sustained concentrations may be unnecessary and perhaps detrimental. As the kinetic governance cannot be predicted, experimental determination of PK-PD relationships is needed for ideal drug management.

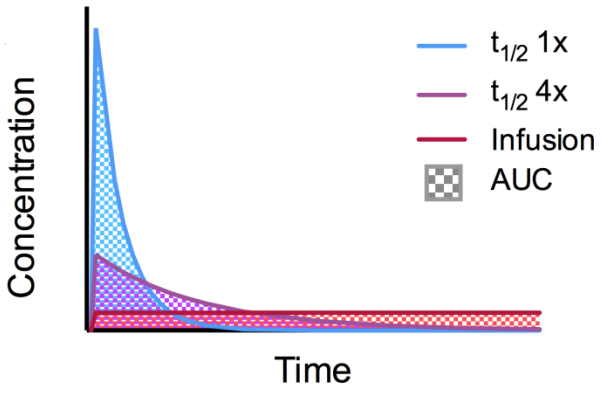

Figure 27. Peak concentration is inversely related to time above a threshold for the same total AUC

Theoretical PKs depicted for the same total AUC (*shaded*) with $t_{1/2}$ 1x (*blue*), $t_{1/2}$ 4x (*purple*) or from a constant infusion (*red*).

In vitro PK-PD methodologies are a valuable translational support. From the very earliest stage of drug discovery, determination of PK-PD can direct choice of lead compound and optimization of PK properties. PK-PD can be used to predict dosing regimens with greatest likelihood of efficacy in vivo. Post-clinical introduction, in vitro PK-PD can provide complementary support to explore alternative dosing regimens and clinical questions difficult to

address in patients. Hollow fiber cartridge systems, culture vessels perfused by porous polymer fibers that allow diffusion of small molecules but restrict passage of cells, are well established for the study of antibacterial and antiviral PK-PD (97,98). Our group developed a novel apparatus for PK-PD of antimalarials (99). This work describes, to our knowledge the first, dynamic in vitro PK-PD studies with *Trypanosoma brucei*. A simple but powerful method is proposed, conducted with artificial PK conditions, to identify the principal kinetic driver of a compound's efficacy.

Trypanosoma brucei is an ancient divergent eukaryotic parasite. It causes the neglected but deadly infection human African trypanosomiasis (sleeping sickness), passed to humans by the tsetse fly in rural regions of sub-Saharan Africa. As an extracellular parasite, it causes non-specific symptoms and is difficult to diagnose (2). Unfortunately the infection progresses to the CNS, where it becomes difficult to treat. Current therapies are less than desirable, requiring lengthy injection regimens and causing severe toxicities (1). The worst case of this is organic arsenical melarsoprol, the only option for treating the late-stage of the acute east-African subspecies. Melarsoprol causes a reactive encephalopathy leading to death in 2-10% of patients. The potential of repurposing Hsp90 inhibitors against *T. brucei* was investigated and it was found that 17-(allylamino)-17-demethoxygeldanamcyin (17-AAG) and 17-(dimethylethylamino)-17-demothxygeldanamycin (17-DMAG), derivatives of geldanamycin, were both potent and selective against the parasite (Chapter I)(30). Importantly, both were able to cure mouse acute early-stage infections, including when 17-DMAG was delivered orally (30). *T. brucei* contains an Hsp90 homologue, HSP83, encoded by ten tandem gene copies (14). HSP83 is 60% identical to human Hsp90, and contains the conserved Hsp90 N-terminal ATP binding site, the Bergerat fold (46).

Geldanamycin and radicicol, a benzoquinone ansamycin and resorcinol respectively, are natural products and were two of the earliest identified Hsp90 inhibitors (20,41). They both bind

in the ATP pocket (Bergerat fold) of the *N*-terminal domain of Hsp90 (100). Their scaffolds have been derivatized extensively, comprising two of the three major chemical classes of Hsp90 inhibitors (24). The first Hsp90 inhibitor to enter clinical trials for oncology was 17-AAG (tanespimycin) which displayed promising activity in multiple myeloma and Her2 positive breast cancer (24,101). Improving on 17-AAG in solubility and pharmacokinetics, 17-DMAG (alvespimycin) was the second ansamycin in the clinic (102). Building off of the resorcinol scaffold, half a dozen inhibitors have been tested in cancer patients, with the greatest experience obtained for NVP-AUY922 and STA-9090 (ganetispib)(24). A third major class of Hsp90 inhibitors are fully synthetic compounds discovered through high-throughput screening, that are based off a purine scaffold and also bind in the ATP pocket (82). Several of these have oral formulations, and various selected pharmacokinetic properties, such as blood-brain barrier penetration for CUDC-305/Debio 0932 (42).

Clinical work with Hsp90 inhibitors has thus far focused on cancer therapy, where most treatment regimens are prolonged cyclical schedules with doses at the limit of tolerability. These schedules and doses are unlikely to be optimal for protozoan parasites with very distinct lifecycles and cell biology. By understanding the pharmacokinetic-pharmacodynamic (PK-PD) relationships of anti-protozoan activity, we can further the potential of Hsp90 inhibitors for treating parasitic infections. PK-PD can be used to build a target product profile for lead compound optimization of Hsp90 inhibitors for parasites. PK-PD can also be used to guide dosing strategies for in vivo investigation of compounds. We desired to develop a method to expose trypanosome parasites to programmable dynamic concentration-time profiles of drugs in vitro. This requires dilution of drug from the system, but retention of parasites. In order to further investigate the potential of Hsp90 inhibitors against *T. brucei*, in this study a hollow-fiber cartridge methodology was developed for in vitro study of antitrypanosomal PK-PD and the effect of the PK shape on PD examined for 17-AAG, 17-DMAG, NVP-AUY922, and CUDC-305.

MATERIALS AND METHODS

Cell Culture and Reagents. *T. b. brucei* (MiTat 1.2 strain 427) were maintained in log growth at 37°C, 5% CO_2, in phenol red-free HMI9, 10% FBS, 10% Serum Plus (Sigma). Number of live (motile) parasites was determined by hemocytometer and light microscopy. Drug stocks were in DMSO, stored aliquoted at -20°C. 17-AAG and 17-DMAG were obtained from the Open Chemical Repository of the National Cancer Institute Developmental Therapeutics Program. NVP-AUY922 (LC Laboratories) and CUDC-305 (ChemieTek) were purchased. [^{3}H]17-AAG (48.5 Ci/mmol, Moravek) was used as a tracer of 17-AAG drug levels.

Cytotoxicity and Bioassays. 96-well plate cytotoxicity assays were performed as described previously (Chapter I)(39). Briefly, cells were seeded at 1 x 10^5 cells/mL in quadruplicate at various drug concentrations. At 24 h cells were lysed and phosphatase substrate added. After 3-6 h incubation at 37°C, absorbance was read at 405 nm, and treated wells were compared to untreated control wells. For bioassay of drug concentrations, unknown samples were incubated with 1 x 10^5 cells/mL for 24 h, and compared to a standard curve of known drug concentrations.

In vitro PK-PD system for *T. brucei.* Several systems were tested for in vitro PK-PD of antitrypanosomals (Fig. 28).

A) Glass cartridge, blown by Adams and Chittendon, perfused by dialysis membrane

    1) 50kDa pore-size, regenerated cellulose 28 mm membrane (Spectrum Labs), with 0 – 200 gauge 27 perforations
    2) 1000 kDa pore-size, cellulose ester 15 mm membrane (Spectrum Labs)

B) Glass cartridge, blown by Adams and Chittendon, capped with hydrophilic polytetrafluoroethylene 1 μm pore-size membrane (JAWP02500, Millipore).

C) One-compartment open dilution in 50 mL bottle

D) Hollow-fiber cartridges

1) 0.1 µm pore, mixed cellulose ester fibers (MidiKros, Spectrum Labs)

2) 0.2 µm pore, polypropylene fibers (Cellmax, Spectrum Labs)

3) 30 kDa pore, polysulfone fibers (Cellmax, Spectrum Labs)

4) 20 kDa pore, polysulfone fibers (C2011, FiberCell Systems)

5) 0.1 µm pore, polyvinylidene difluoride fibers (C2025, FiberCell Systems)

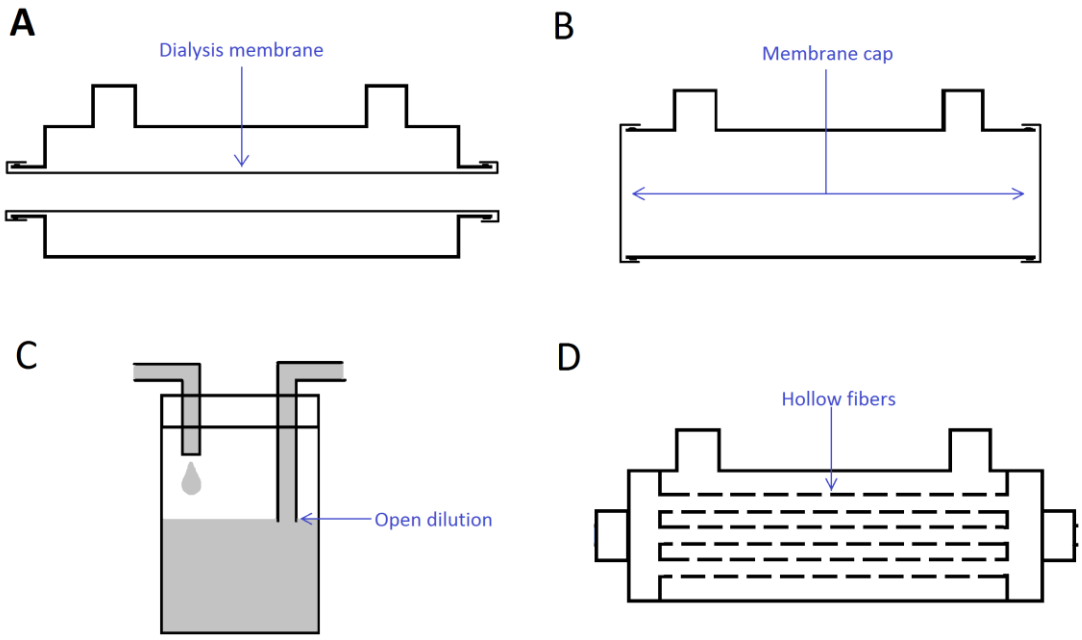

Figure 28. In vitro PK-PD systems tested for antitrypanosomals

(A) Glass cartridges were threaded through with dialysis membrane. Trypanosomes were cultured outside the membrane and PK profiles of drug pumped through the lumen. *(B)* Glass cartridges were sealed on each end with porous membrane. Trypanosomes were grown in the cartridge and PK profiles of drug were pumped through the membranes and cartridge. *(C)* Trypanosomes and t_0 drug were placed in a bottle. Drug free medium was added to the bottle and fluid was removed by a tube placed at the meniscus. *(D)* Trypanosomes were grown in the extra-fiber space of hollow fiber cartridges, and drug solution either pumped through the fibers or pumped directly in to the extra-fiber space.

To achieve dynamic PK profiles, a central reservoir contained a drug solution at desired t_0 (initial) concentration. Using flexible platinum-cured silicone tubing (Masterflex, Cole-Parmer and 2-stop 1.52 mm ID, IDEX Health & Science) and a precise peristaltic pump (IPC, Ismatec), drug was diluted out of the central reservoir by addition of drug free medium from an input reservoir while removing drug solution at the same rate. This changing drug solution was then pumped through the apparatus containing trypanosomes, except in the case of the open dilution (Fig. 28*C*) where trypanosomes were in the central reservoir. In the final system used, trypanosomes were cultured in the extra-fiber space of a C2025 (FiberCell Systems) cartridge and PK profiles were pumped directly into the extra-fiber space and then out via the lumen of the fibers. Cartridges were kept sterile, and rinsed thoroughly with 70% EtOH, water, then HMI9 between experiments. The standard PK-PD experiment involved three cartridges; one drug-free control cartridge, and two cartridges given the same total AUC and dose of drug but delivered in contrasting regimens to either favor time above a threshold or to favor C_{max}. To achieve initial t_0 drug concentrations, cartridges were pre-incubated with calculated concentrations of drug to satisfy non-specific binding to the fibers (Table 4). At t_0, extra-fiber medium was replaced with trypanosomes at $1x10^5$ cells/mL and t_0 drug levels, and the cartridge connected to a central and waste reservoir. Pumps were set to 0.45 mL/min (1.52 mm id two-stop tubing, Cole Parmer) and medium pumped continuously from an input reservoir to the central reservoir, and from the central reservoir into the extra-fiber space of the cartridge, across the fibers and out through the lumen of the fibers to waste. The control cartridge was exposed to drug-free medium. To achieve the constant infusion (time-intensive) regimen, input and central reservoirs and cartridge contained the same concentration of drug. To achieve the C_{max} regimen, the central reservoir contained drug at t_0 levels, but the input reservoir contained drug-free medium, leading to a steady dilution of drug over time. To adjust half-life, volume of the central reservoir was adjusted. Half-lives were initially determined without cells in the extra-fiber space of the cartridge, sampling from the distal port and determining drug concentration using cognate radiolabeled tracer or bioassay. Half-lives were confirmed to be within 10% of desired for every drug. For PK-PD experiments,

the end point was removal of trypanosomes from each cartridge and determination of number of live parasites using hemocytometer and light microscope.

Assessment of Non-specific Binding. Isolated cartridges were incubated with known high concentrations of drug. The extra-fiber space was sampled over time and drug concentration determined. At equilibrium, the percentage of drug loss was calculated and this value used to calculate the concentration required to pre-incubate cartridges to achieve t_0 values for experiments (Table 4). In the range of concentrations studied, non-specific binding was concentration independent.

Table 4. Hsp90 inhibitor non-specific binding and conditions to attain desired kinetics

Drug	Drug loss in cartridge (%)[a]	Cartridge pre-incubation[b]		Central reservoir volume (mL)[c]
		xt_0	duration (h)	
17-AAG	95	20	3	21
17-DMAG	94	15	16	21
NVP-AUY922	90	10	1	25
CUDC-305	90	10	3	20

[a]Drug bound at equilibrium after incubation in an isolated cartridge with high drug concentration

[b]Conditions used for pre-incubation to compensate for nonspecific binding of drug to cartridge. Based on the percentage of drug lost, the indicated multiple (x) of the t_0 drug concentration was incubated in the cartridge for indicated duration before start of experiment

[c]Volume in central reservoir for C_{max} regimens to ensure $t_{1/2}$ of 1 h in extra-fiber space of cartridge

Statistical Analysis. Where indicated, an unpaired, two-tailed, equal variance Student's *t*-test assessed significance. Modified Thompson's Tau test was used on the 24 h trypanosome population in the control cartridge (% of parallel flask for uncontaminated experiments, $n = 162$) to discard experiments where the control grew too poorly (8 cases).

Establishment of an in-vitro PK-PD System for Antitrypanosomals. Multiple in vitro PK-PD systems were tested for robust growth and recovery of trypanosomes, and reproducible desired pharmacokinetics (Fig. 28). Due to trypanosome motility, glass cartridges perfused by perforated dialysis membranes did not retain trypanosomes, and without perforation drug diffusion could not achieve desired pharmacokinetics (Fig 28*A*). Capping a glass cylinder with hydrophilic membrane and rapidly pumping PK profiles of drug through the system produced desired PK; however, membranes were toxic to trypanosomes (Fig. 28*B*). A one-compartment system with constant dilution was impractical due to near complete loss of trypanosomes over 24 h (Fig. 28*C*). Five commercially available hollow-fiber cartridges were tested (Fig. 28*D*). The Cellmax systems with polypropylene or polysulfone fibers were toxic to trypanosome growth, even after extensive washing with HMI9. Trypanosomes grew in the cellulose Midikros and polysulfone C2011 cartridges; however, due to the density of fibers in the cartridge, recovery of trypanosomes was highly variable. Under final flow conditions in the polyvinylidene difluoride C2025 cartridge (FiberCell Systems), trypanosome growth initially equaled then surpassed that in parallel T25 vented flasks (Fig. 29). Extended viability may be due to constant provision of fresh nutrients and removal of byproducts.

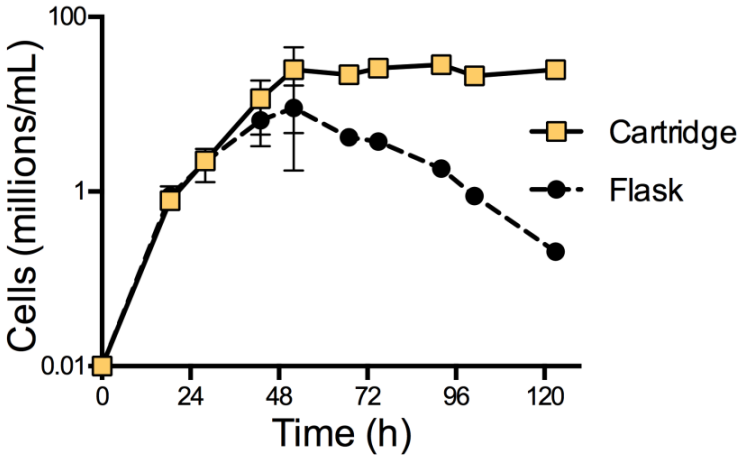

Figure 29. Trypanosomes grow well in C2025 cartridge with cross-fiber flow.

Trypanosome growth in cartridges with flowing drug-free medium into extra-fiber space and across fibers, or in parallel flasks seeded with the same culture. *Mean* (*±SD* for n≥3).

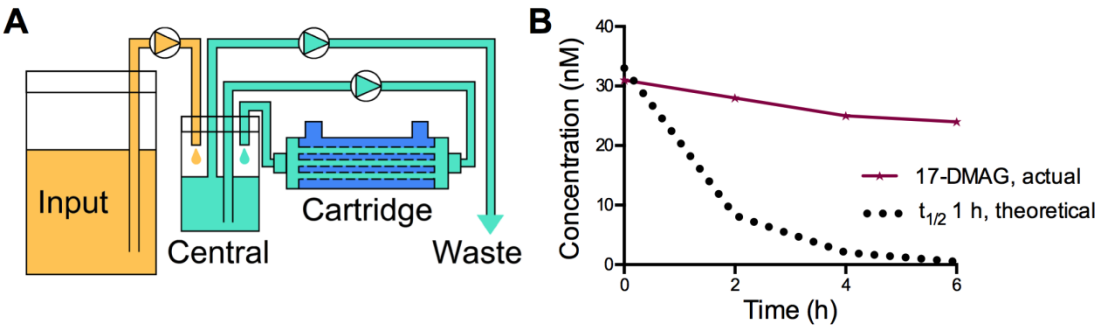

Figure 30. Standard circular loop flow path limits attainable PK parameters.

(A) Schematic of standard circular loop design. Snapshot during a dynamic drug dilution for a C_{max} regimen, produced when a high starting concentration of drug (*blue*) in the central reservoir is diluted with medium (*yellow* to form *green*) from an input reservoir. This is circulated through the lumen of the fibers and back to the central reservoir. Medium is removed from the central reservoir to waste at the same rate as diluent enters from the input bottle. *Arrowhead*, site of directional pump. (*B*) Actual PK obtained for Hsp90 inhibitor 17-DMAG (*red*) in extra-fiber space of C2025 cartridge when pumps where set to achieve $t_{1/2}$ 1 h (*Dotted curve*).

Early efforts to obtain desired PK profiles with conventional flow pathways in the C2025 cartridge failed (Fig. 30), likely because of extensive nonspecific and reversible drug binding to fibers (Table 4). Pre-coating of fibers with polyethylene glycol, gamma globulins, or bovine serum albumin had no effect on PK. Likewise, pre-treatment with trypsin to destroy bound proteins did not improve PK. To circumvent the reversible binding, a single pass cross-fiber flow path was used, pumping medium directly into the extra-fiber space then into the lumen of the fibers and out to waste (Fig. 31). Pre-incubation with calculated concentrations of drug prior to PK-PD (Table 4) led to accurate t_0 drug levels. Half-life was adjusted by varying the volume of the central reservoir and confirmed to be within 10% of desired in the extra-fiber space for all drugs tested. Flow rates were kept constant across experiments to control for effects on trypanosome growth. During PK-PD experiments, mean growth in the extra-fiber space at 24 h was 77 ± 13 percent (n = 127) that of flasks. In some 170 experiments (500 cartridges) over 24 months, 45 cartridge results were discarded due to contamination, and 8 experiments were discarded due to poor control cartridge growth. Contamination by autoclave- and bleach-resistant

spores was traced to lab wipes and was significantly reduced after paper products were eliminated from cartridge set-up areas.

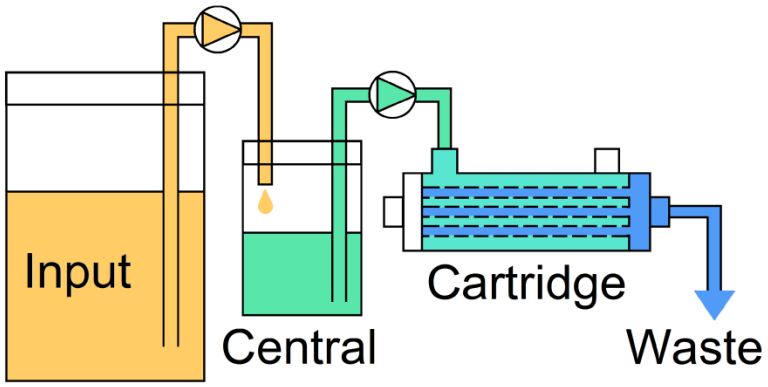

Figure 31. PK-PD system for in vitro study of antitrypanosomals.

Schematic of hollow fiber cartridge system. A snapshot during a dynamic C_{max} regimen, produced when a high starting concentration of drug (*blue*) in the central reservoir is diluted over time with medium from an input reservoir (*yellow, to form green*). The ever-changing dilution is pumped into the extra-fiber space of a cartridge and out via the lumen of the fibers to waste. Parasites are maintained in the extra-fiber space. *Arrowhead*, directional pump.

17-AAG is Concentration-driven Against *T. brucei*. To diagnose the intrinsic antitrypanosomal PK driver, two contrasting PK shapes are artificially generated of the same total drug exposure (AUC), a steady constant infusion (time-intensive) or a transient high peak (C_{max}-intensive), and compared the efficacy against trypanosomes (Fig. 32)(103). The regimen that gives greater efficacy is designated the PK driver and has important implications for drug optimization and in vivo use. The constant concentration infusion maximizes the time drug is present above a threshold. To begin, experiments were 24 h, which allows four doubling times of untreated controls in log growth (*T. brucei* cell cycle is 6 h in our hands) and comparison to our standard 24 h cytotoxicity assays. To contrast the time-intensive regimen, a C_{max}-intensive regimen of the same $AUC_{0\text{-}24}$ was initially generated with $t_{1/2}$ 1 h (Fig. 32*B*). This ensures the drug concentration has dropped 98% over the length of one cell cycle, and generates a peak 16.8-fold the infusion concentration.

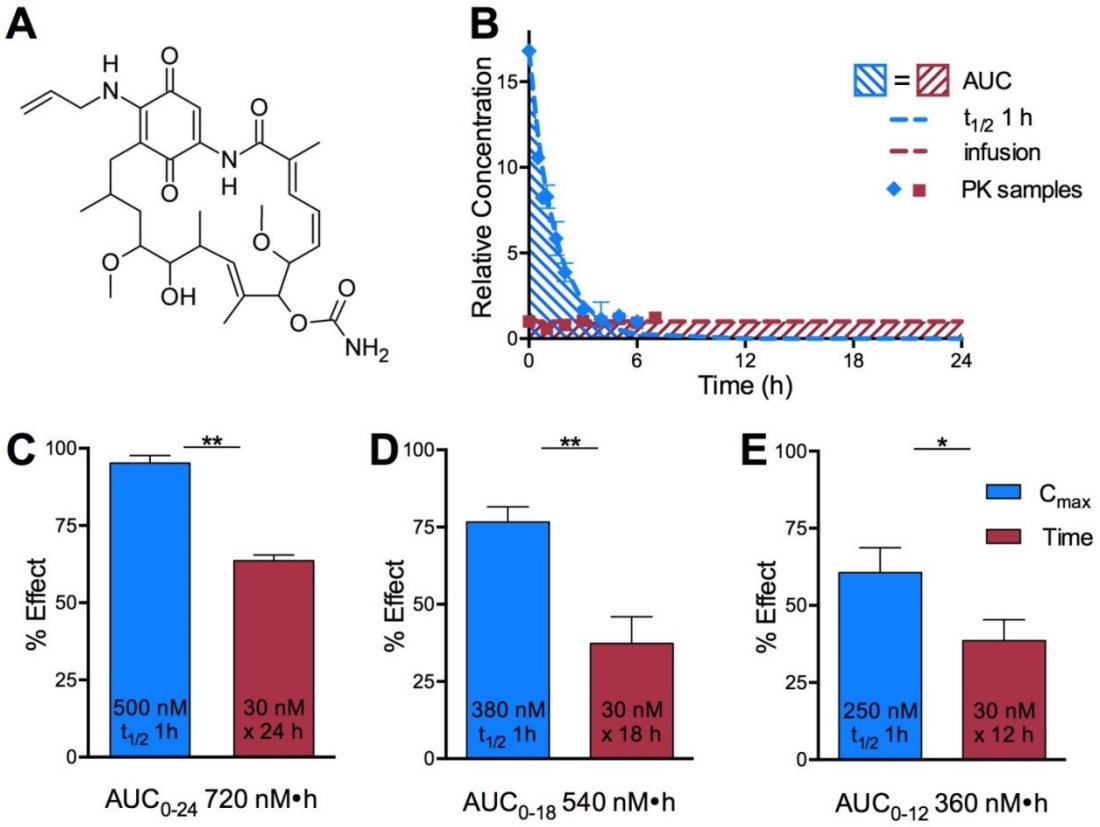

Figure 32. 17-AAG is concentration-driven against trypanosomes.

(A) Structure of the benzoquinone ansamycin 17-AAG. *(B)* The same total AUC (*shaded*) is dosed over 24 h against trypanosomes as either a constant concentration infusion (*red*) or as a high peak that is rapidly cleared with $t_{1/2}$ 1 h (*blue*). Pharmacokinetics were confirmed by radioactive tracer in cartridges sampling (*symbols*) from the extra-fiber space. *(C)* An $AUC_{0\text{-}24}$ 720 nM•h of 17-AAG is significantly more efficacious dosed as a 500 nM peak with $t_{1/2}$ 1 h than as a constant infusion of 30 nM. *(D)* Over 18 h, the same 17-AAG $AUC_{0\text{-}18}$ of 540 nM•h is more effective dosed as a high peak of 380 nM, $t_{1/2}$ 1 h, than as a 30 nM infusion. *(E)* Over 12 h, 17-AAG is more effective dosed as a 250 nM peak, $t_{1/2}$ 1 h, than as an infusion of 30 nM, resulting in the same $AUC_{0\text{-}12}$ of 360 nM•h. *Mean±SD*, $n \geq 3$, * $p<0.05$, ** $p<0.01$.

To begin 17-AAG was delivered at an $AUC_{0\text{-}24}$ of 720 nM•h, for which the 30 nM infusion had an efficacy of 64%, in the linear dose-response range (Fig. 32*C*). When this same $AUC_{0\text{-}24}$ was dosed to favor C_{max}, 504 nM with $t_{1/2}$ 1 h, 17-AAG was 95% effective (Fig. 32*C*). When the shape of the PK curve favors peak concentration, 17-AAG has significantly greater efficacy. The length of the experiment was varied to examine the effect of end-point on the PK driver of 17-

AAG. Trypanosomes were exposed to an infusion of 30 nM, and the equivalent AUC as a high C_{max}, $t_{1/2}$ 1 h, for 18 h or 12 h (Fig. 32*D,E*). In all cases the C_{max} regimen was more efficacious. 17-AAG efficacy is concentration- rather than time-driven.

17-AAG Exposure-response Curve Shifts Left When PK Shape is C_{max}-intensive. Multiple $AUC_{0\text{-}24}$s of 17-AAG were dosed in the two contrasting ways, time-intensive infusion or C_{max}-intensive ($t_{1/2}$ 1 h) transitory peak, to obtain full exposure-response curves for these different PK shapes (Fig. 33). The exposure-response curves were significantly separated. The greatest vertical efficacy separation was seen at an $AUC_{0\text{-}24}$ of 300 nM•h, where infusion dosing was just 20% effective, but by shifting the same $AUC_{0\text{-}24}$ to a transient high C_{max} 90% efficacy was obtained. The linear portions of the curves were horizontally separated three-fold. The EA_{50} 'potency' of 17-AAG with C_{max}-intensive ($t_{1/2}$ 1 h) dosing was 190 nM•h versus 610 nM•h for time-intensive infusion. These exposure-response curves demonstrate the significantly greater benefit that is obtained when the shape of 17-AAG exposure is C_{max}-intensive. For the greatest efficacy with the least total exposure, 17-AAG is most efficiently dosed by transient high peak concentrations.

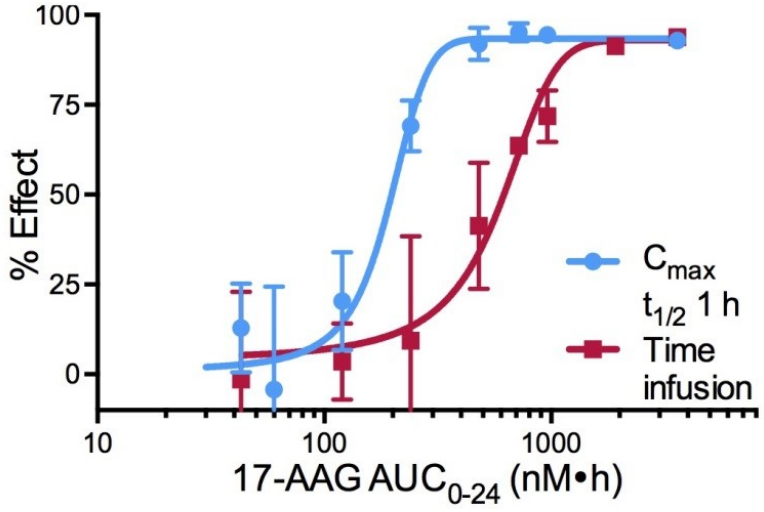

Figure 33. 17-AAG is more potent dosed as C_{max}-intensive PK shape.

Trypanosomes were exposed to 17-AAG in contrasting PK shapes, as either constant infusions (time-intensive, *red*), or as rapidly cleared high peaks (C_{max}-intensive, $t_{1/2}$ 1 h, *blue*), and efficacy determined at 24 h compared to untreated control.

17-AAG Exposure Shape is Optimal with the Highest Peak. To further examine PK shape preference, the relationship between peak, half-life, and efficacy was determined. The same total $AUC_{0\text{-}24}$ of 480 nM•h was dosed with a $t_{1/2}$ of 1 h, 2 h, 4 h, or as a constant infusion (Fig. 34*A*). As the half-life increased and the C_{max} decreased, the efficacy decreased (Fig. 34*B*). C_{max} is the strongest driver of 17-AAG efficacy, with the greatest effect obtained from an $AUC_{0\text{-}24}$ by delivering it as the highest peak, and therefore most transient exposure.

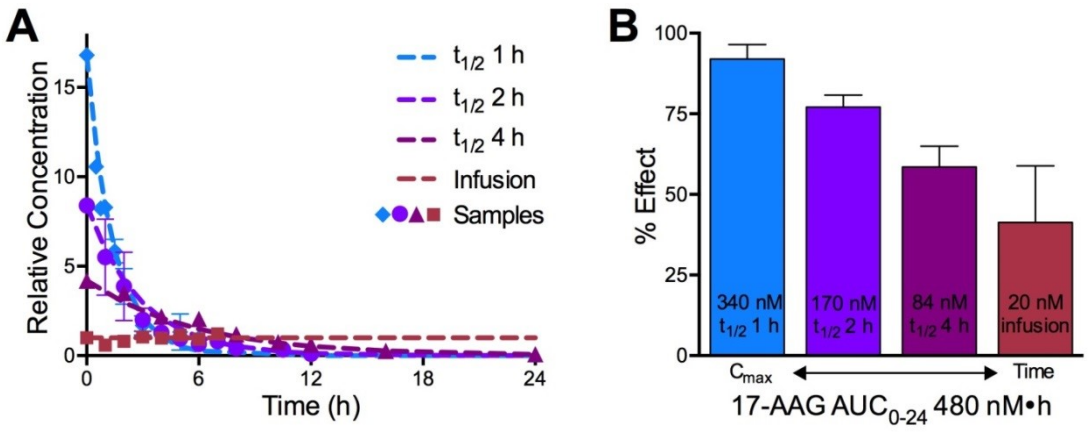

Figure 34. 17-AAG is most effective dosed with the highest peak and shortest half-life.

Trypanosomes were exposed to the same total AUC of 17-AAG of 480 nM•h over 24 h with $t_{1/2}$ 1 h (*blue*), 2 h (*lavender*), 4 h (*violet*), or as a constant infusion (*red*). *(A)* Pharmacokinetics were confirmed by sampling (*symbols*) cartridges for all regimens. *(B)* 17-AAG at an $AUC_{0\text{-}24}$ of 480 nM•h was most effective with the highest peak concentration and shortest half-life (340 nM, $t_{1/2}$ 1 h) and least effective as a constant infusion of 20 nM. *Mean±range/SD, n≥2*.

Three Hsp90 Inhibitors from Different Chemical Classes are Concentration-driven. There are multiple different chemical classes of Hsp90 inhibitors in the clinic. The ansamycins (e.g. 17-AAG) were the original class to enter clinical development; however, the most promising candidates are now from the resorcinol and purine scaffolds (Fig. 4). The intrinsic PK driver was tested for the ansamycin 17-DMAG, the resorcinol NVP-AUY922, and the purine-based CUDC-305 (Fig. 35). Each of these Hsp90 inhibitors, with very different chemical structures, were more

efficacious dosed as a C_{max}-intensive regimen ($t_{1/2}$ 1 h) than as a time-intensive constant infusion (Fig. 35). This suggests a class wide concentration-driven activity for Hsp90 inhibitors, regardless of chemical structure.

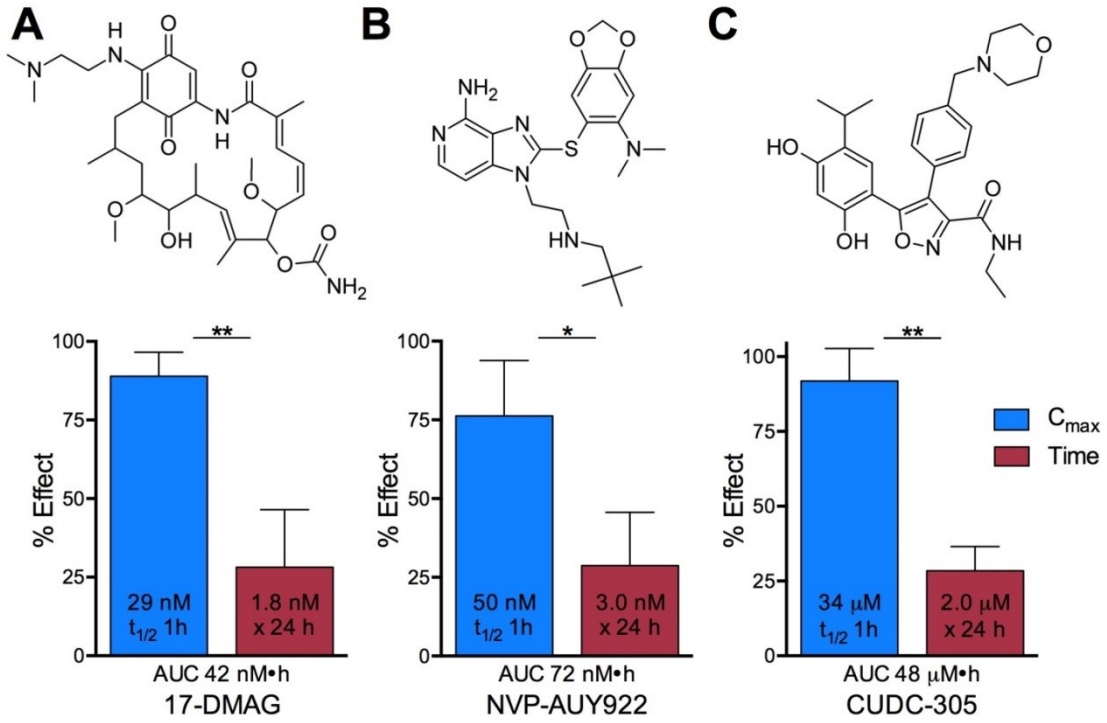

Figure 35. Hsp90 inhibitors from three chemical scaffolds are concentration-driven.

The same $AUC_{0\text{-}24}$ was more effective dosed as a C_{max}-intensive regimen (*blue*, $t_{1/2}$ 1 h) than as a time-intensive constant infusion (*red*). *(A)* Benzoquinone ansamycin 17-DMAG, *(B)* resorcinol NVP-AUY922, *(C)* purine CUDC-305.

DISCUSSION

In vitro PK-PD methodologies are valuable translational tools for studying drugs. However, in order to be able to study in vitro PK-PD a system is needed that provides robust maintenance of the organism of interest, recovery for PD purposes, and accurate and reproducible delivery of adjustable PK profiles. With trypanosomes we encountered difficulty with either retaining and supporting robust growth, or recovering accurate numbers of cells. The other foremost difficulty was obtaining the PK profiles we desired to study. Without large porous surface areas, diffusion did not produce rapid equilibration between extra-membrane/fiber and luminal spaces. Reversible drug binding to system components also greatly hindered attainment of correct peaks and then rapid dilution of drug. These problems were solved by pre-incubating cartridges to reach equilibrium at free desired t_0 levels, and then active pumping of drug PK profiles into the space containing trypanosomes (the extra-fiber space) and then across the porous fiber membranes and out to waste. In this set-up, the fibers act as a filter retaining the trypanosomes but allowing drug and medium components to pass through. Although this system places trypanosomes under a constant flow pressure, at the flow rate used (0.45 mL/min) trypanosome growth was equivalent to that of control populations in flasks (Fig. 29), and constant fluid flow is the in vivo condition of trypanosomes in the bloodstream.

17-AAG has potent activity against African trypanosomes. This activity is a function of the shape of the exposure, as separate dose-response curves are generated based on dosing that is either C_{max}- or time-intensive (Fig. 33). The activity of 17-AAG is concentration-driven. When delivered as high peak concentrations (with $t_{1/2}$ 1 h) 17-AAG is even more 'potent' than constant concentration infusions, generating the same effect with a three-fold lower AUC or total exposure to drug. In other words, C_{max} dosing is more efficient than infusion dosing, as a lower total exposure to 17-AAG is needed for maximal efficacy against trypanosomes. If the AUC of 17-AAG is on the linear portion of the dose-response curves, changing the shape of the AUC in these contrasting ways can mean the difference between almost no activity as a constant infusion

but almost complete activity as a high C_{max} $t_{1/2}$ 1 h. The versatility of in vitro hollow fiber PK-PD systems allowed us to generate these contrasting shapes and to explore artificial PK conditions. For a single AUC, the half-life was varied from 1, to 2, to 4 h, and compared to constant infusion dosing. The efficacy decreased with increasing half-life and therefore decreasing C_{max} (Fig. 34). Peak concentration is the strongest driver of 17-AAG efficacy. This experiment has an important implication: for a given drug, there will be optimal PK properties that produce the shape of exposure resulting in most efficient activity.

17-DMAG is a structurally similar benzoquinone to 17-AAG, with increased water solubility and increased potency and selectivity for trypanosomes (30). 17-DMAG, like 17-AAG, is concentration-driven against trypanosomes. C_{max}-intensive ($t_{1/2}$ 1 h) regimens were significantly more effective than time-intensive (constant infusion) regimens in the cartridge (Fig. 35A). Both 17-AAG and 17-DMAG have $t_{1/2}$s of approximately 1 h in mice (49,104), and were able to cure mice of an acute trypanosome infection with Q24 h dosing (30). The C_{max}-driven activity observed in the cartridge provides rationale for the efficacy of once daily dosing in mice. These results show that a single dose with a $t_{1/2}$ 1 h within the 24 h dosing interval would be more efficacious than delivering the drug in alternative methods to maintain levels above a threshold.

The intrinsic PK driver was identified for a further two Hsp90 inhibitors from very different chemical classes. The resorcinol NVP-AUY922 was chosen due to its experience in the clinic (24), and the purine CUDC-305 chosen for its reported blood-brain barrier penetration (a requirement for second-stage trypanosomiasis drugs) (42). Both Hsp90 inhibitors were concentration-drive. For the same AUC dosed in the contrasting ways of a constant infusion or as a C_{max} with $t_{1/2}$ 1 h, the C_{max}-intensive regimen was significantly more efficacious (Fig. 35). The benzoquinone ansamycins, resorcinols, and the purines all bind in the ATP binding pocket of Hsp90 (24). The shared driver observed with compounds from all three chemical scaffolds may suggest a class-wide PK driver of Hsp90 inhibitor anti-trypanosomal activity, as defined by the

target not chemical structure. If there is development of inhibitors specific for HSP83 (Hsp90), then they too may be concentration-driven. This knowledge provides rationale for target PK properties of specific inhibitors. To generate high peak concentrations that are rapidly cleared, prompt and efficient absorption is vital for oral formulations, and short half-lives are preferred over long half-lives. Moreover, this class wide PK driver of Hsp90 inhibitor activity against trypanosomes can be used to assess in vivo dosing regimens for repurposing the Hsp90 inhibitors with clinical experience.

17-AAG, 17-DMAG, NVP-AUY922, and CUDC-305 have all been in human trials for oncology. Their concentration driven activity against trypanosomes suggests that intermittent dosing regimens obtaining high peak levels will be optimal for treating trypanosomiasis. 17-AAG has a relatively short half-life of 3 – 5 h in plasma (105), which according to cartridge results is a good match for antitrypanosomal activity. Unfortunately, not as good a match for their concentration-dependence, CUDC-305 has a longer half-life of 10-20 h (106), and 17-DMAG and NVP-AUY922 have terminal $t_{1/2}$s of 20 and 60 h respectively (102,107). 17-AAG, 17-DMAG, and NVP-AUY922 all have nanomolar potencies against trypanosomes, and their maximally tolerated doses in oncology trials give C_{max} and AUCs in plasma in the micromolar range, well above what is needed for trypanosomal activity whether dosing is time- or concentration-intensive. Specifically, in oncology trials, the MTD of 17-AAG is 300-450 mg/m^2 (once weekly) giving C_{max} 15 μM and AUC 50 μM•h (105,108), the MTD of 17-DMAG is 20 mg/m^2 (twice weekly) giving C_{max} 1 μM and AUC 4 μM•h (102,109), and the MTD of NVP-AUY922 is 70 mg/m^2 (once weekly) giving C_{max} 3 μM and AUC 30 μM•h (107), in plasma. In second stage disease, trypanosomes cross the blood-brain barrier in humans. In mice, 17-AAG and 17-DMAG do enter the brain, achieving a C_{max} one third and one tenth that of plasma, and a total AUC one half and equal to that of plasma, respectively (49,104). If this is also the case in humans, 17-AAG and 17-DMAG, given their potency, may be able to achieve sufficiently high concentrations in the brain to be effective against second-stage HAT; however, differential

protein binding in tissue versus plasma may impact the AUC achieved in brain interstitial fluid. Although the long half-life of 17-DMAG is not ideal for its use as an antitrypanosomal, it does have the highly desirable property of being orally bioavailable (in mice, 50%) (49). CUDC-305 is also orally bioavailable, and impressively in mice achieves a four-fold higher AUC in brain than in plasma (42). In favor of its optimal antitrypanosomal PK shape, in mice it is cleared faster from the brain than plasma (4 vs 8 h half-life), and also cleared rapidly from tissues (2 h half-life in liver) (42). Unfortunately, it is not highly potent against trypanosomes, with an EC_{50} of 3 μM in cytotoxicity assays. In human oncology phase I trials, the MTD for daily dosing was 1000 mg, which led to a plasma C_{max} of 0.5 μM for parent, and 2 μM for the active demethylated metabolite, not promising for antitrypanosomal indications (106). More encouragingly the incidence of grade 3 adverse events (notably asthenia) decreased with dosing every second day. If the brain exposures in humans are similarly larger, and with a faster clearance than plasma, as in mice, then CUDC-305 may just have potential activity for second-stage HAT. However, large amounts of drug would need to be given. This is not without precedent in trypanosomes, DFMO is clinically used for second-stage HAT and has an EC_{50} of 20 μM in vitro and is given in large gram quantities in humans (110).

Pharmacokinetic-pharmacodynamic relationships not only apply to desired drug activities, but also to undesirable toxicities. One concern with the ansamycin Hsp90 inhibitors is their hepatotoxicity, caused by the benzoquinone moiety (111). Intriguingly, hepatotoxicity was the major adverse event seen in 17-AAG clinical trials when dosing favored a time-intensive exposure, given once daily, and was not a major toxicity when dosed twice or once weekly (101,105). This time-driven toxicity is in contrast to concentration-driven activity against trypanosomes. A second toxicity seen with Hsp90 inhibitors is vision disturbance, in particular night blindness. This has been most frequently observed with 17-DMAG and NVP-AUY922 (102,107), and not seen with 17-AAG or the resorcinol STA-9090 (112). In a rat study of retinal damage from Hsp90 inhibitors, this difference in toxicity was correlated with the clearance of

these inhibitors from the retina, as 17-DMAG and NVP-AUY922 had a much longer retention (112). This may suggest, that like 17-AAG hepatotoxicity, this is a time-driven effect. Hsp90 inhibitors with PK properties that lead to high peak concentrations that are rapidly cleared will optimize activity against trypanosomes, and may minimize undesired toxicities.

With the many Hsp90 inhibitors that have been in clinical trials or developed by academia and industry, there are several potential compounds that may have optimal PK properties for antitrypanosomal use. For example, the clinically tested resorcinols STA-9090 and KW-2478 have half-lives of 7.5 and 6 h respectively (113,114), shorter than that of NVP-AUY922. The purine based Hsp90 inhibitor BIIB021 and its metabolites have half-lives of just 0.5 – 2 h, which would provide C_{max}-intensive exposures (115). NVP-BEP800 is a potent Hsp90 inhibitor developed from fragment based screening and has a novel scaffold, with a 2-aminotheinopyrimidine (116). Pre-clinical data in mice show oral bioavailability, brain penetration (concentrations are one fifth to one tenth that of plasma), and rapid clearance from plasma, liver, and brain ($t_{1/2}$ 1-3h) (116). Understanding the optimal PK shape of Hsp90 inhibitors for optimal PD against trypanosomes provides a valuable criterion for judging potential candidates.

PK-PD relationships are an essential part of understanding the activity of a drug, and the optimal way to utilize it. Hsp90 inhibitors have shown promising activity against protozoan parasites, including *T. brucei*, with the ability to cure in vivo model infections. Using in vitro PK-PD with artificial PK conditions, Hsp90 inhibitors from each of the three major chemical classes all had concentration-driven activity against *T. brucei*. The Hsp90 inhibitors are more efficiently dosed against trypanosomes by transient high peak concentrations than by constant levels above a threshold. This provides parameters for ideal pharmacological properties for future development of specific HSP83 inhibitors. It also provides valuable rationale to assess the feasibility of repurposing clinically used Hsp90 inhibitors and to design dosing regimens with the greatest likelihood of success against HAT.

CHAPTER IV. Shape of the concentration-time curve drives potency: in vitro study of antitrypanosomal pharmacokinetic-pharmacodynamics

INTRODUCTION

T. brucei is an extracellular flagellated and highly motile single-celled eukaryotic parasite spread by the tsetse fly vector in sub-Saharan Africa, subspecies of which cause human African trypanosomiasis (sleeping sickness). In early disease parasites infect the periphery, then subsequently invade the CNS, causing fatality if untreated (2). Epidemics in the early twentieth century killed an estimated 800,000 people before pioneering drug discovery efforts produced several antitrypanosomals, among the very first of the anti-infective drugs (1). Suramin, pentamidine, and melarsoprol, all introduced between 1920 and 1950, remain in use (chemical structures of antitrypanosomals, Fig. 36). All three require lengthy courses of injections and have severe toxicities. The trivalent organic arsenical melarsoprol is particularly toxic, causing a fatal encephalopathy in 2-10% of recipients. Until the 1980s it was the best drug available to treat CNS disease. Despite its requirement for a lengthy dosing schedule, DFMO was repurposed

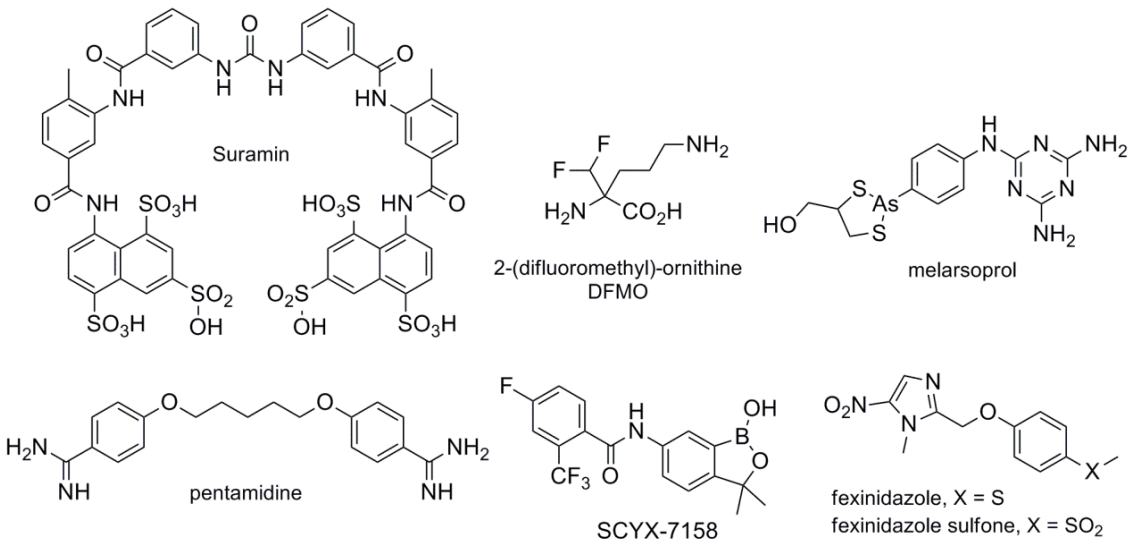

Figure 36. Structures of clinically used and experimental antitrypanosomal drugs.

from the cancer field and has largely replaced melarsoprol for late-stage west African infections. DFMO is ineffective against east African CNS disease, where melarsoprol remains the only option. In recent years concerted efforts to develop new treatments have resulted in two compounds in clinical trials. Fexinidazole is a nitro-heterocycle nearing completion of Phase II/III evaluation and benzoxaborole SCYX-7158 is in Phase I studies (117).

An in vitro hollow fiber cartridge system and experimental method to reveal the pharmacokinetic (PK) drivers of antitrypanosomal drugs was developed (Chapter III). Total exposure to a drug reflects both concentration and time. A given exposure can be achieved with very different concentration-time curves. For a given drug there is a preferred shape to that curve, where best efficacy is achieved with least total exposure. Understanding the preferred shape allows efficient and effective drug development, and provides a rational basis for dosing regimens in humans. The in vitro hollow fiber system and method was used to explore pharmacokinetic-pharmacodynamic (PK-PD) relationships for several classic antitrypanosomals and current clinical candidates. Dynamic in vitro PK-PD has not previously been explored for these agents. Knowledge of PK governance provides a rational basis for assessing and improving their dosing regimens.

MATERIALS AND METHODS

Cell Culture and Reagents. Bloodstream form *T. b. brucei* (MiTat 1.2 strain 427) was maintained in log growth at 37°C, 5% CO_2 in phenol red-free HMI9, 10% FBS, 10% Serum Plus (Sigma). Motile cells were counted by hemocytometer and light microscope. Drug stocks were stored aliquoted (-20°C): suramin (Mobay Chemical Corp.), pentamidine (American Pharmaceutical Partners), D,L-DFMO (National Cancer Institute (NCI) Developmental Therapeutics Program) in water; melarsoprol (Centers for Disease Control and Prevention) in 1,2-propanediol; SCYX-7158, fexinidazole (and sulfone), in DMSO. Using published methods (118-121) fexinidazole, fexinidazole sulfone, and SCYX-7158 were synthesized (Appendix). Tracers were U[^{3}H]suramin (42 Ci/mmol; Moravek) and [^{14}C]pentamidine (32 mCi/mmol; NCI).

Cartridge Assembly, PK Determination, and PK-PD Studies. Methods were as in Chapter III. Briefly, reservoirs and platinum-cured silicone tubing were autoclaved then assembled in a biosafety cabinet. Non-specific binding was assessed by determining concentration (bioassay or cognate radiolabeled tracer) over time of drug in HMI9 incubated in an isolated cartridge (C2025, FiberCell Systems) (Table 5). Prior to experiments, cartridges were pre-incubated with drug solutions calculated to achieve desired t_0 free drug concentrations (Table 5). Reservoirs, tubing, and cartridges were then filled with t_0 solutions, and flow rate set to 0.45 mL/min (IPC, Ismatec). PKs were first determined in the absence of parasites, sampling the extra-fiber space from the distal cartridge port. For C_{max} regimens, central reservoir volume was iteratively adjusted to provide desired $t_{1/2}$ (within 10% of 1 h; or pentamidine 1.7 h). For the fexinidazole infusion regimen, over 24 h a consistent loss of drug in tubing was observed between the infusion input reservoir and the cartridge. The reservoir concentration was increased to give the desired infusion concentration entering the cartridge. To achieve 20 μM, the infusion reservoir was at 66 μM to account for a 70% loss (Table 5). For PK-PDs, pre-incubation medium in cartridges was replaced with 10^5 cells/mL at t_0 drug concentrations, and incubated at 37°C, 5% CO_2. The culture used to inoculate cartridges was maintained in parallel flasks. Cells were harvested at 24 h and number of live parasites in drug-treated cartridges compared to that of untreated control cartridge.

Table 5. Antitrypanosomal non-specific binding and conditions to attain desired kinetics

Drug	Drug loss in cartridge (%)[a]	Cartridge pre-incubation[b]		Central reservoir volume (mL)[c]	Drug loss in tubing (%)[d]
		xt_0	duration (h)		
Suramin	50	2	2	25	0
DFMO	5	-	-	30	0
Melarsoprol	67	3	3	25	0
Pentamidine	90	10	1	13.5 ($t_{1/2}$ 1.7 h)	0
SCYX-7158	67	3	1	30	0
Fexinidazole	90	10	1	13.5	70
Fexinidazole sulfone	88	8	3	20	0

[a]Drug bound at equilibrium after incubation in an isolated cartridge with high drug concentration

[b]Conditions used for pre-incubation to compensate for nonspecific binding of drug to cartridge. Based on the percentage of drug lost, the indicated multiple (x) of the t_0 drug concentration was incubated in the cartridge for indicated duration before start of experiment

[c]Volume in central reservoir for C_{max} regimens to ensure $t_{1/2}$ of 1 h in extra-fiber space of cartridge

[d]Drug loss between the input reservoir and point of entry into cartridge. Fexinidazole infusion input concentrations were increased to account for 70% loss

Drug Cytotoxicity and Concentration Bio-assays. Cytotoxicity assays in 96 well plates used an established acid phosphatase-based method (Chapter I)(39). By this method PK samples were bioassayed, comparing cytotoxicity of unknowns with a standard curve of drug concentrations.

Time-kill and Reversibility. $2x10^5$ cells/mL in 24-well plates were exposed to 20x EC_{99} (except fexinidazole, 5x EC_{99}) for 6 h then split. One population remained in drug; the other was washed thrice in drug-free medium (>4000x drug dilution). Cells were counted by hemocytometer.

Statistical Analysis. Unpaired, two-tailed, equal variance Student's *t*-test assessed significance.

Design to Determine Kinetic Driver of Efficacy. PK-PD studies comprised three cartridges: one no-drug control and two drug-treated, with efficacy based on counting motile parasites at 24 h. Starting density of 10^5 cells/mL resulted in log growth of control cells for 24 h. Cells in the treated cartridges had the same total drug exposure (dose, or $AUC_{0\text{-}24}$), deployed as either a steady infusion of a constant concentration ("time-intensive") or as a contrastingly high peak concentration with $t_{1/2}$ 1 h ("C_{max}-intensive")(Fig. 37*A*). Pharmacokinetics of C_{max} regimens were confirmed in the extra-fiber space of the cartridge for all drugs (Fig. 37*B*). To diagnose the intrinsic PK driver, initially an $AUC_{0\text{-}24}$ was chosen where efficacy of the infusion was in the linear dose-response range, typically around 50%. This allowed detection of a positive or negative efficacy shift in the comparator C_{max}-intensive regimen. The artificial $t_{1/2}$ 1 h yields a 16.8-fold greater C_{max} than the infusion, and concentration drops by 98% over 6 h, the length of one cell cycle of *T. brucei* (Fig. 37*A*). The infusion also allowed direct comparison with the same concentration in microtiter plate assays (Fig. 38). Suramin, pentamidine, SCYX-7158, and fexinidazole sulfone infusions in the cartridge were more effective than the same concentrations in plates, DFMO and melarsoprol had equivalent efficacies, and fexinidazole was less effective in

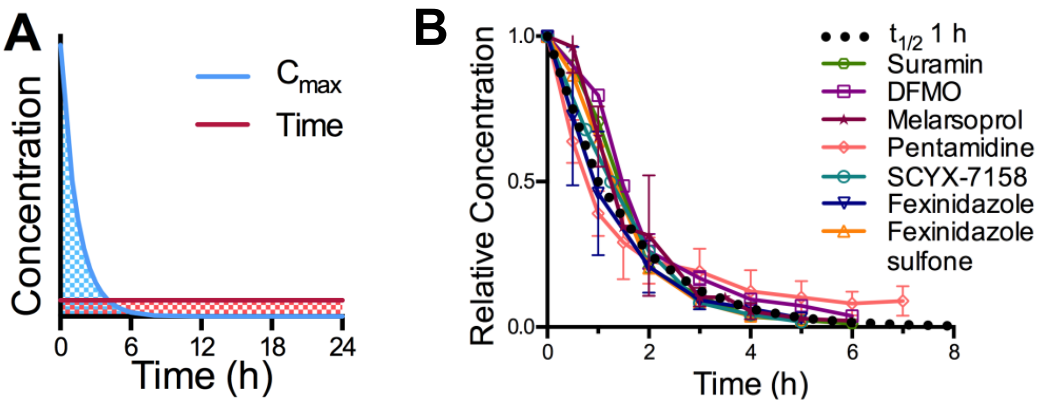

Figure 37. PK of antitrypanosomals in hollow-fiber cartridges

(*A*) Two cartridges are exposed to the same $AUC_{0\text{-}24}$ (*shaded*), but in contrasting regimens as either a high peak with $t_{1/2}$ 1h (*blue*) or as a constant infusion (*red*). (*B*) For C_{max} regimens actual PKs of indicated drugs obtained from the extra-fiber space were assayed in two or more experiments, and achieved $t_{1/2}$ within 10% of 1 h (*dotted curve*), except pentamidine which achieved and was studied at $t_{1/2}$ 1.7 h. *Mean±SD* for $n \geq 3$.

the cartridge. Efficacy in the cartridge may be enhanced by constant provision of fresh drug (two hundred-fold greater total mass of drug passed by cells in the cartridge versus in wells), or alternatively may be hindered by fresh nutrients and removal of waste. In any case it is likely that cartridge conditions more closely mimic those in vivo.

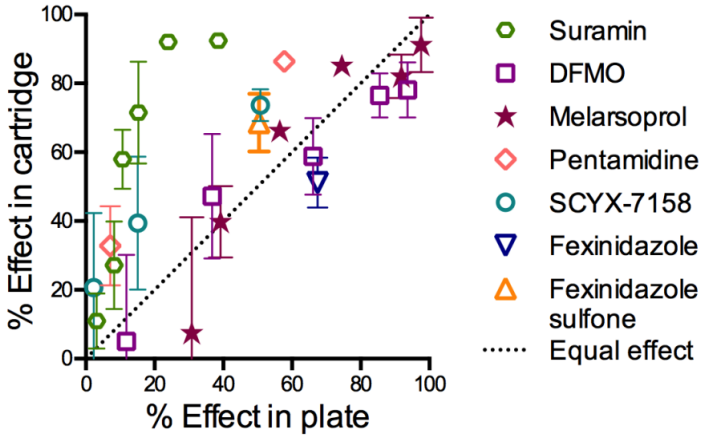

Figure 38. Comparison of efficacy in cartridge versus microtiter plate

Efficacy relative to no drug control in the cartridge system of constant infusions of drug compared to efficacy of the same concentration in microtiter plate assays. *Mean±SD,* for $n \geq 3$.

Suramin Efficacy is Driven by Peak Concentration. Suramin, an antitrypanosomal introduced in the 1920s, was examined in the dynamic in vitro PK-PD system. A time-intensive constant infusion of 0.3 μM over 24 h caused 58% reduction in final cell number compared to drug-free controls. The same total $AUC_{0\text{-}24}$ applied as a 5.0 μM C_{max} with $t_{1/2}$ 1 h resulted in 98% reduction (Fig. 39*A*). Thus, for the same drug exposure, efficacy was nearly doubled by simply changing the shape of the AUC to favor peak concentration (Fig. 37*A*). Suramin is concentration-driven and does not require sustained levels for efficacy, a finding that held with human pathogenic subspecies *T. b. gambiense* (Fig. 40). To further investigate PK-PD, a wide $AUC_{0\text{-}24}$ range was tested, dosed either with $t_{1/2}$ 1 h or as an infusion, and two complete exposure-response curves were generated for these contrasting regimens (Fig. 39*B*). The linear response range of the curves was widely separated, systematically favoring C_{max}- over time-intensive dosing. Vertically, for the

same AUC, a substantial gain was achieved by C_{max} regimens: for example, 85% efficacy at AUC_{0-24} 5 μM•h versus 15% for infusion. Horizontally, suramin was 2-fold more 'potent' if applied to favor C_{max}: EA_{50} values (AUC_{0-24} that gives 50% response) were 3.6 μM•h for C_{max} but 7.2 μM•h for time. Likewise, and notably, concentration-intensive dosing achieved maximal efficacy with a 2-fold lower total dose (AUC_{0-24}).

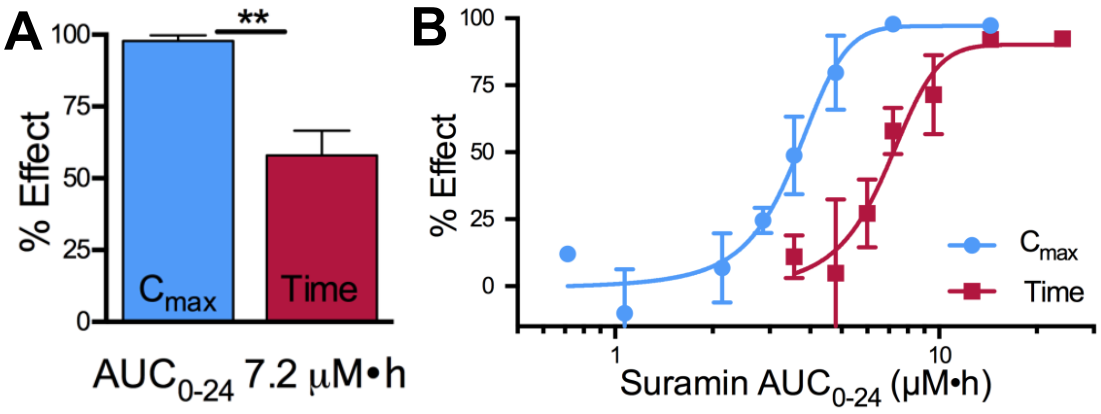

Figure 39. Suramin is more efficacious when dosed to favor high peak concentration.

(A) Suramin AUC_{0-24} of 7.2 μM•h applied as a high C_{max} of 5.0 μM with $t_{1/2}$ 1 h (*blue*) or as a constant infusion of 0.30 μM (*red*), ** p<0.01. (*B*) Exposure-response curves. Suramin was applied as high C_{max} with $t_{1/2}$ 1 h (*blue*, EA_{50} 3.7 μM•h) or as a constant infusion (*red*, EA_{50} 7.2 μM•h), across a range of AUC_{0-24}. Percent effect is reduction at 24 h in trypanosome count compared to untreated control cartridge. *Mean±SD* for $n \geq 3$.

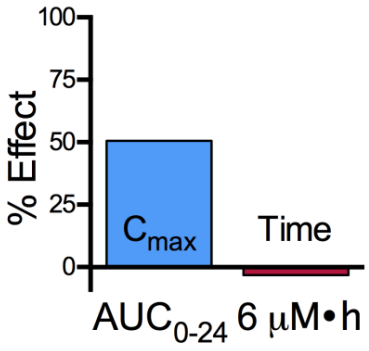

Figure 40. Suramin is concentration-driven against *T. b. gambiense*.

Reduction in cell number of *T. b. gambiense* (strain 348 BT) at 24 h for AUC_{0-24} 6 μM•h, applied as a high C_{max} of 4.2 μM with $t_{1/2}$ 1 h (*blue*) or constant infusion of 0.25 μM (*red*). Cells were adapted in HMI9, doubling time 6 h. n = 1

DFMO Efficacy is Driven by Time of Exposure. DFMO at an $AUC_{0\text{-}24}$ of 2400 μM•h was 76% effective as a time-intensive infusion, but only 55% effective as high C_{max} with $t_{1/2}$ 1 h (p<0.05, Fig. 41). Thus, in contrast to suramin, the antiparasitic activity of DFMO is time- rather than peak concentration-driven. DFMO infusions had an EA_{50} of 600 μM•h versus 1500 μM•h for C_{max} dosing (Fig. 41), a 2.5-fold 'potency' difference. The exposure-response curves had shallow slopes, and for the same $AUC_{0\text{-}24}$ greatest vertical difference in efficacies was 25 points. Interestingly this difference was maintained at the maxima, such that C_{max} dosing achieved at best only a 55% reduction in parasite count, whereas infusion dosing reached 80%. By all measures DFMO is most advantageously applied to maintain concentrations over time rather than to favor peak concentration, and sustained levels are necessary for maximum effect.

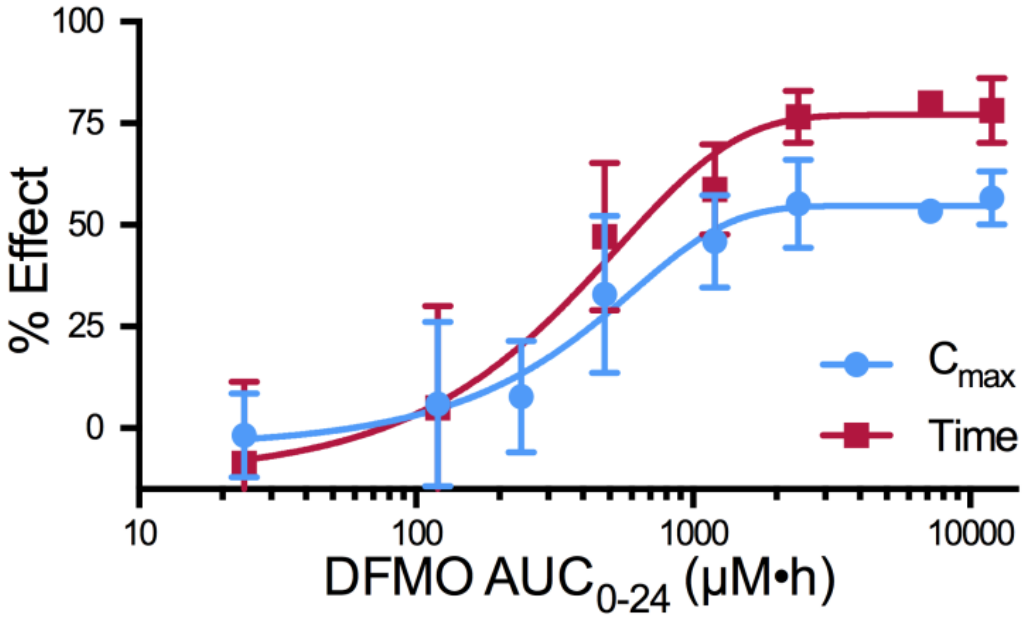

Figure 41. DFMO efficacy is time-driven.

Across three logs of $AUC_{0\text{-}24}$, the efficacy of a time-intensive constant infusion (*red,* EA_{50} 600 μM•h) was compared to that of a short-lived high C_{max}, $t_{1/2}$ 1 h (*blue*, EA_{50} 1500 μM•h). Percent effect is cell count reduction versus controls. *Mean±SD* for $n \geq 3$.

Melarsoprol, Pentamidine, SCYX-7158, and Fexinidazole are Concentration-Driven. The remaining antitrypanosomals studied were all significantly more efficacious with C_{max}-intensive dosing rather than time-intensive infusions (Fig. 42). Fexinidazole in vivo is metabolized to a sulfoxide and then sulfone, both active. The PK driver of fexinidazole sulfone was tested, which as for parent fexinidazole was concentration-driven (Fig. 42), consistent with the class-wide kinetic governance of other anti-infectives (90).

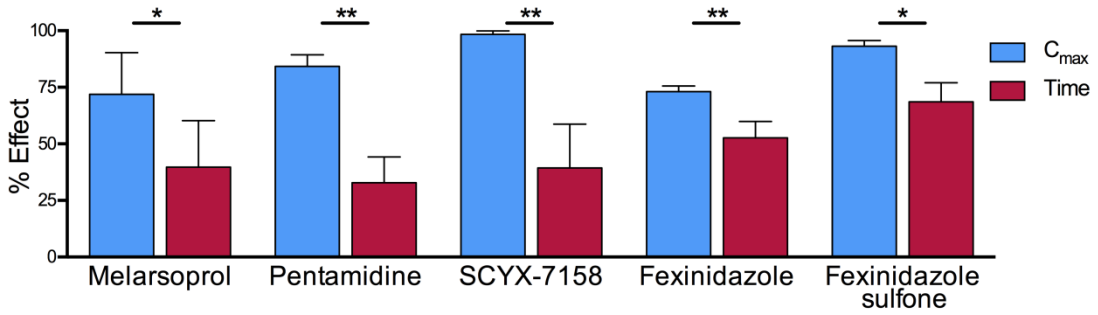

Figure 42. Melarsoprol, pentamidine, SCYX-7158, fexinidazole, and fexinidazole sulfone are concentration-driven.

A given $AUC_{0\text{-}24}$ was applied as a transient high concentration (*blue*) or as a constant infusion (*red*). Unless indicated otherwise, $t_{1/2}$ 1 h for C_{max} regimens. Conditions were ($AUC_{0\text{-}24}$; C_{max}, Infusion): melarsoprol (310 nM•h; 220 nM, 13 nM), pentamidine (53 nM•h; 22 nM $t_{1/2}$ 1.7 h, 2.2 nM), SCYX-7158 (24 μM•h; 17 μM, 1 μM), fexinidazole (480 μM•h; 336 μM, 20 μM), and fexinidazole sulfone (110 μM•h; 80 μM, 4.8 μM). Percent effect is cell count reduction versus controls. *Mean±SD*, $n \geq 3$; * $p<0.05$, ** $p<0.01$.

Time-kill and Reversibility of Drug Action. As C_{max} regimens have relatively transient drug levels, concentration-driven compounds likely rapidly initiate cell-killing, or have a significant post-antiparasitic effect. To assess some of these factors trypanosomes were exposed in plates to drug, with either wash-out at 6 h or maintained presence, and cell viability determined over 48 h by counting motile cells. Concentrations were high, 20-times the microtiter plate EC_{99} (~peak

concentration of an equivalent C_{max} cartridge regimen), and reversibility was analyzed after 6 h (one doubling time). (Fexinidazole was just 5-times the EC_{99} due to solubility limits.)

Each drug had a distinctive time-effect profile, with different rates of growth inhibition, cell killing, and post-drug effect (Fig. 43). Melarsoprol, fexinidazole sulfone, SCYX-7158, pentamidine, and suramin (in order of onset time and log kill rate) were all cytocidal ('cidal) at these exposures, causing a progressive fall in cell number whether drug concentrations were sustained for 48 h or pulsed for 6 h then chased for 42 h. Both pentamidine and suramin exhibited delayed death effects. In contrast, fexinidazole and DFMO were cytostatic ('static): growth resumed after drug was washed away. In 10 mM DFMO onset of action was slow, with trypanosomes continuing to increase for 12 h, then stopping, but not declining. Fexinidazole caused immediate arrest and if maintained cell numbers slowly declined; on wash-out at 6 h there were several further hours of post-antiparasitic effect before growth resumed at 10 h.

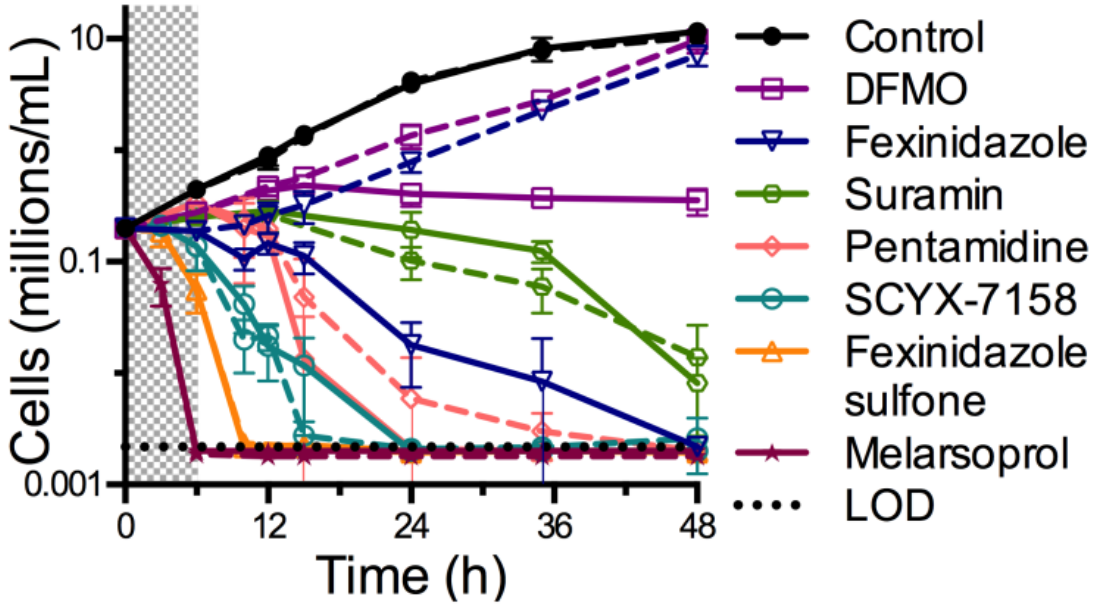

Figure 43. Time-kill and reversibility of antitrypanosomals.

Trypanosomes were exposed to high concentrations of the indicated drugs, either continuously (*solid lines*) or for a 6 h period then washed (*shaded grey interval, dotted lines*). Motile cells were counted at indicated time points over 48 h. *LOD*, limit of detection, 0.0025 million cells/mL. *Mean±SD* for $n \geq 3$.

DISCUSSION

In order to identify the intrinsic PK driver of drug efficacy sharply contrasting shapes of exposure were generated with artificial kinetics. By plotting AUC-response curves based on the shape of exposure delivered (Fig. 39*B* and Fig. 41) information was captured that is unattainable through conventional in vitro assays, and not readily obtained in vivo. The results were highly informative. Shape of the AUC determines 'potency' and efficacy, with clear separation between the response curves of C_{max}- or time-intensive regimens. Suramin and DFMO were governed by opposite drivers, and their curves had various slopes and separations, suggesting that each drug is uniquely affected by shape of exposure changes. Vertical separation of AUC-response curves highlights the efficacy that is gained from an optimally shaped exposure. Horizontal separation reflects differences in potency: the exposure required for equi-efficacy. Importantly, maximal efficacy is achieved with lower total AUC when the PK driver is favored. In fact, time-intensive dosing was necessary for DFMO to achieve maximal efficacy. C_{max}-dosing yielded a lower efficacy plateau, perhaps reflecting DFMO's static nature and inability to eradicate parasites (Fig. 41 and Fig. 43). The AUC-response curves reveal that each drug has intrinsic PK-PD governance, a fundamental kinetic driver of antitrypanosomal activity, and therefore ideal PK properties for optimal potency and efficacy.

Melarsoprol, pentamidine, SCYX-7158, and fexinidazole all had greater activity deployed as a high C_{max} regimen (Fig. 42). Though most of these drugs were 'cidal, fexinidazole had 'static activity (Fig. 43), demonstrating that concentration- or time-driven efficacy does not equate with 'cidal or 'static activity, as is recognized for antibacterials (90). As C_{max} regimens in the cartridge incorporate immediate, delayed, and post-drug effects, fexinidazole's C_{max} governance may reflect the early onset arrest and then significant post-antiparasitic delay in cell growth (Fig. 43). Interestingly fexinidazole sulfone, like parent, was concentration-driven, but unlike parent it was 'cidal (Fig. 42 and Fig. 43). The PK driver of a drug is an empirical description that captures the sum of multiple factors. For all drugs studied a significant separation between the efficacies of C_{max}- or time- intensive regimens was observed (Fig. 39-41); however, the degree of separation

differed, and it is possible that for some drugs there would be insignificant separation. Testing a single AUC in the two contrasting ways allows efficient diagnosis of the preferred kinetic driver, and full exposure-response curves provide even greater insight.

These findings have important inferences for drug development and clinical use. In vitro PK-PD is particularly valuable for trypanosomes, as resource-limited remote settings and invasive diagnostic procedures make human studies unusually challenging. In early-stage drug development knowledge of the intrinsic PK driver can inform lead candidate choice and PK property optimization. In vivo, although the complexity of living systems (tissue specific PK, protein binding, and immune effects, for example) will change the absolute values of concentration and AUC required for efficacy, knowing the optimal shape of exposure is a simple and powerful guide for assessing a dosing regimen. Time-dependency predicts that concentrations must be sustained for best efficacy in vivo, whereas concentration-driven efficacy predicts intermittent dosing achieving high peaks will be optimal.

DFMO was the only time-driven drug, and reported results from in vivo studies support this finding. In mice, multiple day dosing of DFMO in the drinking water is required for cure (122,123). The inopportune 3.5 h half-life of DFMO in humans requires frequent dosing to maintain concentrations (124), and efforts to dose every 12 h instead of 6 h resulted in greater frequency of relapse (125). DFMO is now most commonly given every 12 h in combination with nifurtimox. Clinical trials have demonstrated non-inferiority of this combination to monotherapy (126); however, given the in vitro findings that DFMO resistance can be selected by exposure to low DFMO concentrations and that nifurtimox and DFMO are antagonistic (127), time-driven efficacy suggests a return to dosing DFMO every 6 h in the combination may lower the risk of efficacy failure or emergence of resistance.

The classic drugs, suramin, pentamidine, and melarsoprol, were originally established with lengthy dosing regimens and little PK-PD knowledge. The need to optimize and shorten these regimens is recognized (110). These results of concentration-driven efficacy provide rationale for this, and are supported by in vivo evidence. A single dose of each of these drugs can be curative in mice, and clear trypanosomes from human body fluids, indicating long exposures are not necessary for activity (3,128-130). In *T. b. gambiense*-infected guinea pigs, single dose pentamidine (5 mg/kg) was curative, but when split into ten twice weekly doses animals relapsed (129). Early investigators of suramin and melarsoprol concluded initial large doses were the most important determinant of efficacy and potentially sufficient for cure in humans (131-133). As suramin and pentamidine are effective against early-stage infection, concentration-driven efficacy suggests their activity in blood may stem from the peak of their biphasic distributions (134,135). Melarsoprol however is used against CNS infection, so concentration-driven efficacy would predict high peaks in that compartment would enhance efficacy. Melarsoprol's regimen has already been revised to just 10 consecutive daily doses (136); from our findings this might be improved further by administering fewer but larger doses. Melarsoprol toxicity, an important concern, will also have a PK-PD component. Intriguingly, doubling the starting dose from 1.8 to 3.6 mg/kg decreased the incidence of reactive encephalopathy (137), and in a leukemia trial neurotoxicity was only seen in the second week of injections, perhaps a time-driven effect (8). In any optimization of dosing, the PK-PD relationship for efficacy must be balanced with those for toxicities, and when possible discrepant drivers should be exploited to favor efficacy and minimize side-effects.

Oxaborole SCYX-7158 is in early clinical development. In the cartridge it was optimally dosed by C_{max}-intensive regimens (Fig. 42). This seems inconsistent with previous in vitro results that an AUC 41 μM•h given as 1.7 μM for 24 h was irreversible (at 72 h), whereas the same AUC as 6.8 μM for 6 h was reversible (138,139). However, higher concentrations of SCYX-7158 can be 'cidal on exposures of 6 h or less (Fig. 43)(138). In the cartridge an $AUC_{0\text{-}24}$ of just 24 μM•h distributed as a 17 μM peak with $t_{1/2}$ 1 h caused maximal effect (Fig. 42). This highlights the

importance of studying dynamic AUC shapes. SCYX-7158 has been tested in mouse models of early- and late-stage trypanosomiasis. Its 26 h plasma half-life makes it impossible to restructure the AUC in vivo so as to generate high peaks that are rapidly cleared (138). However, in mouse brain tissue the half-life is closer to 4 h (139). In Phase I trials SCYX-7158 had a 16 day plasma half-life in humans, again making short-lived peaks impossible (117). However, if CNS half-lives are substantially shorter as in rodents, cartridge results suggest achieving early high concentrations in the CNS will lead to clinical success.

Fexinidazole is efficacious in early- and late-stage murine models, and has progressed to Phase II/III trials (117,140-142). Both parent and active sulfone metabolite are concentration-driven (Fig. 42). Consonant with this finding, despite the short half-lives (≤2 h) of fexinidazole and its metabolites in mouse plasma (and likely similar in brain), in the mouse chronic infection model once-daily dosing with 200 mg/kg achieves greater cures than twice-daily dosing with 100 mg/kg (141,142). In humans plasma half-lives are longer, on the order of 10 h for fexinidazole and sulfoxide, and 25 h for the subsequent sulfone (140). The Phase II/III clinical trial assessing once daily doses relies on accumulation of, and sustained exposure to, the sulfone (simulated in Fig. 44)(140). Unfortunately, in mice the sulfone is the least brain-penetrant of the three moieties (141). Given the cartridge finding that high peaks are more effective than sustained levels, the regimen may better be deployed as larger doses on intermittent and fewer days, if tolerability allows. This would optimize the shape of exposure and resulting efficacy of all three compounds (simulations Fig. 44).

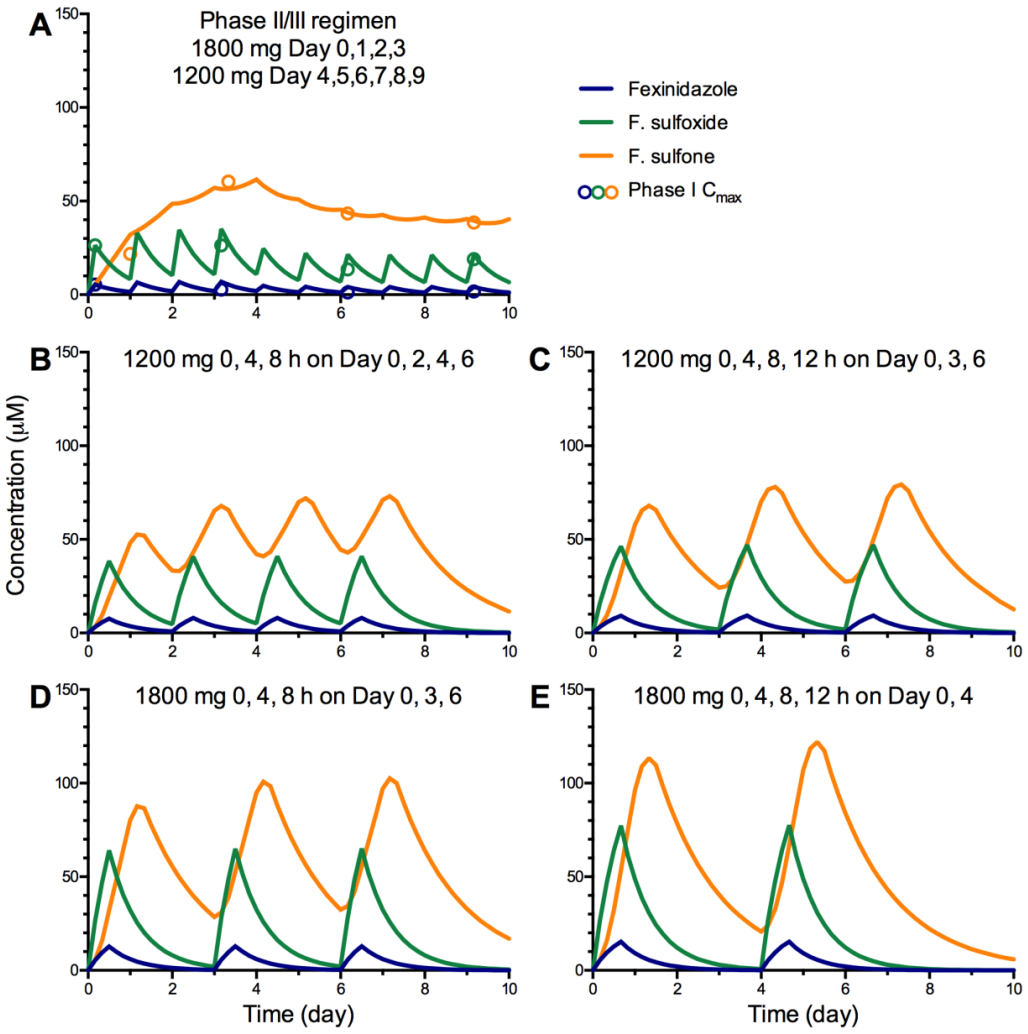

Figure 44. Simulations of alternative fexinidazole dosing regimens.

To generate higher peaks of all three metabolites the same total dose used in the Phase II/III regimen could be restructured as larger doses on intermittent days. As absorption is dose-limiting, the larger dose would need to be split over several administrations, here hypothetically given in 4 h intervals. These simulations illustrate how dose schedule can modify the shape of exposure, and are not intended as clinical recommendations. Simulations performed in Excel using approximate t_{max}, C_{max}, and $t_{1/2}$ values from Phase I study data (140) as follows: 1800 mg dose fexinidazole (4 h, 5.4 μM, 11 h), sulfoxide (4 h, 26 μM, 12 h), sulfone (24 h, 32 μM, 25 h); 1200 mg dose fexinidazole (4 h, 3.2 μM, 11 h), sulfoxide (4 h, 16 μM, 12 h), sulfone (24 h, 19 μM, 25 h). (*A*) Simulation of Phase II/III regimen of 1800 mg per day for four days, followed by 1200 mg per day for six days, total dose 14,400 mg. *Open circles*, reported C_{max} values (140). (*B*) Simulation of 1200 mg at 0, 4, and 8 h on Day 0, 2, 4, and 6, total dose 14,400 mg. (*C*) Simulation of 1200 mg at 0, 4, 8, and 12 h on Day 0, 3, and 6, total dose 14,400 mg. (*D*) Simulation of 1800 mg at 0, 4, and 8 h on Day 0, 3, and 6, total dose 16,200 mg. (*E*) Simulation of 1800 mg at 0, 4, 8, and 12 h on Day 0 and 4, total dose 14,400 mg.

Shape of the concentration-time curve is a critical determinant of antitrypanosomal efficacy. Clearly demonstrated by plotting exposure-response curves, maximal effect will be achieved with the least total drug exposure when the shape of the PK profile favors a drug's driver. Concentration- or time-driven efficacy is a useful simplification of a complex multidimensional relationship. The findings with five clinical, and two candidate, antitrypanosomals are consistent with reported in vivo results. This in vitro methodology is efficient, convenient, and versatile, particularly valuable for the resource-limited and clinically challenging field of antitrypanosomal chemotherapy. These concepts and approaches are likely also relevant for other therapeutic indications. In drug development, knowledge of the PK-PD governance can be used as selection criterion for leads and to direct development such that in vivo PK properties are matched with efficacy driver. Dynamic in vitro PK-PD is a powerful tool that can inform all stages of drug development and clinical use.

CONCLUDING REMARKS

This thesis details investigation into the pharmacology of Hsp90 inhibitors against *T. brucei*. Potent in vitro growth inhibition was discovered (Chapter I), and in particular disruption to both cytokinesis and kDNA replication (Chapter II). Phenotypes observed with RNAi knock-down of the trypanosome *HSP83* and putative mitochondrial *TbTRAP* were similar to the cell cycle aberrations seen with Hsp90 inhibitor treatment, validating target suppositions (Chapter II). To investigate dosing requirements, an in vitro PK-PD system was established for *T. brucei* (Chapter III and IV). Hsp90 inhibitors were significantly more efficacious against trypanosomes when dosed as transient high peaks rather than as prolonged lower concentrations (Chapter III), implying that long half-lives are not required for efficacy in vivo and that intermittent dosing regimens should be efficacious and in fact optimal. Intermittent once daily dosing of the short-lived inhibitor 17-DMAG was efficacious and able to cure mouse trypanosomiasis, including when dosed orally (Fig. 8).

The promising results with Hsp90 inhibitors provide further proof that repurposing oncology drugs is a viable drug development strategy for *T. brucei*. Despite a homologous target, a therapeutic index is possible due to divergent cell biology. RNAi results of disrupted cleavage furrow ingression and kDNA replication provide evidence of how within the unique context of the trypanosome inhibiting HSP83 has unique effects (Chapter II). Several groups have reported activity of Hsp90 inhibitors against protozoan parasites (143), and this work provides valuable supportive evidence that Hsp90 inhibitors can be effective anti-protozoals. Furthermore, novel insight has been gained of the roles of *T. brucei* HSP83 and putative mitochondrial TbTRAP.

Ultimately, therapeutic index is a question of dosing. In vivo, drug exposures are not static but have a dynamic concentration-time profile. For trypanosomes resource-limited remote

settings and invasive diagnostic procedures make human studies unusually challenging (1), therefore in vitro methods to study PK-PD are particularly valuable. A method to study dynamically changing concentration-time profiles against trypanosomes in vitro was developed. Several challenges were overcome, namely balancing robust growth of parasites with tractable PK. Shape of the drug exposure was demonstrated to be a vital determinant of antitrypanosomal efficacy. Conventionally, PK-PD is considered late in the drug development pathway after a drug has been introduced in vivo. In the antibiotic and antiviral field, in vitro PK-PD is increasingly recognized as an important contribution; however, PK-PD is simply used to model in vivo half-lives and predict clinical targets (28,29). In this thesis, artificial kinetics were employed and highlighted the fact that compounds have *intrinsic* drivers of efficacy, and therefore a certain shape of exposure which will allow maximal response for the least total exposure (Chapter III and IV). Both concentration and duration of drug exposure need to be considered as dynamic variables. The discrimination of compounds as either concentration- or time-driven as detailed in this thesis has important implications for target product profiles of lead candidates. Conventional methods used to investigate drug efficacy would be much enhanced by considering in vitro PK-PD from the earliest stages of drug development.

Hsp90 inhibitors were significantly more efficacious dosed in concentration-intensive rather than time-intensive exposures against trypanosomes, as were three of the clinically used antitrypanosomals and two current clinical candidates (Chapter III and IV). Importantly DFMO was found to be time-driven (Fig. 41). For 17-AAG, suramin, and DFMO the shape and magnitude of separation between delineated concentration- vs time-intensive exposure-response curves differed, revealing each drug has unique response to changes in shape of exposure (Chapter III and IV). Concentration- or time-driven efficacy is a useful simplification of the complex PK-PD multidimensional response-surface. What determines whether a drug will be concentration- or time-driven? Presumably it is some interplay between the kinetics of target inactivation and down-stream consequences in the cell. For DFMO, rapid reversibility of growth

inhibition on drug removal is likely the reason for time-driven efficacy (Fig. 43). Concentration-driven drugs in contrast likely initiate irreversible damage or have significant post-drug effects, as the drug effect outlasts the presence of the drug. For the Hsp90 inhibitors, even short exposures cause significant disruption of down-stream clients and pathways as evidenced by cell cycle lesions (Chapter II). As 9 out of the 10 drugs tested were concentration-driven, trypanosomes seem particularly prone to irreversible damage, likely due to the lack of cell cycle checkpoints and therefore insufficient time and resources to fully repair injury (19).

In vitro PK-PD results suggest that Hsp90 inhibitors with fast absorption rates and short half-lives in vivo will be ideal for antitrypanosomal use. Dosing regimens do not need to maintain drug levels, but rather achieve sufficient peaks. However, mouse results with 17-DMAG demonstrate that concentration-driven activity does not necessarily mean single dose cure (Fig. 8). Toxicity, always a vital consideration in drug dosing, may limit the AUC achievable with a single dose and pharmacological sanctuaries in tissues may enable trypanosomes to escape the peak of drug. Within a dosing interval concentration-intensive exposures will be the most efficacious, but repeated dosing may still be necessary for radical cure. 17-DMAG, despite a short $t_{1/2}$ of 1 h, was able to achieve cures with once daily multiple day dosing both intraperitoneally and orally.

In summary, this thesis research has enhanced understanding of *T. brucei* Hsp90s and the potential for use of Hsp90 inhibitors against trypanosomes. The development of an in vitro PK-PD system to study antitrypanosomals allows a greater understanding of efficacy and enhances translation of drugs.

APPENDICES

APPENDIX I

Alignment of *HSP83* coding sequences

Tb927.10.10890/10900/10910/10920/10930/10940/10950/10960/10970/10980 (69).

Synonymous variations highlighted in green, nonsynonymous variations highlighted in yellow, RNAi sequence in red

```
CLUSTAL O(1.2.1) multiple sequence alignment

Tb...10930      ATGACGGAGACATTCGCATTCCAGGCTGAAATCAATCAGCTAATGTCCCTTATTATTAAT   60
Tb...10970      ATGACGGAGACATTCGCATTCCAGGCTGAAATCAATCAGCTAATGTCCCTTATTATTAAT   60
Tb...10980      ATGACGGAGACATTCGCATTCCAGGCTGAAATCAATCAGCTAATGTCCCTTATTATTAAT   60
Tb...10960      ATGACGGAGACATTCGCATTCCAGGCTGAAATCAATCAGCTAATGTCCCTTATTATTAAT   60
Tb...10950      ATGACGGAGACATTCGCATTCCAGGCTGAAATCAATCAGCTAATGTCCCTTATTATTAAT   60
Tb...10940      ATGACGGAGACATTCGCATTCCAGGCTGAAATCAATCAGCTAATGTCCCTTATTATTAAT   60
Tb...10910      ATGACGGAGACATTCGCATTCCAGGCTGAAATCAATCAGCTAATGTCCCTTATTATTAAT   60
Tb...10920      ATGACGGAGACATTCGCATTCCAGGCTGAAATCAATCAGCTAATGTCCCTTATTATTAAT   60
Tb...10900      ATGACGGAGACATTCGCATTCCAGGCTGAAATCAATCAGCTAATGTCCCTTATTATTAAT   60
Tb...10890      ATGACGGAGACATTCGCATTCCAGGCTGAAATCAATCAGCTAATGTCCCTTATTATTAAT   60
                ************************************************************

Tb...10930      ACCTTCTATTCAAACAAGGAAATTTTTCTTCGCGAGCTAATTAGTAATTCGTCAGATGCG   120
Tb...10970      ACCTTCTATTCAAACAAGGAAATTTTTCTTCGCGAGCTAATTAGTAATTCGTCAGATGCG   120
Tb...10980      ACCTTCTATTCAAACAAGGAAATTTTTCTTCGCGAGCTAATTAGTAATTCGTCAGATGCG   120
Tb...10960      ACCTTCTATTCAAACAAGGAAATTTTTCTTCGCGAGCTAATTAGTAATTCGTCAGATGCG   120
Tb...10950      ACCTTCTATTCAAACAAGGAAATTTTTCTTCGCGAGCTAATTAGTAATTCGTCAGATGCG   120
Tb...10940      ACCTTCTATTCAAACAAGGAAATTTTTCTTCGCGAGCTAATTAGTAATTCGTCAGATGCG   120
Tb...10910      ACCTTCTATTCAAACAAGGAAATTTTTCTTCGCGAGCTAATTAGTAATTCGTCAGATGCG   120
Tb...10920      ACCTTCTATTCAAACAAGGAAATTTTTCTTCGCGAGCTAATTAGTAATTCGTCAGATGCG   120
Tb...10900      ACCTTCTATTCAAACAAGGAAATTTTTCTTCGCGAGCTAATTAGTAATTCGTCAGATGCG   120
Tb...10890      ACCTTCTATTCAAACAAGGAAATTTTTCTTCGCGAGCTAATTAGTAATTCGTCAGATGCG   120
                ************************************************************

Tb...10930      TGCGACAAAATCCGGTACCAGAGTCTGACGAGCCAGTCCGTGCTCGGAGATGAACCCCAT   180
Tb...10970      TGCGACAAAATCCGGTACCAGAGTCTGACGAACCAGTCCGTGCTCGGAGATGAACCCCAT   180
Tb...10980      TGCGACAAAATCCGGTACCAGAGTCTGACGAACCAGTCCGTGCTCGGAGATGAACCCCAT   180
Tb...10960      TGCGACAAAATCCGGTACCAGAGTCTGACGAACCAGTCCGTGCTCGGAGATGAACCCCAT   180
Tb...10950      TGCGACAAAATCCGGTACCAGAGTCTGACGAACCAGTCCGTGCTCGGAGATGAACCCCAT   180
Tb...10940      TGCGACAAAATCCGGTACCAGAGTCTGACGAACCAGTCCGTGCTCGGAGATGAACCCCAT   180
Tb...10910      TGCGACAAAATCCGGTACCAGAGTCTGACGAACCAGTCCGTGCTCGGAGATGAACCCCAT   180
Tb...10920      TGCGACAAAATCCGGTACCAGAGTCTGACGAACCAGTCCGTGCTCGGAGATGAACCCCAT   180
Tb...10900      TGCGACAAAATCCGGTACCAGAGTCTGACGAACCAGTCCGTGCTCGGAGATGAACCCCAT   180
Tb...10890      TGCGACAAAATCCGGTACCAGAGTCTGACGAACCAGTCCGTGCTCGGAGATGAACCCCAT   180
                ****************************** ***************************

Tb...10930      TTGCGCATTCGCGTAATCCCCGACCGAGTAAATAAGACACTGACGGTGGAGGACAGTGGC   240
Tb...10970      TTGCGCATTCGCGTAATCCCCGACCGAGTAAATAAGACACTGACGGTGGAGGACAGTGGC   240
Tb...10980      TTGCGCATTCGCGTAATCCCCGACCGAGTAAATAAGACACTGACGGTGGAGGACAGTGGC   240
Tb...10960      TTGCGCATTCGCGTAATCCCCGACCGAGTAAATAAGACACTGACGGTGGAGGACAGTGGC   240
Tb...10950      TTGCGCATTCGCGTAATCCCCGACCGAGTAAATAAGACACTGACGGTGGAGGACAGTGGC   240
Tb...10940      TTGCGCATTCGCGTAATCCCCGACCGAGTAAATAAGACACTGACGGTGGAGGACAGTGGC   240
Tb...10910      TTGCGCATTCGCGTAATCCCCGACCGAGTAAATAAGACACTGACGGTGGAGGACAGTGGC   240
Tb...10920      TTGCGCATTCGCGTAATCCCCGACCGAGTAAATAAGACACTGACGGTGGAGGACAGTGGC   240
Tb...10900      TTGCGCATTCGCGTAATCCCCGACCGAGTAAATAAGACACTGACGGTGGAGGACAGTGGC   240
Tb...10890      TTGCGCATTCGCGTAATCCCCGACCGAGTAAATAAGACACTGACGGTGGAGGACAGTGGC   240
```

```
                ************************************************************

Tb...10930      ATCGGTATGACGAAAGCCGACCTGGTGAACAACCTTGGTACGATTGCTCGCTCCGGTACC    300
Tb...10970      ATCGGTATGACGAAAGCCGACCTGGTGAACAACCTTGGTACGATTGCTCGCTCCGGTACC    300
Tb...10980      ATCGGTATGACGAAAGCCGACCTGGTGAACAACCTTGGTACGATTGCTCGCTCCGGTACC    300
Tb...10960      ATCGGTATGACGAAAGCCGACCTGGTGAACAACCTTGGTACGATTGCTCGCTCCGGTACC    300
Tb...10950      ATCGGTATGACGAAAGCCGACCTGGTGAACAACCTTGGTACGATTGCTCGCTCCGGTACC    300
Tb...10940      ATCGGTATGACGAAAGCCGACCTGGTGAACAACCTTGGTACGATTGCTCGCTCCGGTACC    300
Tb...10910      ATCGGTATGACGAAAGCCGACCTGGTGAACAACCTTGGTACGATTGCTCGCTCCGGTACC    300
Tb...10920      ATCGGTATGACGAAAGCCGACCTGGTGAACAACCTTGGTACGATTGCTCGCTCCGGTACC    300
Tb...10900      ATCGGTATGACGAAAGCCGACCTGGTGAACAACCTTGGTACGATTGCTCGCTCCGGTACC    300
Tb...10890      ATCGGTATGACGAAAGCCGACCTGGTGAACAACCTTGGTACGATTGCTCGCTCCGGTACC    300
                ************************************************************

Tb...10930      AAGTCATTCATGGAGGCATTGGAGGCCGGTGGCGATATGAGCATGATCGGGCAGTTCGGC    360
Tb...10970      AAGTCATTCATGGAGGCATTGGAGGCCGGTGGCGATATGAGCATGATCGGGCAGTTCGGC    360
Tb...10980      AAGTCATTCATGGAGGCATTGGAGGCCGGTGGCGATATGAGCATGATCGGGCAGTTCGGC    360
Tb...10960      AAGTCATTCATGGAGGCATTGGAGGCCGGTGGCGATATGAGCATGATCGGGCAGTTCGGC    360
Tb...10950      AAGTCATTCATGGAGGCATTGGAGGCCGGTGGCGATATGAGCATGATCGGGCAGTTCGGC    360
Tb...10940      AAGTCATTCATGGAGGCATTGGAGGCCGGTGGCGATATGAGCATGATCGGGCAGTTCGGC    360
Tb...10910      AAGTCATTCATGGAGGCATTGGAGGCCGGTGGCGATATGAGCATGATCGGGCAGTTCGGC    360
Tb...10920      AAGTCATTCATGGAGGCATTGGAGGCCGGTGGCGATATGAGCATGATCGGGCAGTTCGGC    360
Tb...10900      AAGTCATTCATGGAGGCATTGGAGGCCGGTGGCGATATGAGCATGATCGGGCAGTTCGGC    360
Tb...10890      AAGTCATTCATGGAGGCATTGGAGGCCGGTGGCGATATGAGCATGATCGGGCAGTTCGGC    360
                ************************************************************

Tb...10930      GTCGGATTTTACTCTGCCTACCTTGTCGCAGACCGCGTAACCGTTGTGTCGAAGAACAAC    420
Tb...10970      GTCGGATTTTACTCTGCCTACCTTGTCGCAGACCGCGTAACCGTTGTGTCGAAGAACAAC    420
Tb...10980      GTCGGATTTTACTCTGCCTACCTTGTCGCAGACCGCGTAACCGTTGTGTCGAAGAACAAC    420
Tb...10960      GTCGGATTTTACTCTGCCTACCTTGTCGCAGACCGCGTAACCGTTGTGTCGAAGAACAAC    420
Tb...10950      GTCGGATTTTACTCTGCCTACCTTGTCGCAGACCGCGTAACCGTTGTGTCGAAGAACAAC    420
Tb...10940      GTCGGATTTTACTCTGCCTACCTTGTCGCAGACCGCGTAACCGTTGTGTCGAAGAACAAC    420
Tb...10910      GTCGGATTTTACTCTGCCTACCTTGTCGCAGACCGCGTAACCGTTGTGTCGAAGAACAAC    420
Tb...10920      GTCGGATTTTACTCTGCCTACCTTGTCGCAGACCGCGTAACCGTTGTGTCGAAGAACAAC    420
Tb...10900      GTCGGATTTTACTCTGCCTACCTTGTCGCAGACCGCGTAACCGTTGTGTCGAAGAACAAC    420
Tb...10890      GTCGGATTTTACTCTGCCTACCTTGTCGCAGACCGCGTAACCGTTGTGTCGAAGAACAAC    420
                ************************************************************

Tb...10930      GAGGACGATGCCTACACGTGGGAATCCTCTGCAGGTGGTACCTTCACTGTAACCTCCACG    480
Tb...10970      GAGGACGATGCCTACACGTGGGAATCCTCTGCAGGTGGTACCTTCACTGTAACCTCCACG    480
Tb...10980      GAGGACGATGCCTACACGTGGGAATCCTCTGCAGGTGGTACCTTCACTGTAACCTCCACG    480
Tb...10960      GAGGACGATGCCTACACGTGGGAATCCTCTGCAGGTGGTACCTTCACTGTAACCTCCACG    480
Tb...10950      GAGGACGATGCCTACACGTGGGAATCCTCTGCAGGTGGTACCTTCACTGTAACCTCCACG    480
Tb...10940      GAGGACGATGCCTACACGTGGGAATCCTCTGCAGGTGGTACCTTCACTGTAACCTCCACG    480
Tb...10910      GAGGACGATGCCTACACGTGGGAATCCTCTGCAGGTGGTACCTTCACTGTAACCTCCACG    480
Tb...10920      GAGGACGATGCCTACACGTGGGAATCCTCTGCAGGTGGTACCTTCACTGTAACCTCCACG    480
Tb...10900      GAGGACGATGCCTACACGTGGGAATCCTCTGCAGGTGGTACCTTCACTGTAACCTCCACG    480
Tb...10890      GAGGACGATGCCTACACGTGGGAATCCTCTGCAGGTGGTACCTTCACTGTAACCTCCACG    480
                ************************************************************

Tb...10930      CCCGACTGTGACCTGAAGCGCGGTACGCGTATCGTCTTGCATTTGAAGGAAGACCAGCAG    540
Tb...10970      CCCGACTGTGACCTGAAGCGCGGTACGCGTATCGTCTTGCATTTGAAGGAAGACCAGCAG    540
Tb...10980      CCCGACTGTGACCTGAAGCGCGGTACGCGTATCGTCTTGCATTTGAAGGAAGACCAGCAG    540
Tb...10960      CCCGACTGTGACCTGAAGCGCGGTACGCGTATCGTCTTGCATTTGAAGGAAGACCAGCAG    540
Tb...10950      CCCGACTGTGACCTGAAGCGCGGTACGCGTATCGTCTTGCATTTGAAGGAAGACCAGCAG    540
Tb...10940      CCCGACTGTGACCTGAAGCGCGGTACGCGTATCGTCTTGCATTTGAAGGAAGACCAGCAG    540
Tb...10910      CCCGACTGTGACCTGAAGCGCGGTACGCGTATCGTCTTGCATTTGAAGGAAGACCAGCAG    540
Tb...10920      CCCGACTGTGACCTGAAGCGCGGTACGCGTATCGTCTTGCATTTGAAGGAAGACCAGCAG    540
Tb...10900      CCCGACTGTGACCTGAAGCGCGGTACGCGTATCGTCTTGCATTTGAAGGAAGACCAGCAG    540
Tb...10890      CCCGACTGTGACCTGAAGCGCGGTACGCGTATCGTCTTGCATTTGAAGGAAGACCAGCAG    540
                ************************************************************

Tb...10930      GAATACCTGGAGGAGCGGCGGCTGAAGGACCTCATCAAAAAACACTCCGAATTTATCGGC    600
Tb...10970      GAATACCTGGAGGAGCGGCGGCTGAAGGACCTCATCAAAAAACACTCCGAATTTATCGGC    600
Tb...10980      GAATACCTGGAGGAGCGGCGGCTGAAGGACCTCATCAAAAAACACTCCGAATTTATCGGC    600
Tb...10960      GAATACCTGGAGGAGCGGCGGCTGAAGGACCTCATCAAAAAACACTCCGAATTTATCGGC    600
Tb...10950      GAATACCTGGAGGAGCGGCGGCTGAAGGACCTCATCAAAAAACACTCCGAATTTATCGGC    600
Tb...10940      GAATACCTGGAGGAGCGGCGGCTGAAGGACCTCATCAAAAAACACTCCGAATTTATCGGC    600
Tb...10910      GAATACCTGGAGGAGCGGCGGCTGAAGGACCTCATCAAAAAACACTCCGAATTTATCGGC    600
Tb...10920      GAATACCTGGAGGAGCGGCGGCTGAAGGACCTCATCAAAAAACACTCCGAATTTATCGGC    600
Tb...10900      GAATACCTGGAGGAGCGGCGGCTGAAGGACCTCATCAAAAAACACTCCGAATTTATCGGC    600
Tb...10890      GAATACCTGGAGGAGCGGCGGCTGAAGGACCTCATCAAAAAACACTCCGAATTTATCGGC    600
                ************************************************************

Tb...10930      TACGACATCGAGTTAATGGTGGAGAACACCACTGAGAAGGAGGTGACAGATGAAGACGAA    660
Tb...10970      TACGACATCGAGTTAATGGTGGAGAACACCACTGAGAAGGAGGTGACAGATGAAGACGAA    660
Tb...10980      TACGACATCGAGTTAATGGTGGAGAACACCACTGAGAAGGAGGTGACAGATGAAGACGAA    660
```

```
Tb...10960      TACGACATCGAGTTAATGGTGGAGAACACCACTGAGAAGGAGGTGACAGATGAAGACGAA   660
Tb...10950      TACGACATCGAGTTAATGGTGGAGAACACCACTGAGAAGGAGGTGACAGATGAAGACGAA   660
Tb...10940      TACGACATCGAGTTAATGGTGGAGAACACCACTGAGAAGGAGGTGACAGATGAAGACGAA   660
Tb...10910      TACGACATCGAGTTAATGGTGGAGAACACCACTGAGAAGGAGGTGACAGATGAAGACGAA   660
Tb...10920      TACGACATCGAGTTAATGGTGGAGAACACCACTGAGAAGGAGGTGACAGATGAAGACGAA   660
Tb...10900      TACGACATCGAGTTAATGGTGGAGAACACCACTGAGAAGGAGGTGACAGATGAAGACGAA   660
Tb...10890      TACGACATCGAGTTAATGGTGGAGAACACCACTGAGAAGGAGGTGACAGATGAAGACGAA   660
                ************************************************************

Tb...10930      GACGAAGAGGCCGCCAAAAAGGCTGAGGAAGGTGAGGAGCCAAAGGTGGAAGAGGTGAAG   720
Tb...10970      GACGAAGAGGCCGCCAAAAAGGCTGAGGAAGGTGAGGAGCCAAAGGTGGAAGAGGTGAAG   720
Tb...10980      GACGAAGAGGCCGCCAAAAAGGCTGAGGAAGGTGAGGAGCCAAAGGTGGAAGAGGTGAAG   720
Tb...10960      GACGAAGAGGCCGCCAAAAAGGCTGAGGAAGGTGAGGAGCCAAAGGTGGAAGAGGTGAAG   720
Tb...10950      GACGAAGAGGCCGCCAAAAAGGCTGAGGAAGGTGAGGAGCCAAAGGTGGAAGAGGTGAAG   720
Tb...10940      GACGAAGAGGCCGCCAAAAAGGCTGAGGAAGGTGAGGAGCCAAAGGTGGAAGAGGTGAAG   720
Tb...10910      GACGAAGAGGCCGCCAAAAAGGCTGAGGAAGGTGAGGAGCCAAAGGTGGAAGAGGTGAAG   720
Tb...10920      GACGAAGAGGCCGCCAAAAAGGCTGAGGAAGGTGAGGAGCCAAAAGTGGAAGAGGTGAAG   720
Tb...10900      GACGAAGAGGCCGCCAAAAAGGCTGAGGAAGGTGAGGAGCCAAAGGTGGAAGAGGTGAAG   720
Tb...10890      GACGAAGAGGCCGCCAAAAAGGCTGAGGAAGGTGAGGAGCCAAAGGTGGAAGAGGTGAAG   720
                ******************************************** ***************

Tb...10930      GACGGCGATGATGCCGATGCCAAGAAAAAGAAAACCAAAAAGGTGAAGGAAGTGAAGCAG   780
Tb...10970      GACGGTGATGATGCCGATGCCAAGAAAAAGAAAACCAAAAAGGTGAAGGAAGTGAAGCAG   780
Tb...10980      GACGGCGATGATGCCGATGCCAAGAAAAAGAAAACCAAAAAGGTGAAGGAAGTGAAGCAG   780
Tb...10960      GACGGCGATGATGCCGATGCCAAGAAAAAGAAAACCAAAAAGGTGAAGGAAGTGAAGCAG   780
Tb...10950      GACGGCGATGATGCCGATGCCAAGAAAAAGAAAACCAAAAAGGTGAAGGAAGTGAAGCAG   780
Tb...10940      GACGGCGATGATGCCGATGCCAAGAAAAAGAAAACCAAAAAGGTGAAGGAAGTGAAGCAG   780
Tb...10910      GACGGCGATGATGCCGATGCCAAGAAAAAGAAAACCAAAAAGGTGAAGGAAGTGAAGCAG   780
Tb...10920      GACGGCGATGATGCCGATGCCAAGAAAAAGAAAACCAAAAAGGTGAAGGAAGTGAAGCAG   780
Tb...10900      GACGGCGATGATGCCGATGCCAAGAAAAAGAAAACCAAAAAGGTGAAGGAAGTGAAGCAG   780
Tb...10890      GACGGCGATGATGCCGATGCCAAGAAAAAGAAAACCAAAAAGGTGAAGGAAGTGAAGCAG   780
                ***** **************************************************

Tb...10930      GAGTTTGTGGTGCAGAACAAGCACAAGCCACTGTGGACGCGCGACCCGAAAGATGTAACA   840
Tb...10970      GAGTTTGTGGTGCAGAACAAGCACAAGCCACTGTGGACGCGCGACCCGAAAGATGTAACA   840
Tb...10980      GAGTTTGTGGTGCAGAACAAGCACAAGCCACTGTGGACGCGCGACCCGAAAGATGTAACA   840
Tb...10960      GAGTTTGTGGTGCAGAACAAGCACAAGCCACTGTGGACGCGCGACCCGAAAGATGTAACA   840
Tb...10950      GAGTTTGTGGTGCAGAACAAGCACAAGCCACTGTGGACGCGCGACCCGAAAGATGTAACA   840
Tb...10940      GAGTTTGTGGTGCAGAACAAGCACAAGCCACTGTGGACGCGCGACCCGAAAGATGTAACA   840
Tb...10910      GAGTTTGTGGTGCAGAACAAGCACAAGCCACTGTGGACGCGCGACCCGAAAGATGTAACA   840
Tb...10920      GAGTTTGTGGTGCAGAACAAGCACAAGCCACTGTGGACGCGCGACCCGAAAGATGTAACA   840
Tb...10900      GAGTTTGTGGTGCAGAACAAGCACAAGCCACTGTGGACGCGCGACCCGAAAGATGTAACA   840
Tb...10890      GAGTTTGTGGTGCAGAACAAGCACAAGCCACTGTGGACGCGCGACCCGAAAGATGTAACA   840
                ************************************************************

Tb...10930      AAGGAGGAGTACGCCTCCTTCTACAAGGCCATCTCGAACGACTGGGAAGAGCAGCTGTCT   900
Tb...10970      AAGGAGGAGTACGCCTCCTTCTACAAGGCCATCTCGAACGACTGGGAAGAGCAGCTGTCT   900
Tb...10980      AAGGAGGAGTACACCTCCTTCTACAAGGCCATCTCGAACGACTGGGAAGAGCAGCTGTCT   900
Tb...10960      AAGGAGGAGTACGCCTCCTTCTACAAGGCCATCTCGAACGACTGGGAAGAGCAGCTGTCT   900
Tb...10950      AAGGAGGAGTACGCCTCCTTCTACAAGGCCATCTCGAACGACTGGGAAGAGCAGCTGTCT   900
Tb...10940      AAGGAGGAGTACGCCTCCTTCTACAAGGCCATCTCGAACGACTGGGAAGAGCAGCTGTCT   900
Tb...10910      AAGGAGGAGTACGCCTCCTTCTACAAGGCCATCTCGAACGACTGGGAAGAGCAGCTGTCT   900
Tb...10920      AAGGAGGAGTACGCCTCCTTCTACAAGGCCATCTCGAACGACTGGGAAGAGCAGCTGTCT   900
Tb...10900      AAGGAGGAGTACGCCTCCTTCTACAAGGCCATCTCGAACGACTGGGAAGAGCAGCTGTCT   900
Tb...10890      AAGGAGGAGTACGCCTCCTTCTACAAGGCCATCTCGAACGACTGGGAAGAGCAGCTGTCT   900
                ************ ************************************************

Tb...10930      ACGAAGCACTTCTCCGTGGAGGGCCAGCTGGAGTTCCGGGCTATCTTATTTCTCCCGAAG   960
Tb...10970      ACGAAGCACTTCTCCGTGGAGGGCCAGCTGGAGTTCCGGGCTATCTTATTTCTCCCGAAG   960
Tb...10980      ACGAAGCACTTCTCCGTGGAGGGCCAGCTGGAGTTCCGGGCTATCTTATTTCTCCCGAAG   960
Tb...10960      ACGAAGCACTTCTCCGTGGAGGGCCAGCTGGAGTTCCGGGCTATCTTATTTCTCCCGAAG   960
Tb...10950      ACGAAGCACTTCTCCGTGGAGGGCCAGCTGGAGTTCCGGGCTATCTTATTTCTCCCGAAG   960
Tb...10940      ACGAAGCACTTCTCCGTGGAGGGCCAGCTGGAGTTCCGGGCTATCTTATTTCTCCCGAAG   960
Tb...10910      ACGAAGCACTTCTCCGTGGAGGGCCAGCTGGAGTTCCGGGCTATCTTATTTCTCCCGAAG   960
Tb...10920      ACGAAGCACTTCTCCGTGGAGGGCCAGCTGGAGTTCCGGGCTATCTTATTTCTCCCGAAG   960
Tb...10900      ACGAAGCACTTCTCCGTGGAGGGCCAGCTGGAGTTCCGGGCTATCTTATTTCTCCCGAAG   960
Tb...10890      ACGAAGCACTTCTCCGTGGAGGGCCAGCTGGAGTTCCGGGCTATCTTATTTCTCCCGAAG   960
                ************************************************************

Tb...10930      CGCGCACCCTTTGACATGTTCGAACCAAACAAGAAGCGCAACAACATCAAGCTATACGTC  1020
Tb...10970      CGCGCACCCTTTGACATGTTCGAACCAAACAAGAAGCGCAACAACATCAAGCTATACGTC  1020
Tb...10980      CGCGCACCCTTTGACATGTTCGAACCAAACAAGAAGCGCAACAACATCAAGCTATACGTC  1020
Tb...10960      CGCGCACCCTTTGACATGTTCGAACCAAACAAGAAGCGCAACAACATCAAGCTATACGTC  1020
Tb...10950      CGCGCACCCTTTGACATGTTCGAACCAAACAAGAAGCGCAACAACATCAAGCTATACGTC  1020
Tb...10940      CGCGCACCCTTTGACATGTTCGAACCAAACAAGAAGCGCAACAACATCAAGCTATACGTC  1020
Tb...10910      CGCGCACCCTTTGACATGTTCGAACCAAACAAGAAGCGCAACAACATCAAGCTATACGTC  1020
Tb...10920      CGCGCACCCTTTGACATGTTCGAACCAAACAAGAAGCGCAACAACATCAAGCTATACGTC  1020
```

```
Tb...10900      CGCGCACCCTTTGACATGTTCGAACCAAACAAGAAGCGCAACAACATCAAGCTATACGTC   1020
Tb...10890      CGCGCACCCTTTGACATGTTCGAACCAAACAAGAAGCGCAACAACATCAAGCTATACGTC   1020
                ************************************************************

Tb...10930      CGCCGCGTGTTCATCATGGACAACTGTGAGGACCTGTGCCCCGAGTGGCTCGGCTTCCTG   1080
Tb...10970      CGCCGCGTGTTCATCATGGACAACTGTGAGGACCTGTGCCCCGAGTGGCTCGGCTTCCTG   1080
Tb...10980      CGCCGCGTGTTCATCATGGACAACTGTGAGGACCTGTGCCCCGAGTGGCTCGGCTTCCTG   1080
Tb...10960      CGCCGCGTGTTCATCATGGACAACTGTGAGGACCTGTGCCCCGAGTGGCTCGGCTTCCTG   1080
Tb...10950      CGCCGCGTGTTCATCATGGACAACTGTGAGGACCTGTGCCCCGAGTGGCTCGGCTTCCTG   1080
Tb...10940      CGCCGCGTGTTCATCATGGACAACTGTGAGGACCTGTGCCCCGAGTGGCTCGGCTTCCTG   1080
Tb...10910      CGCCGCGTATTCATCATGGACAACTGTGAGGACCTGTGCCCCGACTGGCTCGGCTTCCTG   1080
Tb...10920      CGCCGCGTATTCATCATGGACAACTGTGAGGACCTGTGCCCCGAGTGGCTCGGCTTCCTG   1080
Tb...10900      CGCCGCGTATTCATCATGGACAACTGTGAGGACCTGTGCCCCGAGTGGCTCGGCTTCCTG   1080
Tb...10890      CGCCGCGTATTCATCATGGACAACTGTGAGGACCTGTGCCCCGAGTGGCTCGGCTTCCTG   1080
                ******** ********************************** ***************

Tb...10930      CGCGGTGTGGTGGACAGCGAGGACCTGCCACTAAATATCTCCCGTGAGAACCTGCAGCAG   1140
Tb...10970      CGCGGTGTGGTGGACAGCGAGGACCTGCCACTAAATATCTCCCGTGAGAACCTGCAGCAG   1140
Tb...10980      CGCGGTGTGGTGGACAGCGAGGACCTGCCACTAAATATCTCCCGTGAGAACCTGCAGCAG   1140
Tb...10960      CGCGGTGTGGTGGACAGCGAGGACCTGCCACTAAATATCTCCCGTGAGAACCTGCAGCAG   1140
Tb...10950      CGCGGTGTGGTGGACAGCGAGGACCTGCCACTAAATATCTCCCGTGAGAACCTGCAGCAG   1140
Tb...10940      CGCGGTGTGGTGGACAGCGAGGACCTGCCACTAAATATCTCCCGTGAGAACCTGCAGCAG   1140
Tb...10910      CGCGGTGTGGTGGACAGCGAGGACCTGCCACTAAATATCTCCCGTGAGAACCTGCAGCAG   1140
Tb...10920      CGCGGTGTGGTGGACAGCGAGGACCTGCCACTAAATATCTCCCGTGAGAACCTGCAGCAG   1140
Tb...10900      CGCGGTGTGGTGGACAGCGAGGACCTGCCACTAAATATCTCCCGTGAGAACCTGCAGCAG   1140
Tb...10890      CGCGGTGTGGTGGACAGCGAGGACCTGCCACTAAATATCTCCCGTGAGAACCTGCAGCAG   1140
                ************************************************************

Tb...10930      AACAAAATCCTCAAGGTGATCCGTAAGAATATTGTGAAGAAGACCCTGGAGCTCTTCGAG   1200
Tb...10970      AACAAAATCCTCAAGGTGATCCGTAAGAATATTGTGAAGAAGACCCTGGAGCTCTTCGAG   1200
Tb...10980      AACAAAATCCTCAAGGTGATCCGTAAGAATATTGTGAAGAAGGCCCTGGAGCTCTTCGAG   1200
Tb...10960      AACAAAATCCTCAAGGTGATCCGTAAGAATATTGTGAAGAAGGCCCTGGAGCTCTTCGAG   1200
Tb...10950      AACAAAATCCTCAAGGTGATCCGTAAGAATATTGTGAAGAAGGCCCTGGAGCTCTTCGAG   1200
Tb...10940      AACAAAATCCTCAAGGTGATCCGTAAGAATATTGTGAAGAAGGCCCTGGAGCTCTTCGAG   1200
Tb...10910      AACAAAATCCTCAAGGTGATCCGTAAGAATATTGTGAAGAAGGCCCTGGAGCTCTTCGAG   1200
Tb...10920      AACAAAATCCTCAAGGTGATCCGTAAGAATATTGTGAAGAAGGCCCTGGAGCTCTTCGAG   1200
Tb...10900      AACAAAATCCTCAAGGTGATCCGTAAGAATATTGTGAAGAAGGCCCTGGAGCTCTTCGAG   1200
Tb...10890      AACAAAATCCTCAAGGTGATCCGTAAGAATATTGTGAAGAAGGCCCTGGAGCTCTTCGAG   1200
                ********************************************** ***************

Tb...10930      GAGCTCGCAGAGAACAAGGAGGACTACAAGAAGTTCTACGAACAGTTCAGCAAGAACGTG   1260
Tb...10970      GAGCTCGCAGAGAACAAGGAGGACTACAAGAAGTTCTACGAACAGTTCAGCAAGAACGTG   1260
Tb...10980      GAGCTCGCAGAGAACAAGGAGGACTACAAGAAGTTCTACGAACAGTTCAGCAAGAACGTG   1260
Tb...10960      GAGCTCGCAGAGAACAAGGAGGACTACAAGAAGTTCTACGAACAGTTCAGCAAGAACGTG   1260
Tb...10950      GAGCTCGCAGAGAACAAGGAGGACTACAAGAAGTTCTACGAACAGTTCAGCAAGAACGTG   1260
Tb...10940      GAGCTCGCAGAGAACAAGGAGGACTACAAGAAGTTCTACGAACAGTTCAGCAAGAACGTG   1260
Tb...10910      GAGCTCGCAGAGAACAAGGAGGACTACAAGAAGTTCTACGAACAGTTCAGCAAGAACGTG   1260
Tb...10920      GAGCTCGCAGAGAACAAGGAGGACTACAAGAAGTTCTACGAACAGTTCAGCAAGAACGTG   1260
Tb...10900      GAGCTCGCAGAGAACAAGGAGGACTACAAGAAGTTCTACGAACAGTTCAGCAAGAACGTG   1260
Tb...10890      GAGCTCGCAGAGAACAAGGAGGACTACAAGAAGTTCTACGAACAGTTCAGCAAGAACGTG   1260
                ************************************************************

Tb...10930      AAGCTGGGCATCCACGAAGACAGCACAAACCGCAAGAAGCTGATGGAACTGCTGCGCTTC   1320
Tb...10970      AAGCTGGGCATCCACGAAGACAGCACAAACCGCAAGAAGCTGATGGAACTGCTGCGCTTC   1320
Tb...10980      AAGCTGGGCATCCACGAAGACAGCACAAACCGCAAGAAGCTGATGGAACTGCTGCGCTTC   1320
Tb...10960      AAGCTGGGCATCCACGAAGACAGCACAAACCGCAAGAAGCTGATGGAACTGCTGCGCTTC   1320
Tb...10950      AAGCTGGGCATCCACGAAGACAGCACAAACCGCAAGAAGCTGATGGAACTGCTGCGCTTC   1320
Tb...10940      AAGCTGGGCATCCACGAAGACAGCACAAACCGCAAGAAGCTGATGGAACTGCTGCGCTTC   1320
Tb...10910      AAGCTGGGCATCCACGAAGACAGCACAAACCGCAAGAAGCTGATGGAACTGCTGCGCTTC   1320
Tb...10920      AAGCTGGGCATCCACGAAGACAGCACAAACCGCAAGAAGCTGATGGAACTGCTGCGCTTC   1320
Tb...10900      AAGCTGGGCATCCACGAAGACAGCACAAACCGCAAGAAGCTGATGGAACTGCTGCGCTTC   1320
Tb...10890      AAGCTGGGCATCCACGAAGACAGCACAAACCGCAAGAAGCTGATGGAACTGCTGCGCTTC   1320
                ************************************************************

Tb...10930      CACAGTTCGGAATCCGGTGAGGAGATGACGACATTGAAGGACTACGTGACACGCATGAAG   1380
Tb...10970      CACAGTTCGGAATCCGGTGAGGAGATGACGACATTGAAGGACTACGTGACACGCATGAAG   1380
Tb...10980      CACAGTTCGGAATCCGGTGAGGAGATGACGACATTGAAGGACTACGTGACACGCATGAAG   1380
Tb...10960      CACAGTTCGGAATCCGGTGAGGAGATGACGACATTGAAGGACTACGTGACACGCATGAAG   1380
Tb...10950      CACAGTTCGGAATCCGGTGAGGAGATGACGACATTGAAGGACTACGTGACACGCATGAAG   1380
Tb...10940      CACAGTTCGGAATCCGGTGAGGAGATGACGACATTGAAGGACTACGTGACACGCATGAAG   1380
Tb...10910      CACAGTTCGGAATCCGGTGAGGAGATGACGACATTGAAGGACTACGTGACACGCATGAAG   1380
Tb...10920      CACAGTTCGGAATCCGGTGAGGAGATGACGACATTGAAGGACTACGTGACACGCATGAAG   1380
Tb...10900      CACAGTTCGGAATCCGGTGAGGAGATGACGACATTGAAGGACTACGTGACACGCATGAAG   1380
Tb...10890      CACAGTTCGGAATCCGGTGAGGAGATGACGACATTGAAGGACTACGTGACACGCATGAAG   1380
                ************************************************************

Tb...10930      GATGGTCAGAAGTGCATCTACTATGTGACGGGTGACAGCAAGAAGAAGCTCGAAACGTCT   1440
```

```
Tb...10970      GATGGTCAGAAGTGCATCTACTATGTGACGGGTGACAGCAAGAAGAAGCTCGAAACGTCT   1440
Tb...10980      GATGGTCAGAAGTGCATCTACTATGTGACGGGTGACAGCAAGAAGAAGCTCGAAACGTCT   1440
Tb...10960      GATGGTCAGAAGTGCATCTACTATGTGACGGGTGACAGCAAGAAGAAGCTCGAAACGTCT   1440
Tb...10950      GATGGTCAGAAGTGCATCTACTATGTGACGGGTGACAGCAAGAAGAAGCTCGAAACGTCT   1440
Tb...10940      GATGGTCAGAAGTGCATCTACTATGTGACGGGTGACAGCAAGAAGAAGCTCGAAACGTCT   1440
Tb...10910      GATGGTCAGAAGTGCATCTACTATGTGACGGGTGACAGCAAGAAGAAGCTCGAAACGTCT   1440
Tb...10920      GATGGTCAGAAGTGCATCTACTATGTGACGGGTGACAGCAAGAAGAAGCTCGAAACGTCT   1440
Tb...10900      GATGGTCAGAAGTGCATCTACTATGTGACGGGTGACAGCAAGAAGAAGCTCGAAACGTCT   1440
Tb...10890      GATGGTCAGAAGTGCATCTACTATGTGACGGGTGACAGCAAGAAGAAGCTCGAAACGTCT   1440
                ************************************************************

Tb...10930      CCGTTCATCGAGCAGGCGAAGCGCCGCGGCATGGAGGTACTTTTCATGACTGACCCCATC   1500
Tb...10970      CCGTTCATCGAGCAGGCGAAGCGCCGCGGCATGGAGGTACTTTTCATGACTGACCCCATC   1500
Tb...10980      CCGTTCATCGAGCAGGCGAAGCGCCGCGGCATGGAGGTACTTTTCATGACTGACCCCATC   1500
Tb...10960      CCGTTCATCGAGCAGGCGAAGCGCCGCGGCATGGAGGTACTTTTCATGACTGACCCCATC   1500
Tb...10950      CCGTTCATCGAGCAGGCGAAGCGCCGCGGCATGGAGGTACTTTTCATGACTGACCCCATC   1500
Tb...10940      CCGTTCATCGAGCAGGCGAAGCGCCGCGGCATGGAGGTACTTTTCATGACTGACCCCATC   1500
Tb...10910      CCGTTCATCGAGCAGGCGAAGCGCCGCGGCATGGAGGTACTTTTCATGACTGACCCCATC   1500
Tb...10920      CCGTTCATCGAGCAGGCGAAGCGCCGCGGCATGGAGGTACTTTTCATGACTGACCCCATC   1500
Tb...10900      CCGTTCATCGAGCAGGCGAAGCGCCGCGGCATGGAGGTACTTTTCATGACTGACCCCATC   1500
Tb...10890      CCGTTCATCGAGCAGGCGAAGCGCCGCGGCATGGAGGTACTTTTCATGACTGACCCCATC   1500
                ************************************************************

Tb...10930      GACGAGTATGTGATGCAGCAAGTGAAGGACTTTGAGGACAAAAAGTTCGCGTGCCTCACA   1560
Tb...10970      GACGAGTATGTGATGCAGCAAGTGAAGGACTTTGAGGACAAAAAGTTCGCGTGCCTCACA   1560
Tb...10980      GACGAGTATGTGATGCAGCAAGTGAAGGACTTTGAGGACAAAAAGTTCGCGTGCCTCACA   1560
Tb...10960      GACGAGTATGTGATGCAGCAAGTGAAGGACTTTGAGGACAAAAAGTTCGCGTGCCTCACA   1560
Tb...10950      GACGAGTATGTGATGCAGCAAGTGAAGGACTTTGAGGACAAAAAGTTCGCGTGCCTCACA   1560
Tb...10940      GACGAGTATGTGATGCAGCAAGTGAAGGACTTTGAGGACAAAAAGTTCGCGTGCCTCACA   1560
Tb...10910      GACGAGTATGTGATGCAGCAAGTGAAGGACTTTGAGGACAAAAAGTTCGCGTGCCTCACA   1560
Tb...10920      GACGAGTATGTGATGCAGCAAGTGAAGGACTTTGAGGACAAAAAGTTCGCGTGCCTCACA   1560
Tb...10900      GACGAGTATGTGATGCAGCAAGTGAAGGACTTTGAGGACAAAAAGTTCGCGTGCCTCACA   1560
Tb...10890      GACGAGTATGTGATGCAGCAAGTGAAGGACTTTGAGGACAAAAAGTTCGCGTGCCTCACA   1560
                ************************************************************

Tb...10930      AAGGAGGGTGTACACTTCGAGGAGACGGAGGAAGAGAAGAAACAGCGGGAAGAAGAGAAG   1620
Tb...10970      AAGGAGGGTGTACACTTCGAGGAGACGGAGGAAGAGAAGAAACAGCGGGAAGAAGAGAAG   1620
Tb...10980      AAGGAGGGTGTACACTTCGAGGAGACGGAGGAAGAGAAGAAACAGCGGGAAGAAGAGAAG   1620
Tb...10960      AAGGAGGGTGTACACTTCGAGGAGACGGAGGAAGAGAAGAAACAGCGGGAAGAAGAGAAG   1620
Tb...10950      AAGGAGGGTGTACACTTCGAGGAGACGGAGGAAGAGAAGAAACAGCGGGAAGAAGAGAAG   1620
Tb...10940      AAGGAGGGTGTACACTTCGAGGAGACGGAGGAAGAGAAGAAACAGCGGGAAGAAGAGAAG   1620
Tb...10910      AAGGAGGGTGTACACTTCGAGGAGACGGAGGAAGAGAAGAAACAGCGGGAAGAAGAGAAG   1620
Tb...10920      AAGGAGGGTGTACACTTCGAGGAGACGGAGGAAGAGAAGAAACAGCGGGAAGAAGAGAAG   1620
Tb...10900      AAGGAGGGTGTACACTTCGAGGAGACGGAGGAAGAGAAGAAACAGCGGGAAGAAGAGAAG   1620
Tb...10890      AAGGAGGGTGTACACTTCGAGGAGACGGAGGAAGAGAAGAAACAGCGGGAAGAAGAGAAG   1620
                ************************************************************

Tb...10930      GCATCATACGAGCGGCTGTGCAAGGCAATGAAAGAGGTACTTGGTGACAAAGTGGAGAAG   1680
Tb...10970      GCATCATACGAGCGGCTGTGCAAGGCAATGAAAGAGGTACTTGGTGACAAAGTGGAGAAG   1680
Tb...10980      GCATCATACGAGCGGCTGTGCAAGGCAATGAAAGAGGTACTTGGTGACAAAGTGGAGAAG   1680
Tb...10960      GCATCATACGAGCGGCTGTGCAAGGCAATGAAAGAGGTACTTGGTGACAAAGTGGAGAAG   1680
Tb...10950      GCATCATACGAGCGGCTGTGCAAGGCAATGAAAGAGGTACTTGGTGACAAAGTGGAGAAG   1680
Tb...10940      GCATCATACGAGCGGCTGTGCAAGGCAATGAAAGAGGTACTTGGTGACAAAGTGGAGAAG   1680
Tb...10910      GCATCATACGAGCGGCTGTGCAAGGCAATGAAAGAGGTACTTGGTGACAAAGTGGAGAAG   1680
Tb...10920      GCATCATACGAGCGGCTGTGCAAGGCAATGAAAGAGGTACTTGGTGACAAAGTGGAGAAG   1680
Tb...10900      GCATCATACGAGCGGCTGTGCAAGGCAATGAAAGAGGTACTTGGTGACAAAGTGGAGAAG   1680
Tb...10890      GCATCATACGAGCGGCTGTGCAAGGCAATGAAAGAGGTACTTGGTGACAAAGTGGAGAAG   1680
                ************************************************************

Tb...10930      GTGGTGGTGTCCGACCGGTTGGCAACATCACCATGCATTCTCGTGACATCAGAGTTCGGG   1740
Tb...10970      GTGGTGGTGTCCGACCGGTTGGCAACATCACCATGCATTCTCGTGACATCAGAGTTCGGG   1740
Tb...10980      GTGGTGGTGTCCGACCGGTTGGCAACATCACCATGCATTCTCGTGACATCAGAGTTCGGG   1740
Tb...10960      GTGGTGGTGTCCGACCGGTTGGCAACATCACCATGCATTCTCGTGACATCAGAGTTCGGG   1740
Tb...10950      GTGGTGGTGTCCGACCGGTTGGCAACATCACCATGCATTCTCGTGACATCAGAGTTCGGG   1740
Tb...10940      GTGGTGGTGTCCGACCGGTTGGCAACATCACCATGCATTCTCGTGACATCAGAGTTCGGG   1740
Tb...10910      GTGGTGGTGTCCGACCGGTTGGCAACATCACCATGCATTCTCGTGACATCAGAGTTCGGG   1740
Tb...10920      GTGGTGGTGTCCGACCGGTTGGCAACATCACCATGCATTCTCGTGACATCAGAGTTCGGG   1740
Tb...10900      GTGGTGGTGTCCGACCGGTTGGCAACATCACCATGCATTCTCGTGACATCAGAGTTCGGG   1740
Tb...10890      GTGGTGGTGTCCGACCGGTTGGCAACATCACCATGCATTCTCGTGACATCAGAGTTCGGG   1740
                ************************************************************

Tb...10930      TGGAGTGCACACATGGAACAGATCATGCGCAACCAGGCTCTGCGAGACTCCAGCATGTCT   1800
Tb...10970      TGGAGTGCACACATGGAACAGATCATGCGCAACCAGGCTCTGCGAGACTCCAGCATGTCT   1800
Tb...10980      TGGAGTGCACACATGGAACAGATCATGCGCAACCAGGCTCTGCGAGACTCCAGCATGTCT   1800
Tb...10960      TGGAGTGCACACATGGAACAGATCATGCGCAACCAGGCTCTGCGAGACTCCAGCATGTCT   1800
Tb...10950      TGGAGTGCACACATGGAACAGATCATGCGCAACCAGGCTCTGCGAGACTCCAGCATGTCT   1800
Tb...10940      TGGAGTGCACACATGGAACAGATCATGCGCAACCAGGCTCTGCGAGACTCCAGCATGTCT   1800
```

```
Tb...10910      TGGAGTGCACACATGGAACAGATCATGCGCAACCAGGCTCTGCGAGACTCCAGCATGTCT   1800
Tb...10920      TGGAGTGCACACATGGAACAGATCATGCGCAACCAGGCTCTGCGAGACTCCAGCATGTCT   1800
Tb...10900      TGGAGTGCACACATGGAACAGATCATGCGCAACCAGGCTCTGCGAGACTCCAGCATGTCT   1800
Tb...10890      TGGAGTGCACACATGGAACAGATCATGCGCAACCAGGCTCTGCGAGACTCCAGCATGTCT   1800
                ************************************************************

Tb...10930      GCGTACATGATGTCGAAGAAGACCATGGAGATCAACACCACGCACGCCATCGTCAAGGAG   1860
Tb...10970      GCGTACATGATGTCGAAGAAGACCATGGAGATCAACACCACGCACGCCATCGTCAAGGAG   1860
Tb...10980      GCGTACATGATGTCGAAGAAGACCATGGAGATCAACACCACGCACGCCATCGTCAAGGAG   1860
Tb...10960      GCGTACATGATGTCGAAGAAGACCATGGAGATCAACACCACGCACGCCATCGTCAAGGAG   1860
Tb...10950      GCGTACATGATGTCGAAGAAGACCATGGAGATCAACACCACGCACGCCATCGTCAAGGAG   1860
Tb...10940      GCGTACATGATGTCGAAGAAGACCATGGAGATCAACACCACGCACGCCATCGTCAAGGAG   1860
Tb...10910      GCGTACATGATGTCGAAGAAGACCATGGAGATCAACACCACGCACGCCATCGTCAAGGAG   1860
Tb...10920      GCGTACATGATGTCGAAGAAGACCATGGAGATCAACACCACGCACGCCATCGTCAAGGAG   1860
Tb...10900      GCGTACATGATGTCGAAGAAGACCATGGAGATCAACACCACGCACGCCATCGTCAAGGAG   1860
Tb...10890      GCGTACATGATGTCGAAGAAGACCATGGAGATCAACACCACGCACGCCATCGTCAAGGAG   1860
                ************************************************************

Tb...10930      CTGAAACGACGCGTGGAGGCCGACGAAAACGACAAGGCCGCCAAGGACCTGATATTCCTC   1920
Tb...10970      CTGAAACGACGCGTGGAGGCCGACGAAAACGACAAGGCCGCCAAGGACCTGATATTCCTC   1920
Tb...10980      CTGAAACGACGCGTGGAGGCCGACGAAAACGACAAGGCCGCCAAGGACCTGATATTCCTC   1920
Tb...10960      CTGAAACGACGCGTGGAGGCCGACGAAAACGACAAGGCCGCCAAGGACCTGATATTCCTC   1920
Tb...10950      CTGAAACGACGCGTGGAGGCCGACGAAAACGACAAGGCCGCCAAGGACCTGATATTCCTC   1920
Tb...10940      CTGAAACGACGCGTGGAGGCCGACGAAAACGACAAGGCCGCCAAGGACCTGATATTCCTC   1920
Tb...10910      CTGAAACGACGCGTGGAGGCCGACGAAAACGACAAGGCCGCCAAGGACCTGATATTCCTC   1920
Tb...10920      CTGAAACGACGCGTGGAGGCCGACGAAAACGACAAGGCCGCCAAGGACCTGATATTCCTC   1920
Tb...10900      CTGAAACGACGCGTGGAGGCCGACGAAAACGACAAGGCCGCCAAGGACCTGATATTCCTC   1920
Tb...10890      CTGAAACGACGCGTGGAGGCCGACGAAAACGACAAGGCCGCCAAGGACCTGATATTCCTC   1920
                ************************************************************

Tb...10930      CTCTTCGACACCTCGCTGCTGACATCCGGGTTTACACTTGATGACCCCACGGCATACGCT   1980
Tb...10970      CTCTTCGACACCTCGCTGCTGACATCCGGGTTTACACTTGATGACCCCACGGCATACGCT   1980
Tb...10980      CTCTTCGACACCTCGCTGCTGACATCCGGGTTTACACTTGATGACCCCACGGCATACGCT   1980
Tb...10960      CTCTTCGACACCTCGCTGCTGACATCCGGGTTTACACTTGATGACCCCACGGCATACGCT   1980
Tb...10950      CTCTTCGACACCTCGCTGCTGACATCCGGGTTTACACTTGATGACCCCACGGCATACGCT   1980
Tb...10940      CTCTTCGACACCTCGCTGCTGACATCCGGGTTTACACTTGATGACCCCACGGCATACGCT   1980
Tb...10910      CTCTTCGACACCTCGCTGCTGACATCCGGGTTTACACTTGATGACCCCACGGCATACGCT   1980
Tb...10920      CTCTTCGACACCTCGCTGCTGACATCCGGGTTTACACTTGATGACCCCACGGCATACGCT   1980
Tb...10900      CTCTTCGACACCTCGCTGCTGACATCCGGGTTTACACTTGATGACCCCACGGCATACGCT   1980
Tb...10890      CTCTTCGACACCTCGCTGCTGACATCCGGGTTTACACTTGATGACCCCACGGCATACGCT   1980
                ************************************************************

Tb...10930      GACCGTATCCACCGCATGATCAAATTGGGTCTCTCACTCGACGATGATGCGGAAGAGGAG   2040
Tb...10970      GACCGTATCCACCGCATGATCAAATTGGGTCTCTCACTCGACGATGATGCGGAAGAGGAG   2040
Tb...10980      GACCGTATCCACCGCATGATCAAATTGGGTCTCTCACTCGACGATGATGCGGAAGAGGAG   2040
Tb...10960      GACCGTATCCACCGCATGATCAAATTGGGTCTCTCACTCGACGATGATGCGGAAGAGGAG   2040
Tb...10950      GACCGTATCCACCGCATGATCAAATTGGGTCTCTCACTCGACGATGATGCGGAAGAGGAG   2040
Tb...10940      GACCGTATCCACCGCATGATCAAATTGGGTCTCTCACTCGACGATGATGCGGAAGAGGAG   2040
Tb...10910      GACCGTATCCACCGCATGATCAAATTGGGTCTCTCACTCGACGATGATGCGGAAGAGGAG   2040
Tb...10920      GACCGTATCCACCGCATGATCAAATTGGGTCTCTCACTCGACGATGATGCGGAAGAGGAG   2040
Tb...10900      GACCGTATCCACCGCATGATCAAATTGGGTCTCTCACTCGACGATGATGCGGAAGAGGAG   2040
Tb...10890      GACCGTATCCACCGCATGATCAAATTGGGTCTCTCACTCGACGATGATGCGGAAGAGGAG   2040
                ************************************************************

Tb...10930      GAAGCGCAGGCACCCGTTGCCGCTGCTGCCGCCAACTCCAGTACTGGTGCGTCGGGTATG   2100
Tb...10970      GAAGCGCAGGCACCCGTTGCCGCTGCTGCCGCCAACTCCAGTACTGGTGCGTCGGGTATG   2100
Tb...10980      GAAGCGCAGGCACCCGTTGCCGCTGCTGCCGCCAACTCCAGTACTGGTGCGTCGGGTATG   2100
Tb...10960      GAAGCGCAGGCACCCGTTGCCGCTGCTGCCGCCAACTCCAGTACTGGTGCGTCGGGTATG   2100
Tb...10950      GAAGCGCAGGCACCCGTTGCCGCTGCTGCCGCCAACTCCAGTACTGGTGCGTCGGGTATG   2100
Tb...10940      GAAGCGCAGGCACCCGTTGCCGCTGCTGCCGCCAACTCCAGTACTGGTGCGTCGGGTATG   2100
Tb...10910      GAAGCGCAGGCACCCGTTGCCGCTGCTGCCGCCAACTCCAGTACTGGTGCGTCGGGTATG   2100
Tb...10920      GAAGCGCAGGCACCCGTTGCCGCTGCTGCCGCCAACTCCAGTACTGGTGCGTCGGGTATG   2100
Tb...10900      GAAGCGCAGGCACCCGTTGCCGCTGCTGCCGCCAACTCCAGTACTGGTGCGTCGGGTATG   2100
Tb...10890      GAAGCGCAGGCACCCGTTGCCGCTGCTGCCGCCAACTCCAGTACTGGTGCGTCGGGTATG   2100
                ************************************************************

Tb...10930      GAGGAAGTGGACTGA       2115
Tb...10970      GAGGAAGTGGACTGA       2115
Tb...10980      GAGGAAGTGGACTGA       2115
Tb...10960      GAGGAAGTGGACTGA       2115
Tb...10950      GAGGAAGTGGACTGA       2115
Tb...10940      GAGGAAGTGGACTGA       2115
Tb...10910      GAGGAAGTGGACTGA       2115
Tb...10920      GAGGAAGTGGACTGA       2115
Tb...10900      GAGGAAGTGGACTGA       2115
Tb...10890      GAGGAAGTGGACTGA       2115
                ***************
```

Tb427tmp.02.0250/Tb11.02.0250 coding sequence (Putative *TbTRAP*) (69).

RNAi sequence in red

```
ATGATGCGTCGTGTTTGTCAGAGGGTAAACCGACAAGCTCTAACGTCTACCGTTGTGGCT        60
CGCTGTACCGCGACTACCGCTTCGGTGTCTCTAAGAGGAATTTGCCCGCCCGTTTCAACC       120
GATGGTAACCGAAATGCCGGTATTGGACCAATGCAAGGCTCAGTACGTTTCTGCTCCACA       180
CAGGCGGGCGAGAAGGTGCCCGAAGCAGCTGACAATGCCGATGAAGATATTGTTATTGAC       240
CCTGTACCTGATCTAAAGGGCAATGCAGGGGAAAGTGCCGATGAAGGCAGCGCCGGTGGG       300
GTAAAGGCAAACGAGGACAGCGAGAAAGTTGTTGGCAGTGCGGAAGAGATGGGCTTCAAA       360
ACAGAAACCCGTCAGCTTCTGGACATTGTTGCTTGCAGTTTGTACACGGAGAAGGAGGTG       420
TTCATACGTGAACTCGTATCGAATGCAAGCGATGCTCTGGAGAAGCGCCACCTGATGGAG       480
TTGAGCAAACCGGAAGAGTACCCACGCGAGGAAGGTGATGAGGCTCCCATTATTTCCATC       540
ACATGCAATCAAAGCAAGAGCCGATTCGTCATACGTGACACTGGCATTGGTATGACTCGG       600
GAGGAACTAGCGGAGAACCTTGGTACCATTGCTGGCTCGGGCTCAAAGGCATTTGTTCGT       660
GAGTTGCAGAGTCAAGGCGAGAGCAGCAGTGGTGCGGCCGAAAAGATCATTGGTCAGTTT       720
GGCGTTGGTTTCTACGCTGCCTTCATGGTGGCTCGAAATGTCAAGGTGTACAGCCGGAGC       780
GTGAAGAAGGGGAGTAAGGGTTACGTGTGGGAGTCAGATGGTACAGGAACATTTAAGATT       840
GCGGAGTGCGAGGGTGTTGACAAGGGCACGAAAATTGTCCTCGATGTGAAGGACACGGAG       900
CTCTCCTTTTGCACACCGCAGGTGTGTGAGCGCGTGTTGAAACGGTACAGTAACTTTGTC       960
TCCTACGAAATTACACTCAACGGTGGAAAGGTGAACACAGTGGAGGCACTGTGGATGAAG      1020
GATAAGAACTCCGTCACAAATGAGGAGCACATTGATTTCTACAAATTCATCTCCGGTGCG      1080
TACGATAGTCCGATGTTCCGCCTGCATTACGCCGTGGACGCTCCACTTTCTATTCGTGCT      1140
CTTTTGTACGTGCCTCAGTCTCACACGGAGAAGTACGGTGGTGGCCGTATGGAAAGTGGT      1200
GTCAATCTCTACTGCCGCCGAGTACTCATCCAATCGAAGGCGAAGGGAATTCTGCCCGAG      1260
TGGCTCCGCTTCATCAAGGGTGCGGTTGACACAGAGTCTATTCCGCTCAACGTATCACGT      1320
GAACATACCCAGGATGGTAGCATGATGCGCCGGCTCTCAACGGTGCTGACCAAGCGCGTT      1380
ATCCGTTGGATGGAGGAGGAGGCGAAGCAAGACAGGCAAAAGTACGAACGTTTTATAAAG      1440
GAGTACGGTCCTTTCCTGAAGGAGGGAGTTTGTACCGACCAGGTTCACAAGATGGAGCTG      1500
GCGAAGCTTTTGAGGTTTGAAACAACCAAGTCAGACATCGACTACCCCTACGTGTCACTT      1560
GACGAATACCGCGACCGCATGGTGGCAAACCAAACTCACATTTATTACATCAACGCTCCT      1620
TCAAAGGAGATGGCGCTCGAATCTCCCTACTACGAACAGTACAAGGAGCACGACCTCGAG      1680
GTGCTCGTCTGCACAGAACCTATTGATGACTTTGTTATGCAGCACCTTGACACGTATGCG      1740
AAGCATAAACTGCAAAACATTGAACTGTTTGACGCTTCACTTGACGGTAGCGTCCAAAAC      1800
AAGCTTAAACTCGAGGGCGATAAAGGGGAGGTGAAGGTTGAGAAACAACTCACTGAGGCG      1860
```

CAGGTGAAAGCTCTCAGTGACTTTATTTCCAAGCGTCTTGTGGGACGCGTTGGCGTCGTC 1920

AAATCCACCACACGCCTGCGCGATAGTCCTGCTGTTATTGCTGACCATGAATCAGCTCAG 1980

ATGCGCAAGATTTACCGTATCACTGGCCAGATGGCTGGTGCCCCACCCAAGTATAACATG 2040

CATTTCAACCCAAAGCACACCATCGTGCGTAAGTTGTATACCCTTTCCATTTCACCCAAT 2100

TCAGAAGAGGTTGAAACTGCCGGGCTCCTGGTTGAGCAGATGTTTGACAACGCCGTTATC 2160

GCTGCCGGCTTGCTGGAAGATCCGCGTTCCATCGTTTCGCGCCTGAACACCATCATGACG 2220

CGCATGGTGGAAAATGTGGAGGAGCCCACTGCCGATAAGTAG 2262

APPENDIX II

Synthesis of fexinidazole, fexinidazole sulfone, and SCYX-7158, general.

(Performed by David Meyers, PhD, Department of Pharmacology and Molecular Sciences, JHU)

For chemical synthesis, all reagents and solvents were used as supplied by commercial sources without further purification. Anhydrous solvents were purchased from Aldrich (Sure Seal). Reactions involving air and/or moisture-sensitive reagents were carried out under an argon atmosphere. For these reactions, glassware was dried under vacuum with a heat gun and then filled with argon. Reactions were monitored by thin layer chromatography using Analtech chromatography plates (silica gel GHLF, 250 microns). Visualization was performed by UV light (254 and 365 nm) and/or by staining with aqueous potassium permanganate solution. Flash chromatography was performed using a Grace Reveleris flash purification system and Grace silica cartridges (avg. particle size 40 μm). ^{1}H (500 MHz) and ^{13}C (126 MHz) NMR spectra of compounds were obtained using a Varian spectrometer. ^{1}H NMR spectra acquired in $CDCl_3$ were referenced to tetramethylsilane (0 ppm), and spectra acquired in d6-DMSO were referenced to 2.50 ppm. ^{13}C NMR spectra recorded in $CDCl_3$ were referenced to 77.0 ppm. Accurate mass determinations were recorded by the Mass Spectrometry Laboratory, School of Chemical Sciences, University of Illinois.

Synthesis of fexinidazole taken from Samant and Sukhthankar (118). 2-(chloromethyl)-1-methyl-5-nitro-1H-imidazole was obtained from commercially available (1-methyl-5-nitro-1H-imidazol-2-yl)methanol as described (119). Crude product was recrystallized from EtOAc to obtain 107 mg of clear, pale yellow crystals in 95% yield. ^{1}H NMR (500 MHz, CHLOROFORM-d) δ 7.96 (s, 1H), 4.69 (s, 2H), 4.05 (s, 3H). ^{1}H NMR is consistent to Compound **13** reported by Morrow *et al.* (119). Fexinidazole was synthesized as described by Samant and Sukhthankar (Compound **7a**) using Method C. Crude product was purified using a 0 to 100% EtOAc/Hex gradient, and the purified product was recrystallized from EtOAc and hexanes to provide 1.08 g of yellow crystals in 77% yield. ^{1}H NMR (500 MHz, CHLOROFORM-d) δ 7.97 (s, 1H), 7.22 - 7.31 (m, 2H), 6.91 - 7.01 (m, 2H), 5.19 (s, 2H), 4.06 (s,

3H), 2.45 (s, 3H) (Fig. 43*A*). ^{13}C NMR (126 MHz, CHLOROFORM-d) δ 155.6, 147.4, 139.7, 131.7, 130.9, 129.6, 115.4, 62.8, 33.8, 17.4 (Fig. 43*B*). HRMS (m/z): [MH+] calculated for $C_{12}H_{14}N_3O_3S$ 280.0756, found 280.0758.

Synthesis of the sulfone metabolite of fexinidazole, 1-methyl-2-((4-(methylsulfonyl)phenoxy)methyl)-5-nitro-1H-imidazole, taken from Fontana *et al.* (120). ^{1}H NMR (500 MHz, CHLOROFORM-d) δ 7.99 (s, 1H), 7.84 - 7.95 (m, J = 8.96 Hz, 2H), 7.14 - 7.23 (m, J = 8.80 Hz, 2H), 5.30 (s, 2H), 4.07 (s, 3H), 3.03 (s, 3H) (Fig. 43*C*). ^{13}C NMR (126 MHz, CHLOROFORM-d) δ 161.3, 146.3, 139.8, 133.9, 131.6, 129.8, 115.3, 62.8, 44.7, 33.9 (Fig. 43*D*). HRMS (m/z): [MH+] calculated for $C_{12}H_{14}N_3O_5S$ 312.0654, found 312.0651.

Synthesis of SCYX-7158 taken from Jacobs *et al.* (121). 2-(2'-bromophenyl)-6-butyl[1,3,6,2] dioxazaborocan was synthesized from 2-bromophenylboronic acid as described (121). Synthesis of 4-fluoro-N-(1-hydroxy-3,3-dimethyl-1,3-dihydrobenzo[c][1,2]oxaborol-6-yl)-2-(trifluoromethyl)benzamide (SCYX-7158): To a solution of crude 6-amino-3,3-dimethylbenzo[c][1,2]oxaborol-1(3H)-ol (0.85 mmoles, 1.0 equiv.) and iPr_2NEt (435 ul, 2.55 mmoles, 3.0 equiv.) in 5 ml anhydrous CH_2Cl_2 was added 4-fluoro-2-(trifluoromethyl)benzoyl chloride (142 μL, 0.935, 1.1 equiv.) dropwise at 0 °C. After addition was complete, the ice water cooling bath was removed and the reaction was allowed to warm to rt. After stirring for 5 h at rt, the reaction was diluted with CH_2Cl_2, and washed with 5% aq. HCl. The aqueous layer was extracted with CH_2Cl_2 (3 x 10 mL). The organic layers were combined, dried with anhydrous $MgSO_4$, and concentrated in vacuo. Purification by flash chromatography (0 to 100% EtOAc/Hex, then 0 to 10% MeOH/EtOAc) provided 85 mg of an impure solid. A second purification using a gradient of 0 to 10% MeOH/$CHCl_3$ provided 38 mg of the desired product. ^{1}H NMR (500 MHz, DMSO-d6) δ 10.58 (s, 1H), 9.09 (s, 1H), 8.03 (d, J = 1.73 Hz, 1H), 7.76 - 7.87 (m, 2H), 7.69 (dt, J = 2.36, 8.57 Hz, 1H), 7.63 (dd, J = 2.04, 8.33 Hz, 1H), 7.39 (d, J = 8.33 Hz, 1H), 1.44 (s, 6H) (Fig. 44). HRMS (m/z): [MH+] calculated for $C_{17}H_{15}NO_3F_4B$ 368.1081, found 368.1074.

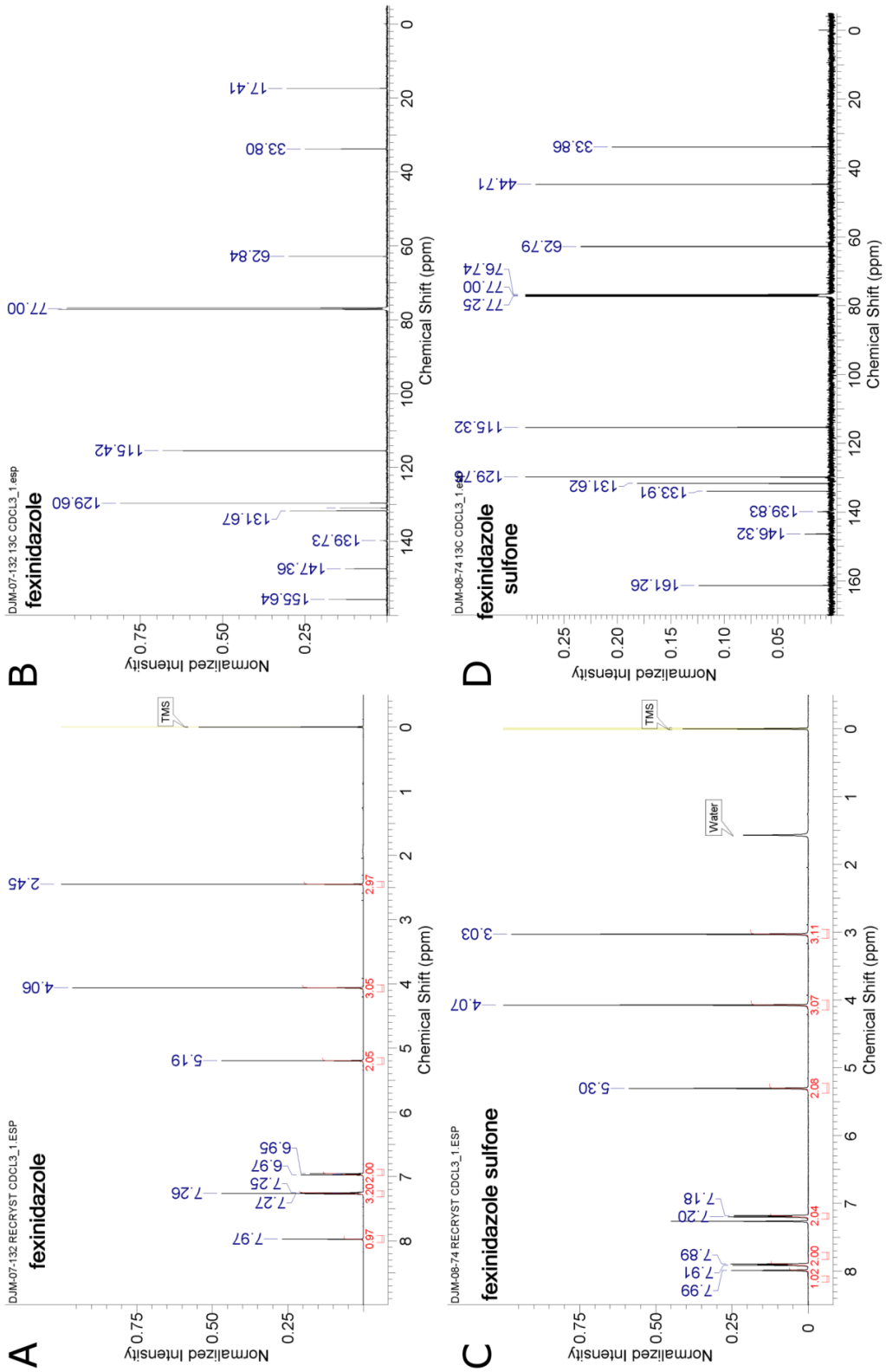

Figure 45. NMR Spectra

NMR spectra for fexinidazole (*A* proton, *B* carbon), and fexinidazole sulfone (*C* proton, *D* carbon), acquired in $CDCl_3$ on a Varian spectrometer, created using ACD/NMR Processor Academic Addition.

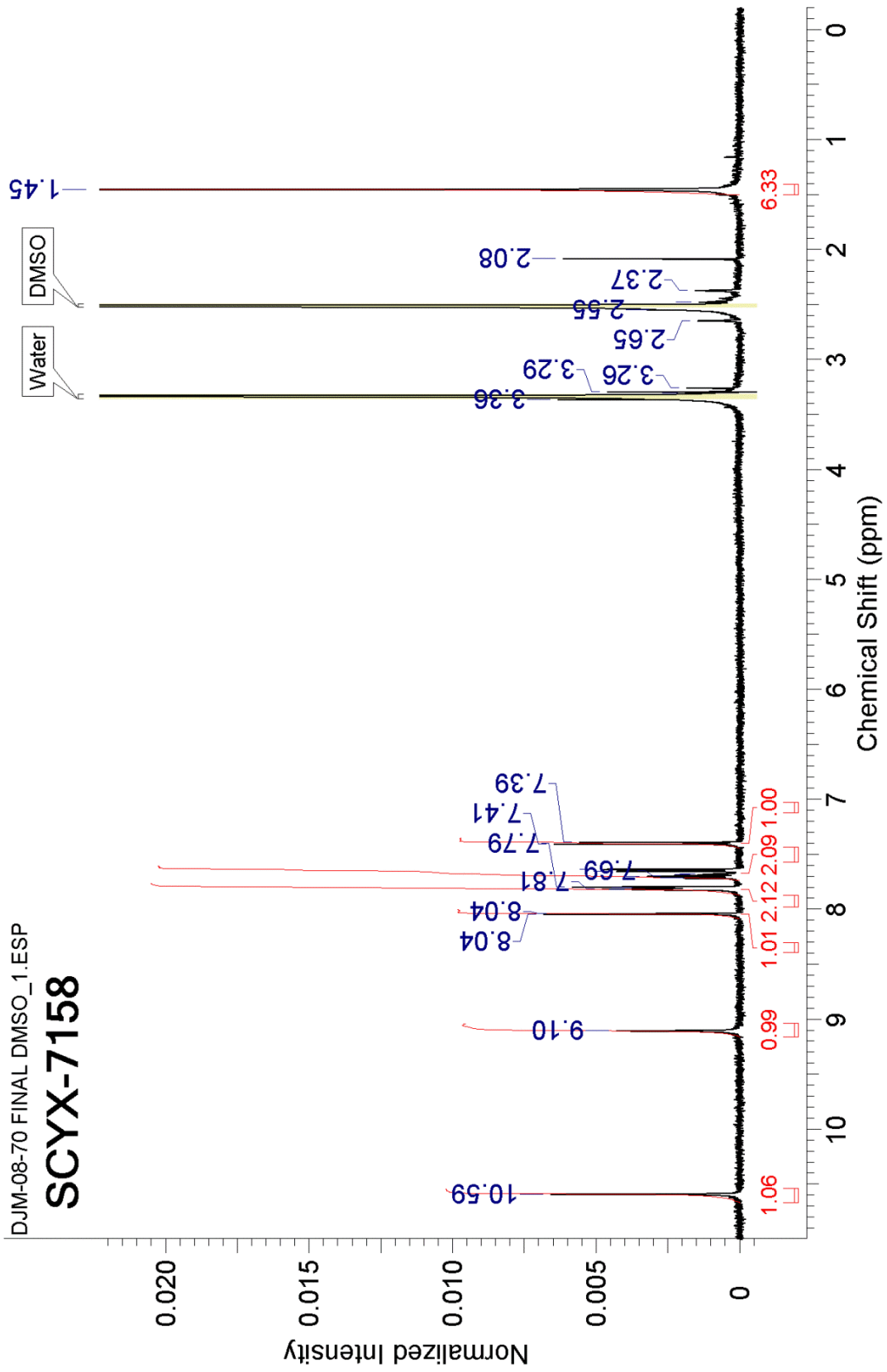

Figure 46. NMR SCYX-7158

^{1}H NMR spectra for SCYX-7158 acquired in d6-DMSO on a Varian spectrometer, created using ACD/NMR Processor Academic Addition.

BIBLIOGRAPHY

1. Brun, R., Blum, J., Chappuis, F., and Burri, C. (2010) Human African trypanosomiasis. *Lancet* **375**, 148-159
2. Kennedy, P. G. (2013) Clinical features, diagnosis, and treatment of human African trypanosomiasis (sleeping sickness). *Lancet Neurol* **12**, 186-194
3. Findlay, G. M. (1930) *Recent advances in chemotherapy*, P. Blakiston's sons & co. inc., Philadelphia
4. Sands, M., Kron, M. A., and Brown, R. B. (1985) Pentamidine: a review. *Rev Infect Dis* **7**, 625-634
5. Steverding, D. (2010) The development of drugs for treatment of sleeping sickness: a historical review. *Parasit Vectors* **3**, 15
6. Van Nieuwenhove, S., Schechter, P. J., Declercq, J., Bone, G., Burke, J., and Sjoerdsma, A. (1985) Treatment of gambiense sleeping sickness in the Sudan with oral DFMO (DL-alpha-difluoromethylornithine), an inhibitor of ornithine decarboxylase; first field trial. *Trans R Soc Trop Med Hyg* **79**, 692-698
7. Stein, C. A., LaRocca, R. V., Thomas, R., McAtee, N., and Myers, C. E. (1989) Suramin: an anticancer drug with a unique mechanism of action. *J Clin Oncol* **7**, 499-508
8. Soignet, S. L., Tong, W. P., Hirschfeld, S., and Warrell, R. P., Jr. (1999) Clinical study of an organic arsenical, melarsoprol, in patients with advanced leukemia. *Cancer chemotherapy and pharmacology* **44**, 417-421
9. Csermely, P., Schnaider, T., Soti, C., Prohaszka, Z., and Nardai, G. (1998) The 90-kDa molecular chaperone family: structure, function, and clinical applications. A comprehensive review. *Pharmacol Ther* **79**, 129-168
10. Csermely, P., Kajtar, J., Hollosi, M., Jalsovszky, G., Holly, S., Kahn, C. R., Gergely, P., Jr., Soti, C., Mihaly, K., and Somogyi, J. (1993) ATP induces a conformational change of the 90-kDa heat shock protein (hsp90). *The Journal of biological chemistry* **268**, 1901-1907
11. Li, J., Soroka, J., and Buchner, J. (2012) The Hsp90 chaperone machinery: conformational dynamics and regulation by co-chaperones. *Biochim Biophys Acta* **1823**, 624-635
12. Mollapour, M., and Neckers, L. (2012) Post-translational modifications of Hsp90 and their contributions to chaperone regulation. *Biochim Biophys Acta* **1823**, 648-655
13. Hartson, S. D., and Matts, R. L. (2012) Approaches for defining the Hsp90-dependent proteome. *Biochim Biophys Acta* **1823**, 656-667
14. Mottram, J. C., Murphy, W. J., and Agabian, N. (1989) A transcriptional analysis of the *Trypanosoma brucei* Hsp83 gene cluster. *Mol Biochem Parasitol* **37**, 115-127
15. Jones, C., Anderson, S., Singha, U. K., and Chaudhuri, M. (2008) Protein phosphatase 5 is required for Hsp90 function during proteotoxic stresses in *Trypanosoma brucei*. *Parasitol Res* **102**, 835-844
16. Muhich, M. L., and Boothroyd, J. C. (1988) Polycistronic transcripts in trypanosomes and their accumulation during heat-shock - evidence for a precursor role in messenger-RNA synthesis. *Mol Cell Biol* **8**, 3837-3846
17. Fairlamb, A. H., and Cerami, A. (1992) Metabolism and functions of trypanothione in the Kinetoplastida. *Annual review of microbiology* **46**, 695-729
18. Zhou, Q., Hu, H., and Li, Z. (2014) New insights into the molecular mechanisms of mitosis and cytokinesis in trypanosomes. *International review of cell and molecular biology* **308**, 127-166
19. Hammarton, T. C. (2007) Cell cycle regulation in *Trypanosoma brucei*. *Mol Biochem Parasitol* **153**, 1-8

20. Whitesell, L., Mimnaugh, E. G., Decosta, B., Myers, C. E., and Neckers, L. M. (1994) Inhibition of Heat-Shock Protein Hsp90-Pp60(V-Src) Heteroprotein Complex-Formation by Benzoquinone Ansamycins - Essential Role for Stress Proteins in Oncogenic Transformation. *Proceedings of the National Academy of Sciences of the United States of America* **91**, 8324-8328
21. Dutta, R., and Inouye, M. (2000) GHKL, an emergent ATPase/kinase superfamily. *Trends in biochemical sciences* **25**, 24-28
22. DeBoer, C., Meulman, P. A., Wnuk, R. J., and Peterson, D. H. (1970) Geldanamycin, a new antibiotic. *J Antibiot (Tokyo)* **23**, 442-447
23. Neckers, L. (2002) Hsp90 inhibitors as novel cancer chemotherapeutic agents. *Trends in Molecular Medicine* **8**, S55-S61
24. Jhaveri, K., Ochiana, S. O., Dunphy, M. P., Gerecitano, J. F., Corben, A. D., Peter, R. I., Janjigian, Y. Y., Gomes-DaGama, E. M., Koren, J., 3rd, Modi, S., and Chiosis, G. (2014) Heat shock protein 90 inhibitors in the treatment of cancer: current status and future directions. *Expert opinion on investigational drugs* **23**, 611-628
25. Vickerman, K., and Cox, F. E. G. (1967) *The Protozoa*, Houghton Mifflin
26. Butler, L. M., Ferraldeschi, R., Armstrong, H. K., Centenera, M. M., and Workman, P. (2015) Maximizing the Therapeutic Potential of HSP90 Inhibitors. *Molecular cancer research : MCR* **13**, 1445-1451
27. Rochani, A. K., Singh, M., and Tatu, U. (2013) Heat shock protein 90 inhibitors as broad spectrum anti-infectives. *Curr Pharm Des* **19**, 377-386
28. Drusano, G. L. (2004) Antimicrobial pharmacodynamics: critical interactions of 'bug and drug'. *Nat Rev Microbiol* **2**, 289-300
29. Schmidt, S., Barbour, A., Sahre, M., Rand, K. H., and Derendorf, H. (2008) PK/PD: new insights for antibacterial and antiviral applications. *Curr Opin Pharmacol* **8**, 549-556
30. Meyer, K. J., and Shapiro, T. A. (2013) Potent antitrypanosomal activities of heat shock protein 90 inhibitors in vitro and in vivo. *The Journal of infectious diseases* **208**, 489-499
31. Taipale, M., Jarosz, D. F., and Lindquist, S. (2010) Hsp90 at the hub of protein homeostasis: emerging mechanistic insights. *Nat Rev Mol Cell Biol* **11**, 515-528
32. Kaplan, K. B., and Li, R. (2012) A prescription for 'stress' - the role of Hsp90 in genome stability and cellular adaptation. *Trends in cell biology* **22**, 576-583
33. Trepel, J., Mollapour, M., Giaccone, G., and Neckers, L. (2010) Targeting the dynamic Hsp90 complex in cancer. *Nat Rev Cancer* **10**, 537-549
34. Whitesell, L., and Lin, N. U. (2012) Hsp90 as a platform for the assembly of more effective cancer chemotherapy. *Biochim Biophys Acta* **1823**, 756-766
35. Travers, J., Sharp, S., and Workman, P. (2012) Hsp90 inhibition: two-pronged exploitation of cancer dependencies. *Drug Discov Today* **17**, 242-252
36. Kamal, A., Thao, L., Sensintaffar, J., Zhang, L., Boehm, M. F., Fritz, L. C., and Burrows, F. J. (2003) A high-affinity conformation of Hsp90 confers tumour selectivity on Hsp90 inhibitors. *Nature* **425**, 407-410
37. Matts, R. L., Brandt, G. E., Lu, Y., Dixit, A., Mollapour, M., Wang, S., Donnelly, A. C., Neckers, L., Verkhivker, G., and Blagg, B. S. (2011) A systematic protocol for the characterization of Hsp90 modulators. *Bioorg Med Chem* **19**, 684-692
38. Lu, X., Xiao, L., Wang, L., and Ruden, D. M. (2012) Hsp90 inhibitors and drug resistance in cancer: the potential benefits of combination therapies of Hsp90 inhibitors and other anti-cancer drugs. *Biochemical pharmacology* **83**, 995-1004
39. Bodley, A. L., McGarry, M. W., and Shapiro, T. A. (1995) Drug cytotoxicity assay for African trypanosomes and Leishmania species. *The Journal of infectious diseases* **172**, 1157-1159

40. Grenert, J. P., Sullivan, W. P., Fadden, P., Haystead, T. A. J., Clark, J., Mimnaugh, E., Krutzsch, H., Ochel, H. J., Schulte, T. W., Sausville, E., Neckers, L. M., and Toft, D. O. (1997) The amino-terminal domain of heat shock protein 90 (Hsp90) that binds geldanamycin is an ATP/ADP switch domain that regulates Hsp90 conformation. *The Journal of biological chemistry* **272**, 23843-23850
41. Schulte, T. W., Akinaga, S., Soga, S., Sullivan, W., Stensgard, B., Toft, D., and Neckers, L. M. (1998) Antibiotic radicicol binds to the N-terminal domain of Hsp90 and shares important biologic activities with geldanamycin. *Cell Stress Chaperones* **3**, 100-108
42. Bao, R., Lai, C. J., Qu, H., Wang, D., Yin, L., Zifcak, B., Atoyan, R., Wang, J., Samson, M., Forrester, J., DellaRocca, S., Xu, G. X., Tao, X., Zhai, H. X., Cai, X., and Qian, C. (2009) CUDC-305, a novel synthetic HSP90 inhibitor with unique pharmacologic properties for cancer therapy. *Clinical cancer research : an official journal of the American Association for Cancer Research* **15**, 4046-4057
43. Marcu, M. G., Chadli, A., Bouhouche, I., Catelli, M., and Neckers, L. M. (2000) The heat shock protein 90 antagonist novobiocin interacts with a previously unrecognized ATP-binding domain in the carboxyl terminus of the chaperone. *The Journal of biological chemistry* **275**, 37181-37186
44. Johnson, V. A., Singh, E. K., Nazarova, L. A., Alexander, L. D., and McAlpine, S. R. (2010) Macrocyclic inhibitors of Hsp90. *Current topics in medicinal chemistry* **10**, 1380-1402
45. Nadeau, K., Sullivan, M. A., Bradley, M., Engman, D. M., and Walsh, C. T. (1992) 83-kilodalton heat shock proteins of trypanosomes are potent peptide-stimulated ATPases. *Protein Sci* **1**, 970-979
46. Pizarro, J. C., Hills, T., Senisterra, G., Wernimont, A. K., Mackenzie, C., Norcross, N. R., Ferguson, M. A., Wyatt, P. G., Gilbert, I. H., and Hui, R. (2013) Exploring the *Trypanosoma brucei* Hsp83 potential as a target for structure guided drug design. *PLoS Negl Trop Dis* **7**, e2492
47. Barker, C. R., McNamara, A. V., Rackstraw, S. A., Nelson, D. E., White, M. R., Watson, A. J., and Jenkins, J. R. (2006) Inhibition of Hsp90 acts synergistically with topoisomerase II poisons to increase the apoptotic killing of cells due to an increase in topoisomerase II mediated DNA damage. *Nucleic acids research* **34**, 1148-1157
48. Mimnaugh, E. G., Xu, W., Vos, M., Yuan, X., Isaacs, J. S., Bisht, K. S., Gius, D., and Neckers, L. (2004) Simultaneous inhibition of hsp 90 and the proteasome promotes protein ubiquitination, causes endoplasmic reticulum-derived cytosolic vacuolization, and enhances antitumor activity. *Mol Cancer Ther* **3**, 551-566
49. Egorin, M. J., Lagattuta, T. F., Hamburger, D. R., Covey, J. M., White, K. D., Musser, S. M., and Eiseman, J. L. (2002) Pharmacokinetics, tissue distribution, and metabolism of 17-(dimethylaminoethylamino)-17-demethoxygeldanamycin (NSC 707545) in CD2F1 mice and Fischer 344 rats. *Cancer chemotherapy and pharmacology* **49**, 7-19
50. Glaze, E. R., Lambert, A. L., Smith, A. C., Page, J. G., Johnson, W. D., McCormick, D. L., Brown, A. P., Levine, B. S., Covey, J. M., Egorin, M. J., Eiseman, J. L., Holleran, J. L., Sausville, E. A., and Tomaszewski, J. E. (2005) Preclinical toxicity of a geldanamycin analog, 17-(dimethylaminoethylamino)-17-demethoxygeldanamycin (17-DMAG), in rats and dogs: potential clinical relevance. *Cancer chemotherapy and pharmacology* **56**, 637-647
51. Amolins, M. W., and Blagg, B. S. (2009) Natural product inhibitors of Hsp90: potential leads for drug discovery. *Mini Rev Med Chem* **9**, 140-152
52. Bangs, J. D., Brouch, E. M., Ransom, D. M., and Roggy, J. L. (1996) A soluble secretory reporter system in *Trypanosoma brucei*. Studies on endoplasmic reticulum targeting. *The Journal of biological chemistry* **271**, 18387-18393

53. Descoteaux, A., Avila, H. A., Zhang, K., Turco, S. J., and Beverley, S. M. (2002) Leishmania LPG3 encodes a GRP94 homolog required for phosphoglycan synthesis implicated in parasite virulence but not viability. *Embo J* **21**, 4458-4469
54. Jensen, R. E., and Englund, P. T. (2012) Network news: The replication of kinetoplast DNA. in *Ann Rev of Microbiol* (Gottesman, S., Harwood, C. S., and Schneewind, O. eds.). pp 473-491
55. McKean, P. G. (2003) Coordination of cell cycle and cytokinesis in *Trypanosoma brucei*. *Curr Opin Microbiol* **6**, 600-607
56. Woodward, R., and Gull, K. (1990) Timing of nuclear and kinetoplast DNA replication and early morphological events in the cell cycle of *Trypanosoma brucei*. *J Cell Sci* **95 (Pt 1)**, 49-57
57. Li, Z. (2012) Regulation of the cell division cycle in *Trypanosoma brucei*. *Eukaryot Cell* **11**, 1180-1190
58. Shapiro, T. A. (1993) Inhibition of topoisomerases in African trypanosomes. *Acta tropica* **54**, 251-260
59. Graefe, S. E. B., Wiesgigl, M., Gaworski, I., Macdonald, A., and Clos, J. (2002) Inhibition of Hsp90 in *Trypanosoma cruzi* induces a stress response but no stage differentiation. *Eukaryot Cell* **1**, 936-943
60. Wiesgigl, M., and Clos, J. (2001) Heat shock protein 90 homeostasis controls stage differentiation in *Leishmania donovani*. *Mol Biol Cell* **12**, 3307-3316
61. Li, Q., Zhou, Y., Yao, C., Ma, X., Wang, L., Xu, W., Wang, Z., and Qiao, Z. (2009) Apoptosis caused by Hsp90 inhibitor geldanamycin in *Leishmania donovani* during promastigote-to-amastigote transformation stage. *Parasitol Res* **105**, 1539-1548
62. Adriano, M. A., Vergnes, B., Poncet, J., Mathieu-Daude, F., da Silva, A. C., Ouaissi, A., and Sereno, D. (2007) Proof of interaction between Leishmania Sir2RP1 deacetylase and chaperone Hsp83. *Parasitol Res* **100**, 811-818
63. Altieri, D. C., Stein, G. S., Lian, J. B., and Languino, L. R. (2012) TRAP-1, the mitochondrial Hsp90. *Biochim Biophys Acta* **1823**, 767-773
64. Rasola, A., Neckers, L., and Picard, D. (2014) Mitochondrial oxidative phosphorylation TRAP(1)ped in tumor cells. *Trends in cell biology* **24**, 455-463
65. Wirtz, E., Leal, S., Ochatt, C., and Cross, G. A. (1999) A tightly regulated inducible expression system for conditional gene knock-outs and dominant-negative genetics in Trypanosoma brucei. *Mol Biochem Parasitol* **99**, 89-101
66. Field, M. C., Allen, C. L., Dhir, V., Goulding, D., Hall, B. S., Morgan, G. W., Veazey, P., and Engstler, M. (2004) New approaches to the microscopic imaging of *Trypanosoma brucei*. *Microsc Microanal* **10**, 621-636
67. Shapiro, T. A., Klein, V. A., and Englund, P. T. (1989) Drug-promoted cleavage of kinetoplast DNA minicircles. Evidence for type II topoisomerase activity in trypanosome mitochondria. *The Journal of biological chemistry* **264**, 4173-4178
68. Church, G. M., and Gilbert, W. (1984) Genomic sequencing. *Proceedings of the National Academy of Sciences of the United States of America* **81**, 1991-1995
69. Aslett, M., Aurrecoechea, C., Berriman, M., Brestelli, J., Brunk, B. P., Carrington, M., Depledge, D. P., Fischer, S., Gajria, B., Gao, X., Gardner, M. J., Gingle, A., Grant, G., Harb, O. S., Heiges, M., Hertz-Fowler, C., Houston, R., Innamorato, F., Iodice, J., Kissinger, J. C., Kraemer, E., Li, W., Logan, F. J., Miller, J. A., Mitra, S., Myler, P. J., Nayak, V., Pennington, C., Phan, I., Pinney, D. F., Ramasamy, G., Rogers, M. B., Roos, D. S., Ross, C., Sivam, D., Smith, D. F., Srinivasamoorthy, G., Stoeckert, C. J., Jr., Subramanian, S., Thibodeau, R., Tivey, A., Treatman, C., Velarde, G., and Wang, H. (2010) TriTrypDB: a functional genomic resource for the Trypanosomatidae. *Nucleic acids research* **38**, D457-462

70. Redmond, S., Vadivelu, J., and Field, M. C. (2003) RNAit: an automated web-based tool for the selection of RNAi targets in Trypanosoma brucei. *Mol Biochem Parasitol* **128**, 115-118
71. Silverman, J. S., Schwartz, K. J., Hajduk, S. L., and Bangs, J. D. (2011) Late endosomal Rab7 regulates lysosomal trafficking of endocytic but not biosynthetic cargo in Trypanosoma brucei. *Mol Microbiol* **82**, 664-678
72. Oberholzer, M., Morand, S., Kunz, S., and Seebeck, T. (2006) A vector series for rapid PCR-mediated C-terminal in situ tagging of Trypanosoma brucei genes. *Mol Biochem Parasitol* **145**, 117-120
73. Borst, P., van der Ploeg, M., van Hoek, J. F., Tas, J., and James, J. (1982) On the DNA content and ploidy of trypanosomes. *Mol Biochem Parasitol* **6**, 13-23
74. Panigrahi, A. K., Ogata, Y., Zikova, A., Anupama, A., Dalley, R. A., Acestor, N., Myler, P. J., and Stuart, K. D. (2009) A comprehensive analysis of Trypanosoma brucei mitochondrial proteome. *Proteomics* **9**, 434-450
75. Tu, X., and Wang, C. C. (2004) The involvement of two cdc2-related kinases (CRKs) in *Trypanosoma brucei* cell cycle regulation and the distinctive stage-specific phenotypes caused by CRK3 depletion. *The Journal of biological chemistry* **279**, 20519-20528
76. Tu, X., Kumar, P., Li, Z., and Wang, C. C. (2006) An aurora kinase homologue is involved in regulating both mitosis and cytokinesis in *Trypanosoma brucei*. *The Journal of biological chemistry* **281**, 9677-9687
77. Hammarton, T. C., Kramer, S., Tetley, L., Boshart, M., and Mottram, J. C. (2007) *Trypanosoma brucei* Polo-like kinase is essential for basal body duplication, kDNA segregation and cytokinesis. *Mol Microbiol* **65**, 1229-1248
78. Hammarton, T. C., Clark, J., Douglas, F., Boshart, M., and Mottram, J. C. (2003) Stage-specific differences in cell cycle control in *Trypanosoma brucei* revealed by RNA interference of a mitotic cyclin. *The Journal of biological chemistry* **278**, 22877-22886
79. Hammarton, T. C., Lillico, S. G., Welburn, S. C., and Mottram, J. C. (2005) *Trypanosoma brucei* MOB1 is required for accurate and efficient cytokinesis but not for exit from mitosis. *Mol Microbiol* **56**, 104-116
80. Rothberg, K. G., Burdette, D. L., Pfannstiel, J., Jetton, N., Singh, R., and Ruben, L. (2006) The RACK1 homologue from *Trypanosoma brucei* is required for the onset and progression of cytokinesis. *The Journal of biological chemistry* **281**, 9781-9790
81. Lange, B. M. H., Rebollo, E., Herold, A., and Gonzalez, C. (2002) Cdc37 is essential for chromosome segregation and cytokinesis in higher eukaryotes. *The EMBO journal* **21**, 5364-5374
82. Caldas-Lopes, E., Cerchietti, L., Ahn, J. H., Clement, C. C., Robles, A. I., Rodina, A., Moulick, K., Taldone, T., Gozman, A., Guo, Y., Wu, N., de Stanchina, E., White, J., Gross, S. S., Ma, Y., Varticovski, L., Melnick, A., and Chiosis, G. (2009) Hsp90 inhibitor PU-H71, a multimodal inhibitor of malignancy, induces complete responses in triple-negative breast cancer models. *Proceedings of the National Academy of Sciences of the United States of America* **106**, 8368-8373
83. Simizu, S., and Osada, H. (2000) Mutations in the Plk gene lead to instability of Plk protein in human tumour cell lines. *Nat Cell Biol* **2**, 852-854
84. Basto, R., Gergely, F., Draviam, V. M., Ohkura, H., Liley, K., and Raff, J. W. (2007) Hsp90 is required to localise cyclin B and Msps/ch-TOG to the mitotic spindle in Drosophila and humans. *J Cell Sci* **120**, 1278-1287
85. Hammarton, T. C., Monnerat, S., and Mottram, J. C. (2007) Cytokinesis in trypanosomatids. *Curr Opin Microbiol* **10**, 520-527
86. Ma, J., Benz, C., Grimaldi, R., Stockdale, C., Wyatt, P., Frearson, J., and Hammarton, T. C. (2010) Nuclear DBF-2-related kinases are essential regulators of cytokinesis in

bloodstream stage Trypanosoma brucei. *The Journal of biological chemistry* **285**, 15356-15368

87. Benz, C., Clucas, C., Mottram, J. C., and Hammarton, T. C. (2012) Cytokinesis in bloodstream stage Trypanosoma brucei requires a family of katanins and spastin. *PloS one* **7**, e30367
88. Hu, L., Hu, H., and Li, Z. (2012) A kinetoplastid-specific kinesin is required for cytokinesis and for maintenance of cell morphology in Trypanosoma brucei. *Mol Microbiol* **83**, 565-578
89. Alsford, S., Turner, D. J., Obado, S. O., Sanchez-Flores, A., Glover, L., Berriman, M., Hertz-Fowler, C., and Horn, D. (2011) High-throughput phenotyping using parallel sequencing of RNA interference targets in the African trypanosome. *Genome Res* **21**, 915-924
90. Martinez, M. N., Papich, M. G., and Drusano, G. L. (2012) Dosing regimen matters: the importance of early intervention and rapid attainment of the pharmacokinetic/pharmacodynamic target. *Antimicrobial agents and chemotherapy* **56**, 2795-2805
91. Eagle, H., Fleischman, R., and Musselman, A. D. (1950) Effect of schedule of administration on the therapeutic efficacy of penicillin; importance of the aggregate time penicillin remains at effectively bactericidal levels. *The American journal of medicine* **9**, 280-299
92. Moore, R. D., Lietman, P. S., and Smith, C. R. (1987) Clinical response to aminoglycoside therapy: importance of the ratio of peak concentration to minimal inhibitory concentration. *The Journal of infectious diseases* **155**, 93-99
93. Rybak, M. J., Abate, B. J., Kang, S. L., Ruffing, M. J., Lerner, S. A., and Drusano, G. L. (1999) Prospective evaluation of the effect of an aminoglycoside dosing regimen on rates of observed nephrotoxicity and ototoxicity. *Antimicrobial agents and chemotherapy* **43**, 1549-1555
94. Shah, N. P., Kantarjian, H. M., Kim, D. W., Rea, D., Dorlhiac-Llacer, P. E., Milone, J. H., Vela-Ojeda, J., Silver, R. T., Khoury, H. J., Charbonnier, A., Khoroshko, N., Paquette, R. L., Deininger, M., Collins, R. H., Otero, I., Hughes, T., Bleickardt, E., Strauss, L., Francis, S., and Hochhaus, A. (2008) Intermittent target inhibition with dasatinib 100 mg once daily preserves efficacy and improves tolerability in imatinib-resistant and -intolerant chronic-phase chronic myeloid leukemia. *J Clin Oncol* **26**, 3204-3212
95. Shah, N. P., Kasap, C., Weier, C., Balbas, M., Nicoll, J. M., Bleickardt, E., Nicaise, C., and Sawyers, C. L. (2008) Transient potent BCR-ABL inhibition is sufficient to commit chronic myeloid leukemia cells irreversibly to apoptosis. *Cancer Cell* **14**, 485-493
96. Jiang, J. B., Li, G. Q., Guo, X. B., Kong, Y. C., and Arnold, K. (1982) Antimalarial activity of mefloquine and qinghaosu. *Lancet* **2**, 285-288
97. Blaser, J., Stone, B. B., and Zinner, S. H. (1985) Two compartment kinetic model with multiple artificial capillary units. *J Antimicrob Chemother* **15 Suppl A**, 131-137
98. Moore, M. R., Hamzeh, F. M., Lee, F. E., and Lietman, P. S. (1994) Activity of (S)-1-(3-hydroxy-2-phosphonylmethoxypropyl) cytosine against human cytomegalovirus when administered as single-bolus dose and continuous infusion in in vitro cell culture perfusion system. *Antimicrobial agents and chemotherapy* **38**, 2404-2408
99. Bakshi, R. P., Nenortas, E., Tripathi, A. K., Sullivan, D. J., and Shapiro, T. A. (2013) Model system to define pharmacokinetic requirements for antimalarial drug efficacy. *Sci Transl Med* **5**, 205ra135
100. Neckers, L., and Workman, P. (2012) Hsp90 molecular chaperone inhibitors: are we there yet? *Clinical cancer research : an official journal of the American Association for Cancer Research* **18**, 64-76

101. Grem, J. L., Morrison, G., Guo, X. D., Agnew, E., Takimoto, C. H., Thomas, R., Szabo, E., Grochow, L., Grollman, F., Hamilton, J. M., Neckers, L., and Wilson, R. H. (2005) Phase I and pharmacologic study of 17-(allylamino)-17-demethoxygeldanamycin in adult patients with solid tumors. *J Clin Oncol* **23**, 1885-1893
102. Kummar, S., Gutierrez, M. E., Gardner, E. R., Chen, X., Figg, W. D., Zajac-Kaye, M., Chen, M., Steinberg, S. M., Muir, C. A., Yancey, M. A., Horneffer, Y. R., Juwara, L., Melillo, G., Ivy, S. P., Merino, M., Neckers, L., Steeg, P. S., Conley, B. A., Giaccone, G., Doroshow, J. H., and Murgo, A. J. (2010) Phase I trial of 17-dimethylaminoethylamino-17-demethoxygeldanamycin (17-DMAG), a heat shock protein inhibitor, administered twice weekly in patients with advanced malignancies. *Eur J Cancer* **46**, 340-347
103. Meyer, K. J. (2015) PK/PD of anti-trypanosomal agents. in *Interscience Conference on Antimicrobial Agents and Chemotherapy 2015*, San Diego
104. Egorin, M. J., Zuhowski, E. G., Rosen, D. M., Sentz, D. L., Covey, J. M., and Eiseman, J. L. (2001) Plasma pharmacokinetics and tissue distribution of 17-(allylamino)-17-demethoxygeldanamycin (NSC 330507) in CD2F1 mice1. *Cancer chemotherapy and pharmacology* **47**, 291-302
105. Ramanathan, R. K., Trump, D. L., Eiseman, J. L., Belani, C. P., Agarwala, S. S., Zuhowski, E. G., Lan, J., Potter, D. M., Ivy, S. P., Ramalingam, S., Brufsky, A. M., Wong, M. K., Tutchko, S., and Egorin, M. J. (2005) Phase I pharmacokinetic-pharmacodynamic study of 17-(allylamino)-17-demethoxygeldanamycin (17AAG, NSC 330507), a novel inhibitor of heat shock protein 90, in patients with refractory advanced cancers. *Clinical cancer research : an official journal of the American Association for Cancer Research* **11**, 3385-3391
106. Isambert, N., Hollebecque, A., Berge, Y., van Ingen, H., Brienza, S., Destaillats, A., Soria, J.-C., Fumoleau, P., and Delord, J.-P. (2012) A phase I study of Debio 0932, an oral HSP90 inhibitor, in patients with solid tumors. *ASCO Meeting Abstracts* **30**, 3026
107. Sessa, C., Shapiro, G. I., Bhalla, K. N., Britten, C., Jacks, K. S., Mita, M., Papadimitrakopoulou, V., Pluard, T., Samuel, T. A., Akimov, M., Quadt, C., Fernandez-Ibarra, C., Lu, H., Bailey, S., Chica, S., and Banerji, U. (2013) First-in-human phase I dose-escalation study of the HSP90 inhibitor AUY922 in patients with advanced solid tumors. *Clinical cancer research : an official journal of the American Association for Cancer Research* **19**, 3671-3680
108. Banerji, U., O'Donnell, A., Scurr, M., Pacey, S., Stapleton, S., Asad, Y., Simmons, L., Maloney, A., Raynaud, F., Campbell, M., Walton, M., Lakhani, S., Kaye, S., Workman, P., and Judson, I. (2005) Phase I pharmacokinetic and pharmacodynamic study of 17-allylamino, 17-demethoxygeldanamycin in patients with advanced malignancies. *J Clin Oncol* **23**, 4152-4161
109. Lancet, J. E., Gojo, I., Burton, M., Quinn, M., Tighe, S. M., Kersey, K., Zhong, Z., Albitar, M. X., Bhalla, K., Hannah, A. L., and Baer, M. R. (2010) Phase I study of the heat shock protein 90 inhibitor alvespimycin (KOS-1022, 17-DMAG) administered intravenously twice weekly to patients with acute myeloid leukemia. *Leukemia* **24**, 699-705
110. Burri, C. (2010) Chemotherapy against human African trypanosomiasis: is there a road to success? *Parasitology* **137**, 1987-1994
111. Moore, G. A., Rossi, L., Nicotera, P., Orrenius, S., and O'Brien, P. J. (1987) Quinone toxicity in hepatocytes: studies on mitochondrial Ca2+ release induced by benzoquinone derivatives. *Arch Biochem Biophys* **259**, 283-295
112. Zhou, D., Liu, Y., Ye, J., Ying, W., Ogawa, L. S., Inoue, T., Tatsuta, N., Wada, Y., Koya, K., Huang, Q., Bates, R. C., and Sonderfan, A. J. (2013) A rat retinal damage model

predicts for potential clinical visual disturbances induced by Hsp90 inhibitors. *Toxicol Appl Pharmacol* **273**, 401-409

113. Goldman, J. W., Raju, R. N., Gordon, G. A., El-Hariry, I., Teofilivici, F., Vukovic, V. M., Bradley, R., Karol, M. D., Chen, Y., Guo, W., Inoue, T., and Rosen, L. S. (2013) A first in human, safety, pharmacokinetics, and clinical activity phase I study of once weekly administration of the Hsp90 inhibitor ganetespib (STA-9090) in patients with solid malignancies. *BMC Cancer* **13**, 152
114. Yong, K., Cavet, J., Johnson, P., Morgan, G., Williams, C., Nakashima, D., Akinaga, S., Oakervee, H., and Cavenagh, J. (2016) Phase I study of KW-2478, a novel Hsp90 inhibitor, in patients with B-cell malignancies. *Br J Cancer* **114**, 7-13
115. Hong, D., Said, R., Falchook, G., Naing, A., Moulder, S., Tsimberidou, A. M., Galluppi, G., Dakappagari, N., Storgard, C., Kurzrock, R., and Rosen, L. S. (2013) Phase I study of BIIB028, a selective heat shock protein 90 inhibitor, in patients with refractory metastatic or locally advanced solid tumors. *Clinical cancer research : an official journal of the American Association for Cancer Research* **19**, 4824-4831
116. Massey, A. J., Schoepfer, J., Brough, P. A., Brueggen, J., Chene, P., Drysdale, M. J., Pfaar, U., Radimerski, T., Ruetz, S., Schweitzer, A., Wood, M., Garcia-Echeverria, C., and Jensen, M. R. (2010) Preclinical antitumor activity of the orally available heat shock protein 90 inhibitor NVP-BEP800. *Mol Cancer Ther* **9**, 906-919
117. Tarral, A. (2014) New treatments for sleeping sickness. in *American Society for Tropical Medicine and Hygiene (ASTMH), 63rd Annual Meeting* Drugs for Neglected Diseases Initiative, http://www.dndi.org/images/stories/events2014/14astmh/Tarral_TreatmentsHAT_ASTMH_2014.pdf, New Orleans
118. Samant, B. S., and Sukhthankar, M. G. (2011) Compounds containing 2-substituted imidazole ring for treatment against human African trypanosomiasis. *Bioorganic & medicinal chemistry letters* **21**, 1015-1018
119. Morrow, N., Ramsden, C. A., Sargent, B. J., and Wallett, C. D. (1998) Oxidative decarbonylation of β-arylpyruvic acids using sodium perborate. *Tetrahedron* **54**, 9603-9612
120. Fontana, E., Pignatti, A., Venegoni, S., and Bray, M. A. (2011) Synthesis of 2H- and 14C-labeled fexinidazole and its primary metabolites labeled with 2H. *Journal of Labelled Compounds and Radiopharmaceuticals* **54**, 714-719
121. Jacobs, R. T., Plattner, J. J., Nare, B., Wring, S. A., Chen, D., Freund, Y., Gaukel, E. G., Orr, M. D., Perales, J. B., Jenks, M., Noe, R. A., Sligar, J. M., Zhang, Y. K., Bacchi, C. J., Yarlett, N., and Don, R. (2011) Benzoxaboroles: a new class of potential drugs for human African trypanosomiasis. *Future Med Chem* **3**, 1259-1278
122. Bacchi, C. J., Nathan, H. C., Hutner, S. H., McCann, P. P., and Sjoerdsma, A. (1980) Polyamine metabolism: a potential therapeutic target in trypanosomes. *Science* **210**, 332-334
123. Jennings, F. W. (1988) Chemotherapy of trypanosomiasis: the potentiation of melarsoprol by concurrent difluoromethylornithine (DFMO) treatment. *Trans R Soc Trop Med Hyg* **82**, 572-573
124. Abeloff, M. D., Slavik, M., Luk, G. D., Griffin, C. A., Hermann, J., Blanc, O., Sjoerdsma, A., and Baylin, S. B. (1984) Phase I trial and pharmacokinetic studies of alpha-difluoromethylornithine--an inhibitor of polyamine biosynthesis. *J Clin Oncol* **2**, 124-130
125. Milord, F., Pepin, J., Loko, L., Ethier, L., and Mpia, B. (1992) Efficacy and toxicity of eflornithine for treatment of Trypanosoma brucei gambiense sleeping sickness. *Lancet* **340**, 652-655

126. Priotto, G., Kasparian, S., Mutombo, W., Ngouama, D., Ghorashian, S., Arnold, U., Ghabri, S., Baudin, E., Buard, V., Kazadi-Kyanza, S., Ilunga, M., Mutangala, W., Pohlig, G., Schmid, C., Karunakara, U., Torreele, E., and Kande, V. (2009) Nifurtimox-eflornithine combination therapy for second-stage African Trypanosoma brucei gambiense trypanosomiasis: a multicentre, randomised, phase III, non-inferiority trial. *Lancet* **374**, 56-64
127. Vincent, I. M., Creek, D., Watson, D. G., Kamleh, M. A., Woods, D. J., Wong, P. E., Burchmore, R. J., and Barrett, M. P. (2010) A molecular mechanism for eflornithine resistance in African trypanosomes. *PLoS Pathog* **6**, e1001204
128. Wenyon, C. M. (1921) The action of "Bayer 205" on trypanosoma equiperdum in experimentally infected mice. *Br Med J* **2**, 746
129. Van Hoof, L., Henrard, C., and Peel, E. (1944) Pentamidine in the prevention and treatment of trypanosomiasis. *Transactions of the Royal Society of Tropical Medicine and Hygiene* **37**, 271-280
130. Friedheim, E. A., and De Jongh, R. T. (1959) Mel W, a new trypanosomicidal agent derived from mel B. *Trans R Soc Trop Med Hyg* **53**, 262-269
131. Low, G. C., and Manson-Bahr, P. (1923) The treatment of human trypanosomiasis by “Bayer 205”. *Transactions of the Royal Society of Tropical Medicine and Hygiene* **16**, 339-383
132. Kellersberger, E. R. (1926) “Bayer 205” (Germanin) in sleeping sickness — report on 150 cases treated. *Transactions of the Royal Society of Tropical Medicine and Hygiene* **20**, 185-194
133. Friedheim, E. A. (1949) Mel B in the treatment of human trypanosomiasis. *The American journal of tropical medicine and hygiene* **29**, 173-180
134. Conte, J. E., Jr., Upton, R. A., Phelps, R. T., Wofsy, C. B., Zurlinden, E., and Lin, E. T. (1986) Use of a specific and sensitive assay to determine pentamidine pharmacokinetics in patients with AIDS. *The Journal of infectious diseases* **154**, 923-929
135. Jodrell, D. I., Reyno, L. M., Sridhara, R., Eisenberger, M. A., Tkaczuk, K. H., Zuhowski, E. G., Sinibaldi, V. J., Novak, M. J., and Egorin, M. J. (1994) Suramin: development of a population pharmacokinetic model and its use with intermittent short infusions to control plasma drug concentration in patients with prostate cancer. *J Clin Oncol* **12**, 166-175
136. Burri, C., Nkunku, S., Merolle, A., Smith, T., Blum, J., and Brun, R. (2000) Efficacy of new, concise schedule for melarsoprol in treatment of sleeping sickness caused by Trypanosoma brucei gambiense: a randomised trial. *Lancet* **355**, 1419-1425
137. Pepin, J., and Mpia, B. (2006) Randomized controlled trial of three regimens of melarsoprol in the treatment of Trypanosoma brucei gambiense trypanosomiasis. *Trans R Soc Trop Med Hyg* **100**, 437-441
138. Jacobs, R. T., Nare, B., Wring, S. A., Orr, M. D., Chen, D., Sligar, J. M., Jenks, M. X., Noe, R. A., Bowling, T. S., Mercer, L. T., Rewerts, C., Gaukel, E., Owens, J., Parham, R., Randolph, R., Beaudet, B., Bacchi, C. J., Yarlett, N., Plattner, J. J., Freund, Y., Ding, C., Akama, T., Zhang, Y. K., Brun, R., Kaiser, M., Scandale, I., and Don, R. (2011) SCYX-7158, an orally-active benzoxaborole for the treatment of stage 2 human African trypanosomiasis. *PLoS Negl Trop Dis* **5**, e1151
139. Wring, S., Gaukel, E., Nare, B., Jacobs, R., Beaudet, B., Bowling, T., Mercer, L., Bacchi, C., Yarlett, N., Randolph, R., Parham, R., Rewerts, C., Platner, J., and Don, R. (2014) Pharmacokinetics and pharmacodynamics utilizing unbound target tissue exposure as part of a disposition-based rationale for lead optimization of benzoxaboroles in the treatment of Stage 2 Human African Trypanosomiasis. *Parasitology* **141**, 104-118

140. Tarral, A., Blesson, S., Mordt, O. V., Torreele, E., Sassella, D., Bray, M. A., Hovsepian, L., Evene, E., Gualano, V., Felices, M., and Strub-Wourgaft, N. (2014) Determination of an optimal dosing regimen for fexinidazole, a novel oral drug for the treatment of human African trypanosomiasis: first-in-human studies. *Clin Pharmacokinet* **53**, 565-580
141. Torreele, E., Bourdin Trunz, B., Tweats, D., Kaiser, M., Brun, R., Mazue, G., Bray, M. A., and Pecoul, B. (2010) Fexinidazole--a new oral nitroimidazole drug candidate entering clinical development for the treatment of sleeping sickness. *PLoS Negl Trop Dis* **4**, e923
142. Kaiser, M., Bray, M. A., Cal, M., Bourdin Trunz, B., Torreele, E., and Brun, R. (2011) Antitrypanosomal activity of fexinidazole, a new oral nitroimidazole drug candidate for treatment of sleeping sickness. *Antimicrobial agents and chemotherapy* **55**, 5602-5608
143. Roy, N., Nageshan, R. K., Ranade, S., and Tatu, U. (2012) Heat shock protein 90 from neglected protozoan parasites. *Biochim Biophys Acta* **1823**, 707-711

CURRICULUM VITAE

The Johns Hopkins University School of Medicine

KIRSTEN J. MEYER August 2016

Born Aug 20 1987, Takapuna, New Zealand

EDUCATION

2010-Present	PhD candidate in Pharmacology and Molecular Sciences Johns Hopkins University (Baltimore, MD, USA)
2006-2009	Bachelor of BioMedical Science, First Class Honours Major: Pharmacology and Medicinal Chemistry Victoria University of Wellington (Wellington, New Zealand)

RESEARCH EXPERIENCE

Aug 2010-Present	PhD research under Theresa Shapiro, MD, PhD. Johns Hopkins University
Feb 2009- Mar 2010	Honours research under John Miller, PhD. Victoria University of Wellington

PUBLICATIONS

1. Meyer KJ, Shapiro TA. Potent antitrypanosomal activities of heat shock protein 90 inhibitors in vitro and in vivo. *The Journal of Infectious Diseases.*2013; 208:489-499

2. Meyer KJ, Singh AJ, Cameron A, Tan AS, Leahy DC, O'Sullivan S, Joshi P, La Flamme AC, Northcote PT, Berridge MV, Miller JH. Mitochondrial genome-knockout cells demonstrate a dual mechanism of action for the electron transport complex I inhibitor mycothiazole. *Marine Drugs*. 2012; 10(4):900-917

3. Bhat S, Olaleye O, **Meyer KJ**, Shi WL, Zhang Y, Liu JO. Analogs of N'-hydroxy-N- (4H,5H-naptho[1,2-d]thiazol-2-yl)methanimidamine inhibit *Mycobacterium tuberculosis* methionine aminopeptidases. *Bioorganic & Medicinal Chemistry*. 2012; 20(14):4507-4513

OTHER PUBLICATIONS (SUBMITTED/IN PREPARATION)

1. Meyer KJ, Caton, E, Shapiro TA. Hsp90 inhibitors display concentration dependent efficacy against *Trypanosoma brucei* and *Plasmodium falciparum*. (In preparation for submission to PNAS)

2. Meyer KJ, Meyers DJ, Shapiro TA. Shape of the concentration-time curve drives drug potency: in vitro pharmacokinetic-pharmacodynamics of antitrypanosomals. (In preparation for submission to PLoS Pathogens)

3. Meyer KJ, Shapiro TA. RNAi of cytosolic and mitochondrial Hsp90 in *Trypanosoma brucei* reveals roles in cytokinesis and kinetoplast replication. (In preparation for submission to JBC)

ORAL PRESENTATIONS AT INTERNATIONAL CONFERENCES

1. Meyer KJ, Shapiro TA. RNAi of *T. brucei* cytosolic HSP83 and mitochondrial TRAP-1 reveals roles for these Hsp90 homologues in cytokinesis and kinetoplast division. *Kinetoplastida: Cellular, Molecular and Immunoparasitology Scientific Session*. 64th Annual Meeting of the American Society for Tropical Medicine and Hygiene, Oct 25-29 2015, Philadelphia, PA **Co-chaired session**

2. Meyer KJ, Shapiro TA. PK/PD of Antitrypanosomal Agents. *Symposium on PK/PD for Neglected Tropical Infections.* 55th Interscience Conference on Antimicrobial Agents and Chemotherapy, Sept 17-21 2015, San Diego, CA **Invited symposium speaker**

3. Meyer KJ, Shapiro TA. Heat shock protein 90 (Hsp90) inhibitors have potent in vitro and in vivo activity against African trypanosomes. 23rd Molecular Parasitology Meeting, Sept 22-26 2012, Woods Hole, MA

POSTER PRESENTATIONS AT INTERNATIONAL CONFERENCES

1. Meyer KJ, Bakshi RP, Shapiro TA. In vitro PK/PD relationships of antitrypanosomals with a hollow fiber system. 54th Interscience Conference on Antimicrobial Agents and Chemotherapy, Sept 5-9 2014, Washington, DC

2. Meyer KJ, Shapiro TA. Cell cycle disruption and inhibition of proliferation of *Trypanosoma brucei* by Hsp90 inhibitors. 62nd Annual Meeting of the American Society for Tropical Medicine and Hygiene, Nov 13-17 2014, Washington, DC

EXTRAMURAL FELLOWSHIP FUNDING

2013-2015 Mustard Seed Foundation, Harvey Fellowship, $26,000

2010-2011 Fulbright New Zealand Ministry of Research, Science, and Technology Award, $25,000

ACADEMIC HONORS & AWARDS

2015 Paul Ehrlich Award, Young Investigator's Day 2015, Johns Hopkins University

2013 Harvey Fellowship, Mustard Seed Foundation

2012 First Place Poster, 13th Pharmacology and Molecular Sciences Research Retreat, Johns Hopkins

2011	Kelly Award, Johns Hopkins University
2010	Fulbright NZ Ministry of Research, Science, and Technology Award
2009	Summer Research Scholarship, Victoria University of Wellington
2009	Victoria Graduate Award, Victoria University of Wellington
2008	New Zealand Institute of Chemistry Prize, Biochemistry 300 Level, Victoria University of Wellington
2007	Bonded Merit Scholarship, Studylink New Zealand
2006	Jenny Whitmarsh Award for Mathematics, Victoria University of Wellington
2006	Rotary Club of Wellington Science Prize for Biology, Victoria University of Wellington
2006	School Leaver for Academic Excellence, Victoria University of Wellington
2006	W.H. (Bill) Vaughan Scholarship in Mathematics, Victoria University of Wellington

ACADEMIC LEADERSHIP/SERVICE

Nov 2015	**Co-chair of session**, Kinetoplastida: Cellular, Molecular and Immunoparasitology Scientific Session, at the 64th meeting of the American Society for Tropical Medicine and Hygiene.
Sep 2015	**Student organizer** for Merck Pharmacology visit to Johns Hopkins Pharmacology department.
Jan 2015-Present	Founding **member of the Pharmacology Student Initiative**, a group that enhances student training opportunities and promotes greater camaraderie in the department of Pharmacology and Molecular Sciences, Johns Hopkins University.
Sep 2014-May 2015	**Research mentor** for undergraduate volunteer, Kathryn Champ, in Shapiro lab
Feb 2012, Jun 2014	**Peer reviewed** publications for EMBO Molecular Medicine, and the Journal of Medicinal Chemistry alongside mentors Rahul Bakshi, PhD., and Theresa Shapiro, MD, PhD.
Jan 2014	Selected **student representative** from the Pharmacology department at the Johns Hopkins-wide Future of PhD Education symposium.
Feb 2009-Nov 2009	**Chemistry Equity Tutor** for Te Ropu Awhina at Victoria University of Wellington.